SPIRE
Design Description

SUBJECT:	SPIRE Design Description		
PREPARED BY:	Douglas Griffin Matt Griffin Bruce Swinyard		
DOCUMENT No:	SPIRE-RAL-PRJ-000620		
ISSUE:	0.1	**Date:**	Thursday, 12 April 2001
APPROVED BY:	**DRAFT**	**Date:**	

Distribution:

All SPIRE Co-Investigators and Institute Managers

Change Record

ISSUE DATE

Glossary

Term	Meaning
ADC	Analogue to Digital Converter
AIV	Assembly, Integration and Verification
AME	Absolute Measurement Error
AOCS	Attitude and Orbit Control System
APART	Arizona's Program for the Analysis of Radiation Transfer
APE	Absolute Pointing Error
ASAP	Advanced Systems Analysis Program
AVM	Avionics Model
BDA	Bolometer Detector Array
BFL	Back Focal Length
BRO	Breault Research Organization
BSM	Beam Steering Mirror
CDMS	Command and Data Management System
CDMU	Command and Data Management Unit
CDR	Critical Design Review
CMOS	Complimentary Metal Oxide Silicon
CPU	Central Processing Unit
CVV	Cryostat Vacuum Vessel
DAC	Digital to Analogue Converter
DAQ	Data Acquisition
DCU	Detector Control Unit = HSDCU
DPU	Digital Processing Unit = HSDPU
DSP	Digital Signal Processor
DQE	Detective Quantum Efficiency
EDAC	Error Detection and Correction
EGSE	Electrical Ground Support Equipment
EMC	Electro-magnetic Compatibility
EMI	Electro-magnetic Interference
ESA	European Space Agency
FCU	FCU Control Unit = HSFCU
FIR	Far Infrared
FIRST	Far Infra-Red and Submillimetre Telescope
FOV	Field of View
F-P	Fabry-Perot
FPGA	Field Programmable Gate Array
FPU	Focal Plane Unit
FTS	Fourier Transform Spectrometer
FWHM	Full Width Half maximum
GSFC	Goddard Space Flight Center
HK	House Keeping
HOB	Herschel Optical Bench
HPDU	Herschel Power Distribution Unit
HSDCU	Herschel-SPIRE Detector Control Unit
HSDPU	Herschel-SPIRE Digital Processing Unit
HSFCU	Herschel-SPIRE FPU Control Unit
HSO	Herschel Space Observatory
IF	Interface
IID-A	Instrument Interface Document - Part A
IID-B	Instrument Interface Document - Part B
IMF	Initial Mass Function

Term	Meaning
IR	Infrared
IRD	Instrument Requirements Document
IRTS	Infrared Telescope in Space
ISM	Interstellar Medium
JFET	Junction Field Effect Transistor
ISO	Infrared Space Observatory
LCL	Latching Current Limiter
LIA	Lock-In Amplifier
LVDT	Linear Variable Differential Transformer
MAC	Multi Axis Controller
LWS	Long Wave Spectrometer (an instrument used on ISO)
MCU	Mechanism Control Unit = HSMCU
M-P	Martin-Puplett
NEP	Noise Equivalent Power
NTD	Neutron Transmutation Doped
OBS	On-Board Software
OMD	Observing Modes Document
OPD	Optical Path Difference
PACS	Photodetector Array Camera and Spectrometer
PCAL	Photometer Calibration source
PID	Proportional, Integral and Differential (used in the context of feedback control loop architecture)
PLW	Photometer, Long Wavelength
PMW	Photometer, Medium Wavelength
POF	Photometer Observatory Function
PROM	Programmable Read Only Memory
PSW	Photometer, Short Wavelength
PUS	Packet Utilisation Standard
RMS	Root Mean Squared
SCAL	Spectrometer Calibration Source
SCUBA	Submillimetre Common User Bolometer Array
SED	Spectral Energy Distribution
SMEC	Spectrometer Mechanics
SMPS	Switch Mode Power Supply
SOF	Spectrometer Observatory Function
SPIRE	Spectral and Photometric Imaging Receiver
SRAM	Static Random Access Memory
SSSD	SubSystem Specification Document
STP	Standard Temperature and Pressure
SVM	Service Module
TBC	To Be Confirmed
TBD	To Be Determined
TC	Telecommand
URD	User Requirements Document
UV	Ultra Violet
WE	Warm Electronics
ZPD	Zero Path Difference

1. INTRODUCTION

1.1 The SPIRE instrument and its scientific programme

SPIRE (the Spectral and Photometric Imaging REceiver) is one of three cryogenic focal plane instruments for ESA's Herschel mission. Its main scientific goals are the investigation of the statistics and physics of galaxy and structure formation at high redshift and the study of the earliest stages of star formation, when the protostar is still coupled to the interstellar medium. These studies require the capabilities to carry out large-area (many tens of square degrees) deep photometric imaging surveys at far-infrared and submillimetre wavelengths, and to follow up these systematic survey observations with spectroscopy of selected sources. SPIRE will exploit the advantages of Herschel: its large-aperture, cold, low-emissivity telescope; the complete lack of atmospheric emission and attenuation giving access to the poorly explored 200-700-μm range, and the large amount of high quality observing time. Because of these advantages, SPIRE will have unmatched sensitivity for deep imaging photometry and moderate-resolution spectroscopy.

Galaxies emit a large amount (from 30% to nearly 100%) of their energy in the far infrared due to re-processing of stellar UV radiation by interstellar dust grains. The far infrared peak is redshifted into the SPIRE wavelength range for galaxies with redshift, z, greater than ~ 1. The total luminosity of a galaxy cannot be determined without an accurate measurement of its Spectral Energy Distribution (SED). The study of the early stages of galaxy evolution thus requires an instrument that can detect emission from high-z galaxies in the submillimetre, enabling their SEDs and luminosities to be derived.

Stars form through the fragmentation and collapse of dense cloud cores in the interstellar medium (ISM), and the very first stages of this process are not well known. A good understanding of this early evolution is crucial, as it governs the origin of the stellar initial mass function (IMF). Sensitive far infrared and submillimetre observations with high spatial resolution are necessary to make complete surveys of protostellar clumps to determine their bolometric luminosities and mass functions. SPIRE will also, for the first time, enable astronomers to observe at high spatial resolution the physical and chemical conditions prevailing in the cold phases of the interstellar medium and to study the behaviour of the interstellar gas and dust before and during star formation. SPIRE's uniquely high sensitivity to very cold dust emission also makes it the ideal instrument to study the material that is ejected in copious quantities from evolved stars, enriching the interstellar medium with heavy elements. Large amounts of matter - as yet undetected - are ejected from stars before the white dwarf stage. Theories of stellar evolution, and of the enrichment of galaxies in heavy elements and dust, will be incomplete until these earlier mass loss phases are characterised and understood. Studies of star formation and of the interaction of forming and evolved stars with the ISM are also, of course, intimately related to the investigation of galaxy formation and evolution, which occur through just these processes.

These high priority programmes for Herschel require sensitive continuum imaging in several bands to carry out surveys, and a low-resolution spectroscopic mode to obtain detailed SEDs of selected objects and measure key spectral lines. Although SPIRE has been optimised for these two main scientific programmes, it will offer the astronomical community a powerful tool for many other astrophysical studies: giant planets, comets, the galactic interstellar medium, nearby galaxies, ultraluminous infrared galaxies, and active galactic nuclei. Its capabilities will remain unchallenged by the ground-based and the airborne observatories which are planned to come into operation over the next decade.

The scientific case for SPIRE is described in more detail in the SPIRE proposal (Griffin *et al.,* 1998a)

1.2 Purpose of this document

This document outlines the essential features of the design and operation of SPIRE. It is intended to provide an introductory account of the key features of the SPIRE system and subsystem design and operation - but not to provide a complete description: for that the reader is referred to other more detailed project documents, particularly the following:

Document	Reference		Abbreviation
SPIRE Scientific Requirements	SPIRE-UCF-PRJ-000064		SRD
SPIRE Instrument Interface Document Part B	SPIRE-ESA-DOC-000275		IID-B
SPIRE Instrument Requirements Specification	SPIRE-RAL-PRJ-000034/1.0 23 Nov. 2000		IRD
Operating Modes for SPIRE	SPIRE-RAL-PRJ-000320		OMD
SPIRE On-Board Software URD	SPIRE-IFSI-PRJ-000444/		OBS URD
Subsystem Specification Documents for each of the SPIRE subsystems	Detector Subsystem Specifications	SPIRE-JPL-PRJ-456	SSSDs
	SPIRE Spectrometer Mirror Mechanism Subsystem Specification	LAM.PJT.SPI.SPT.200002 Ind 4	
	SPIRE Beam Steering Mirror Subsystem Specification Document	SPIRE-ATC-PRJ-0460	
	SPIRE Sorption Cooler Specifications	GS/SBT/SPIRE/2000-01	
	DPU Subsystem Specification Document	SPIRE-IFS-PRJ-000462	
	MCU Design Description	LAM/ELE/SPI/000619/1.1/ 20 Dec. 2000	
	SPIRE Mirrors Specification	LAM.PJT.SPI.SPT.200007 Ind 4	
	DRCU Subsystem Specification	SAp-SPIRE-CCa-25-00	
	SPIRE Filters subsystem specification	SPIRE-PRJ-000454	
	SPIRE Calibrators subsystem specification	SPIRE-QMW-PRJ-000453	
	SPIRE Structure Subsystem Specification Document	SPIRE-MSS-PRJ-0000427	

Additional references are given in Section 7.

1.3 Scope

The document concerns the design and operation of the instrument. It includes:

(i) the Warm Electronics (WE) which is composed of the Digital Processor Unit (DPU), the Detector Control Unit (DCU) and the FPU Control Unit (FCU) and their associated electrical harnesses;
(ii) the Focal Plane Unit (FPU) which contains the optical components, detector arrays, 300-mK sorption cooler, mechanisms, internal calibrators, thermal straps, and various housekeeping units, and the mechanical structure which houses these elements;
(iii) the on-board software (OBS) which allows commanding of the instrument and telemetry of the science and housekeeping data.

The design of the Herschel telescope, which SPIRE shares with the other experiments is only referenced in as much as it influences the design of SPIRE as external inputs. The thermal straps from the Herschel cryostat to the FPU, the interface between the DPU and the spacecraft Power Distribution Unit and the Command and Data Handling System (CDMS) are only referenced only in so far as they impact on the design of the units listed above. The various items of SPIRE ground support equipment also fall outside the scope of the document.

The intention of this document is to provide the reader with an understanding of the rationale for the current design. Although the document will be updated periodically to reflect the evolution and detailing of the instrument design the information contained herein is not necessarily accurate in all details, and this document should therefore not be used as a reliable source of design information. To obtain the most up-to-date information, the reader is directed to the appropriate project documents, viz. IID-B, IRD and the various SSSDs.

2. INSTRUMENT OVERVIEW

SPIRE contains a three-band imaging photometer and an imaging Fourier Transform Spectrometer (FTS), both of which use 0.3-K feedhorn-coupled "spider-web" NTD germanium bolometers cooled by a ^{3}He refrigerator. The photometer and spectrometer are not designed to operate simultaneously. The field of view of the photometer is 4 x 8 arcminutes, the largest that can be achieved given the location of the SPIRE field of view in the Herschel focal plane and the size of the telescope unvignetted field of view. Three bolometer arrays provide broad-band photometry ($\lambda/\Delta\lambda \sim 3$) in wavelength bands centred on 250, 350 and 500 μm. The field of view is observed simultaneously in all three bands through the use of fixed dichroic beam-splitters. Spatial modulation can be provided either by a Beam Steering Mirror (BSM) in the instrument or by scanning the telescope across the sky, depending on the type of observation. An internal thermal calibration source is available to provide a repeatable calibration signal for the detectors. The FTS uses novel broadband intensity beam splitter, and combines high efficiency with spatially separated input ports. One input port covers a 2.6-arcminute diameter field of view on the sky and the other is fed by an on-board calibration source. Two bolometer arrays are located at the output ports, one covering 200-300 μm and the other 300-670 μm. The FTS will be operated in continuous scan mode, with the path difference between the two arms of the interferometer being varied by a constant-speed mirror drive mechanism. The spectral resolution, as determined by the maximum optical path difference, will be adjustable between 0.04 and 2 cm^{-1} (corresponding to $\lambda/\Delta\lambda = 1000 - 20$ at 250 μm wavelength.

2.1 Photometer design drivers

The basic design of the photometer was dictated by the following consideration:

(i) the major scientific priorities for SPIRE require an instrument which is capable of deep mapping of large areas of sky efficiently with full spatial sampling and multi-wavelength coverage;
(ii) observations of point and compact sources should also be possible with good efficiency;
(iii) the instrument should be as simple as possible for affordability, reliability and ease of operation;
(iv) the wavelength coverage should complement that of the PACS instrument on board Herschel and ground-based facilities operating at near-millimetre wavelengths;

These considerations led to the choice of a system with fixed dichroic beamsplitters allowing simultaneous observation of a large field of view in the three chosen submillimetre bands, with the inclusion of a beam steering mirror to allowed point source observations and small maps to be carried out efficiently.

2.2 Spectrometer design drivers

Fabry-Perot and grating spectrometer designs were also studied for SPIRE (Griffin, 1997; Griffin *et al.* 1998b). The FTS was chosen for a number of reasons:

(i) it allows for two-dimensional imaging spectroscopy, which is not possible with the grating instrument;
(ii) the spectral resolution can easily be adjusted and tailored to the scientific requirements of the observation;
(iii) the detectors can be operated at 300 mK because the photon noise limited NEP is higher for the FTS, whose detectors observe broad-band, than for grating or Fabry-Perot spectrometers in which they observe in narrow-band mode - this allowed a ^{3}He sorption cooler to be adopted for SPIRE - a considerable simplification over the 100-mK dilution cooler that would have been needed for a grating or F-P instrument;
(iv) whilst the grating is more sensitive, at least in principle, for observations of known spectral lines, there is little difference in the sensitivities of the two options for spectral survey observations, which are of greater scientific priority for SPIRE;

(v) the FTS is less vulnerable to degradation in performance arising from stray light and out-of-band leaks which can be problematic with a low-background grating instrument;
(vi) practical implementation of either a grating or an F-P instrument within the constraints of the Herschel system would have posed serious accommodation problems (grating) or risk of FPU failure due to having multiple mechanisms in series (F-P).

2.3 Instrument functional block diagram

Figure 2-1 shows a functional block diagram of the SPIRE instrument. The subsystems are prefixed HS standing for Herschel-SPIRE. The focal plane unit is mounted on the Herschel Optical Bench as shown in Figure 2-2. It is approximately 690 x 410 x 410mm in size, and has three separate temperature stages at nominal temperatures of 4 K, 2 K (both provided by the Herschel cryostat) and 300 mK (provided by SPIRE's internal cooler). The main 4-K structural element of the FPU is an optical bench panel which is supported from the 10-K cryostat optical bench by stainless steel blade mounts. The photometer and spectrometer are located on either side of this panel. The majority of the optics are at 4 K, but the detector arrays and final optics are contained within 2-K enclosures. The ^{3}He refrigerator cools all of the five detector arrays to 0.3 K. Two JFET preamplifier boxes (one for the photometer and one for the FTS) are attached to the 10-K optical bench close to the 4-K enclosure, with the JFETs heated internally to their optimum operating temperature of ~ 120 K. Note that the shutter is not designed for flight operation and is controlled by SPIRE EGSE.

The SPIRE warm electronics consist of a Detector Readout Unit (DCU), a FPU Control Unit (FCU) and a Digital Processing Unit (DPU). The DCU provides bias and signal conditioning for the arrays and cold readout electronics and reads out the detector signals; the FCU controls the FPU mechanisms, the ^{3}He cooler and the internal calibrators, and housekeeping thermometers. The DPU acts as the interface to the spacecraft, including instrument commanding, and formats science and housekeeping data for telemetry to the ground.

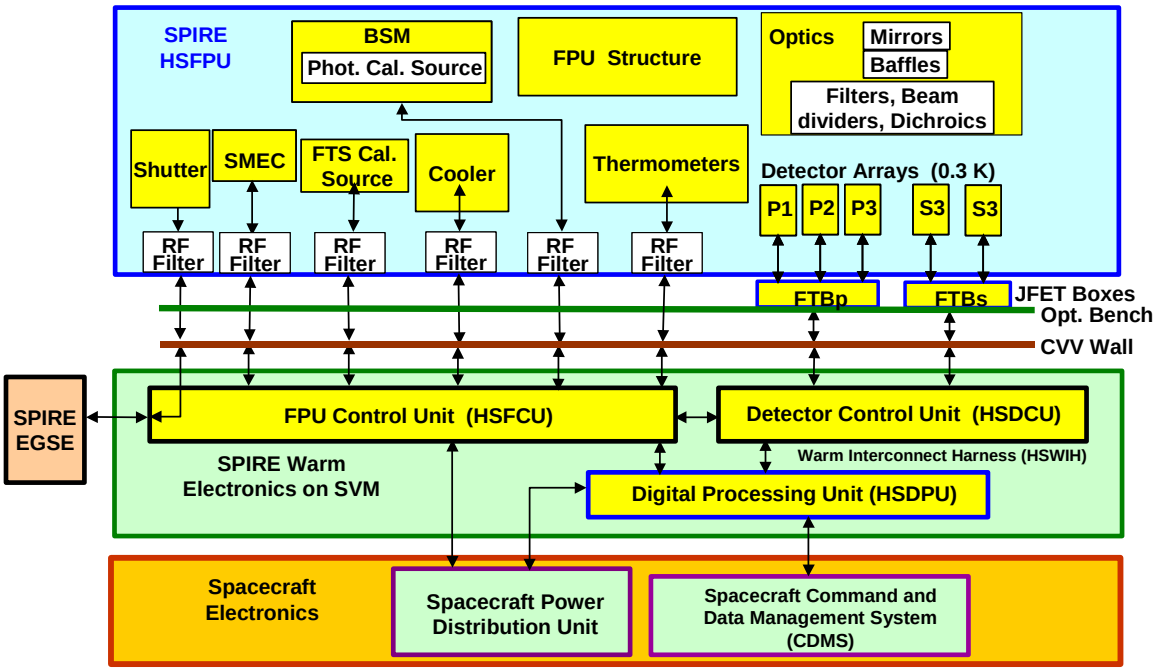

Figure 2-1 - Functional block diagram of the SPIRE instrument

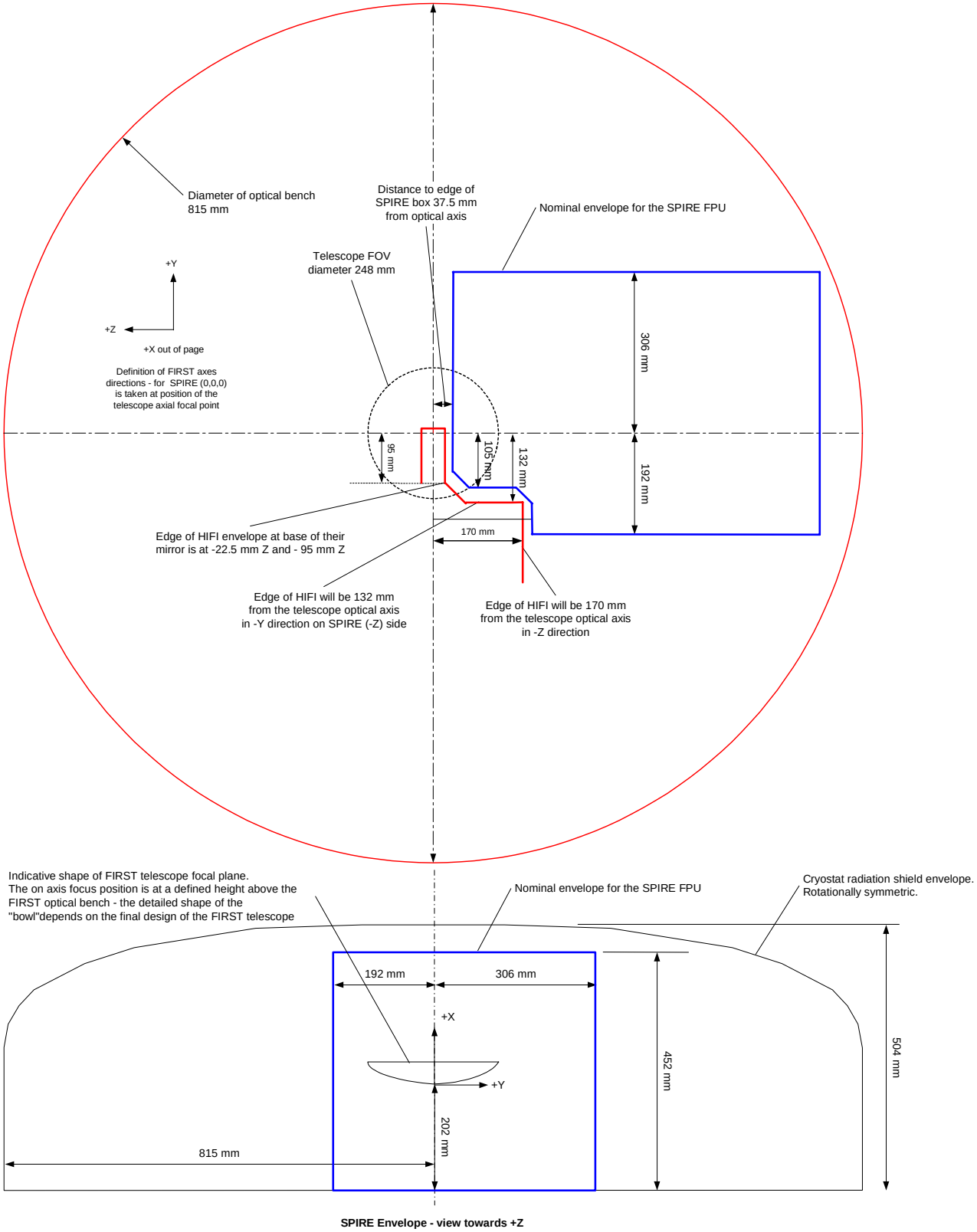

Figure 2-2 Location of the SPIRE FPU on the Herschel Optical Bench

2.3.1 Imaging photometer

2.3.1.1 Optical Design and FPU layout

The photometer layout is shown in Fig. 2.3. The 4-K optical elements are mounted directly from the optical bench panel. The 2-K enclosure is also supported from the panel by stainless steel blades, and contains the detector arrays, dichroics, and fold mirrors. The three array modules are bolted to the outside wall of the 2-K box. Within each module, the detector arrays, feedhorns and the final filter are thermally isolated from the 2-K structure by Kevlar wires, and are cooled by a thermal strap to the ^{3}He refrigerator (see §4.11 below). The photometer input optics are shared with the spectrometer. The separate spectrometer field of view is directed to the other side of the optical bench panel by a pick-off mirror.

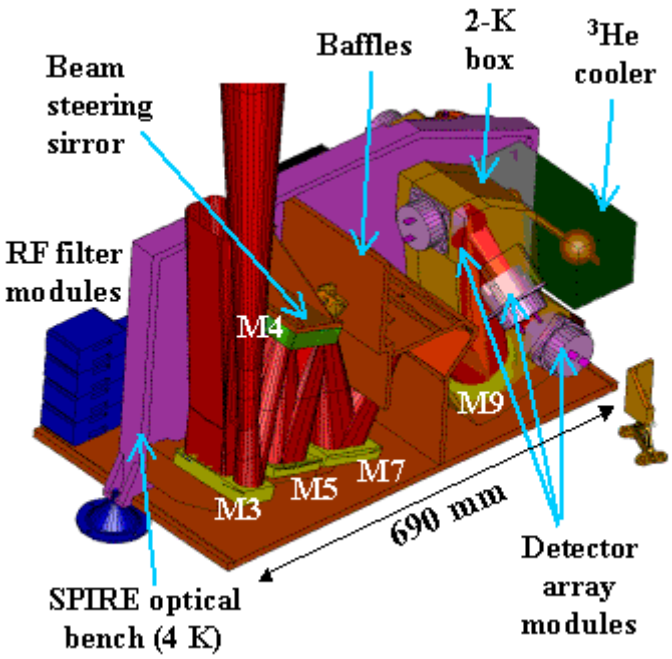

Figure 2-3 Computer-generated picture of the SPIRE photometer layout (4-K cover not shown)

The photometer optical design is shown in Figure 2-4, and is described in more detail by Dohlen *et al.* (2000) and in §4.4 below. It is an all-reflective system except for two dichroic beam splitters used to direct the three wavelength bands onto different bolometer arrays, and various transmissive band-pass and edge filters used to reject out-of-band radiation. It is optimised to give close to diffraction-limited imaging across the whole 4 x 8 arcminute field of view. The SPIRE field of view is offset by 11 arcminutes from the centre of the Herschel telescope's highly curved focal surface. Mirror M3, which lies below the focus, receives the f/8.68 beam from the telescope and forms a pupil image of the telescope secondary at the flat beam steering mirror, M4. Mirror M5 converts the focal ratio to f/5 and provides an intermediate focus at the next mirror, M6, which re-images the aperture stop at M4 to a cold stop located at the entrance to a 2-K enclosure. M7, M8 and M9 constitute a one-to-one optical relay to bring the M6 focus to the three detector arrays. The beams for the three bands are directed onto the arrays at f/5 by a combination of flat folding mirrors and fixed dichroics set at 25º to the beam axis. M3 - M8 are at 4 K and the cold stop and all subsequent optics are at 2 K.

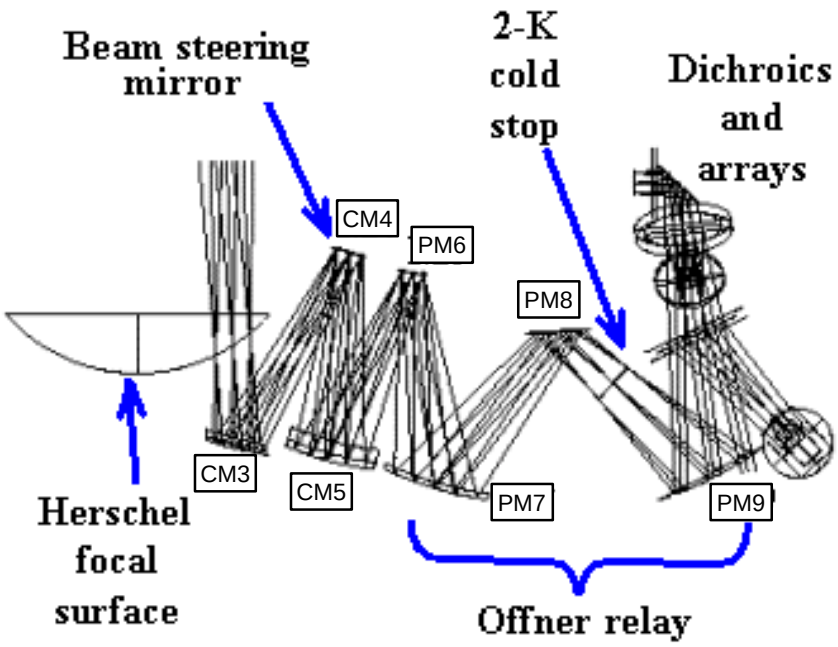

Figure 2-4 Imaging photometer optical design

A shutter at the entrance aperture of the instrument (just above the telescope focus) can be inserted to block the beam. This will be important for ground testing in the Herschel cryostat where the background radiation from the cryostat shields and lid will be much greater than in flight. The shutter will allow the detector performance to be tested and verified under controlled flight-representative conditions. Flight operation of the shutter is not planned.

An internal calibration source provides a repeatable signal for the bolometer arrays. It radiates through a 1-mm hole in the centre of the beam steering mirror, M4. As this is at a pupil image, the illumination is close to uniform over the arrays. The source can be modulated at frequencies up to 5 Hz, and operated at temperatures up to 80 K to give sufficient signal on the arrays, with peak power dissipation < 2 mW. The beam steering mirror is capable of chopping (2 arcminutes along the long axis of the 4 x 8 arcminute field of view, at frequencies up to 2 Hz with an efficiency of 90% and power dissipation < 2 mW. It can operate at higher frequencies with reduced efficiency and increased power dissipation. The beam steering mechanism can simultaneously chop at up to 1 Hz in the orthogonal direction by up to 30 arcseconds. Two axis motion allows "jiggling" of the pointing to create a fully sampled image of the sky with the feedhorn-coupled detectors whose diffraction-limited beams on the sky are separated by approximately twice the beam FWHM.

The SPIRE filtering scheme is designed to provide precise definition of the spectral passbands with high out-of-band rejection and maximum in-band transmission, and also to minimise the thermal loading on the 4-K, 2-K and 0.3-K stages by reflecting short-wavelength radiation. To achieve complete rejection out to UV wavelengths, four blocking filters are needed in the chain in addition to high-pass and low-pass edge filters which define the band.

2.3.1.2 Detector arrays

SPIRE will use spider-web bolometers with NTD germanium thermometers (Mauskopf *et al.* 1997; Bock *et al.* 1998). The bolometers are coupled to the telescope by hexagonally close-packed single-mode conical feedhorns, providing diffraction limited beams. The horn diameters are 2Fλ where F is the focal ratio of the final optics and λ is the wavelength: this provides a diffraction-limited beam with maximum coupling efficiency of the detector to a point source. Modelling of the complete optical train predicts FWHM beam widths of 17.1, 24.4 and 34.6

arcseconds at 250, 350 and 500 μm, respectively. The numbers of detectors in the three arrays are 139, 88, and 43 for 250, 350 and 500 μm respectively, making a total of 270 detectors for the photometer. The detector arrays are shown schematically in Figure 4-19, and a photograph of a prototype array module is shown in

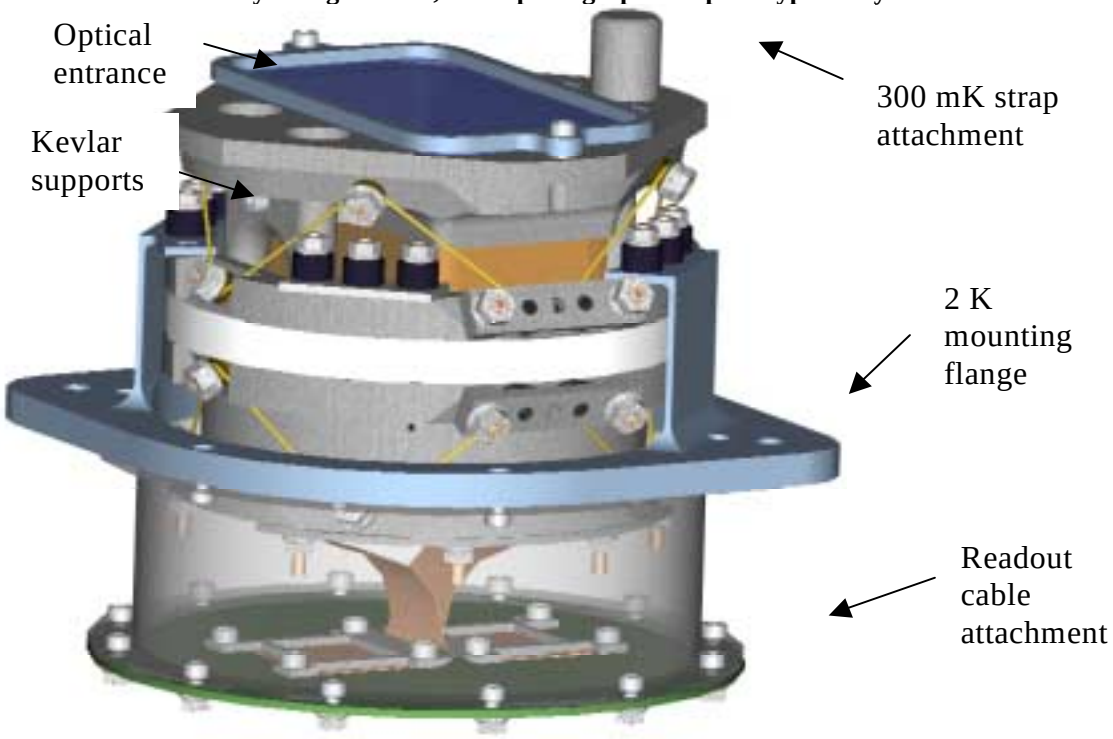

Figure 4-21. Each array unit has an interface to the 2-K box, with a thermal strap from the ^{3}He cooler to the 0.3-K stage, which is supported by Kevlar strings from the 2-K level. The electrical connections to the detectors are made with Kapton ribbon cables within the array modules and with woven manganin cables between the array modules and the JFET units. The bolometers are excited by an AC bias at approx. 100 Hz, which eliminates 1/f noise from the JFETs, giving a 1/f knee for the system of less than 100 mHz. Conservative estimates of the bolometer Detective Quantum Efficiency (DQE) vary between 0.6 and 0.7 ensuring that the overall NEP will be dominated by the thermal emission from the Herschel telescope.

2.3.1.3 Photometer observing modes

The photometer will have three principal observing modes, as illustrated in Figure 2-6 and described below. These modes are described in greater detail in OMD.

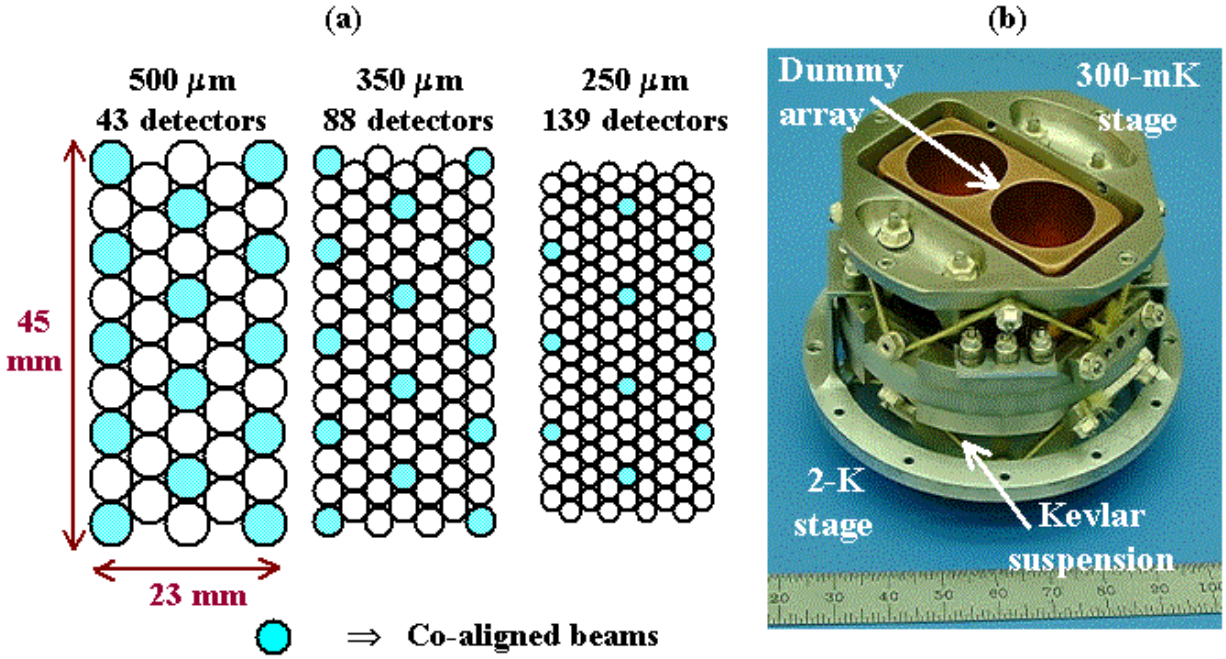

Figure 2-5 - : (a) layout of the three photometer arrays; (b) photograph of array mechanical prototype

Point source photometry: For photometric observations of point or compact sources, chopping will be used. There are several sets of three detectors for which the beams at the three wavelengths are exactly co-aligned on the sky, indicated by the shaded circles in Figure 2-5. By chopping through the appropriate angle (approx. 126 arcseconds), 3-band photometric observations can be carried out simultaneously with maximum efficiency. To account for the possibility of positional errors due to telescope pointing inaccuracy or imperfect knowledge of the source position, the beam steering mirror can be used to implement a seven-point mapping routine in this mode. Assuming an angular offset of 6" for the seven-point, the loss in S/N for a given integration time varies between 6% at 500 μm and 20% at 250 μm, which is a small penalty to pay for assurance that telescope pointing or source position errors do not result in an underestimate of the source flux density.

Field mapping: For mapping of regions a few arcminutes in extent, the beam steering mirror will be used to carry out a jiggle map, similar to the mode of operation of the SCUBA bolometer camera on the JCMT (Holland *et al.* 1999). A 64-point jiggle pattern is needed to achieve full spatial sampling in all bands simultaneously, with a step size of 9 arcseconds (half-beam spacing at 250 μm). A maximum field size of 4 x 4 arcminutes is available in this mode as the 2-arcminute regions at each end of the array will be chopped outside the field of view admitted by the photometer optics.

Scan mapping: This mode will be used for mapping large areas of sky (much bigger than the SPIRE field of view), including deep survey observations. The telescope will be scanned across the sky (at up to 1 arcminute per second, the maximum rate that the spacecraft can provide). Because of the excellent 1/f stability of the NTD detectors, the beam steering mirror does not need to be operated - signal modulation is provided by the telescope motion. To provide the necessary beam overlap for full spatial sampling over the strip defined by a single scan, the scan angle must be 14.5^{o} with respect to one of the array axes.

The available telemetry rate of 100 kbs allows all of the 270 photometer detectors to be sampled with 16-bit resolution at up to 28 Hz and the data telemetered directly to the ground with no on-board processing.

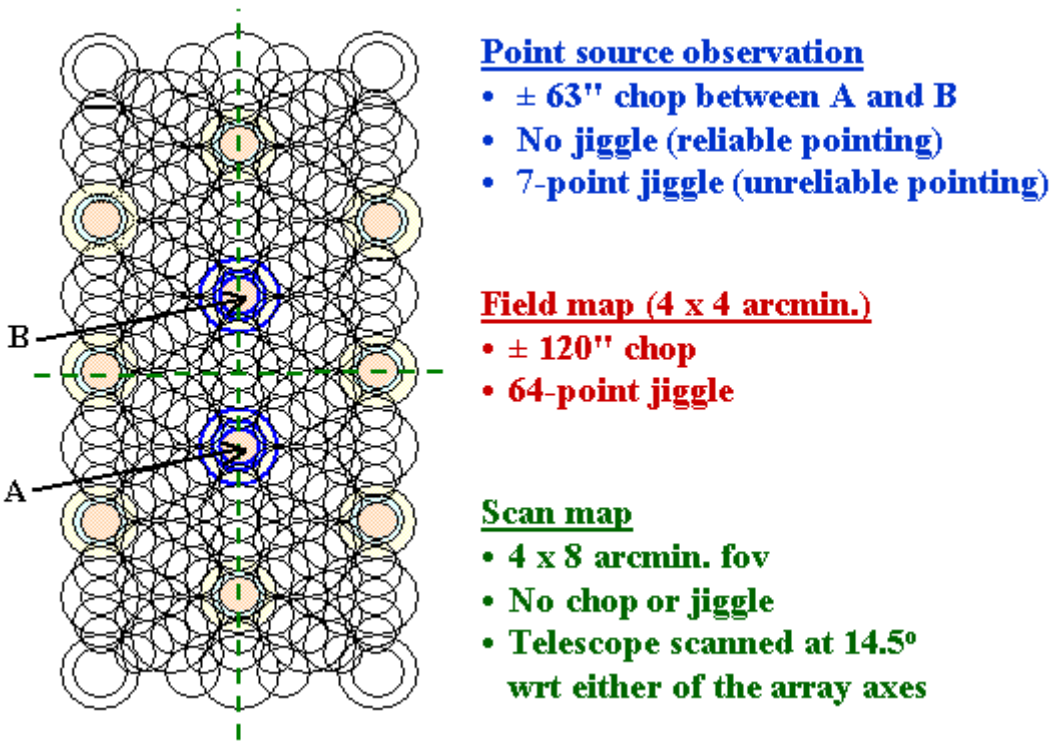

Figure 2-6 Overlaid photometer arrays and summary of photometer observing modes.

2.3.2 Fourier transform spectrometer

2.3.2.1 Optical design and FPU layout

The layout of the FTS and its optical scheme are shown in Figure 2-7 and Figure 2-8 respectively. The main design features of the FTS are described in Swinyard *et al.* (2000) and in §3.4.2 below. It uses two broadband, high-efficiency, intensity beam splitters in a Mach-Zehnder configuration rather than the traditional polarising beam splitters. This configuration has the advantage that all four ports are separately accessible, as in the classical Martin Puplett (M-P) polarising FTS (Martin, 1982). But the throughput is a factor of two higher than for the M-P as none of the incoming radiation is rejected. This design is also insensitive to the polarisation of the incident radiation. The performance of the beam splitters and of a bench-top implementation of this design has been demonstrated (Ade *et al.* 1999). A thermal calibrator is located at a pupil image in the second input port of the FTS, and provides a thermal input that mimics the dilute 80-K black body emission of the telescope. This allows the large telescope background to be nulled, thereby reducing the dynamic range requirements for the detector sampling. Two band-limited detector arrays are placed in the two output ports, covering 200-300 μm and 300-670 μm. A single back-to-back moving roof-top mechanism serves both arms of the interferometer, with a frictionless carriage mechanism using double parallelogram linkage and flex pivots. The pick-off mirror (on the photometer side of the optical bench panel and located at the intermediate field image) directs the spectrometer field of view through a hole in the optical bench panel into the FTS side of the instrument. A 4-K pupil stop is located between the pick-off mirror and the input fold mirror. The input relay mirror focuses the beam to an intermediate image plane located just after the first beam splitter, after which the beam is collimated and sent to the moving corner cube assembly. The corner cube shifts the beam and sends it towards the camera mirror, which produces an image plane just before the output beam splitter. The output relay mirror focuses the beam onto the detector arrays. A pupil image is located near the final fold mirror, making this a convenient location for the entrance aperture to the 2-K enclosure. As this pupil moves when the optical path difference changes, it is not a good place for a limiting cold stop. Instead, the limiting aperture is located at the 4-K pupil plane between the pick-off mirror and the input fold mirror.

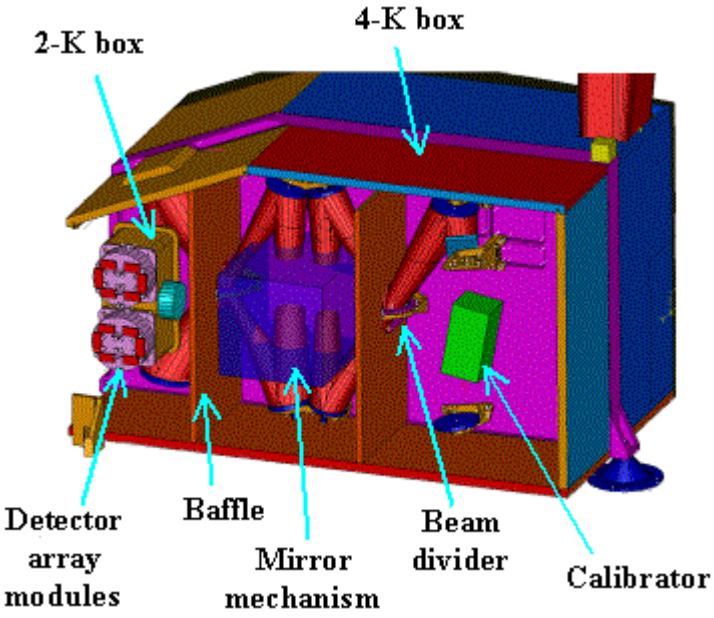

Figure 2-7 - Physical layout of the spectrometer.

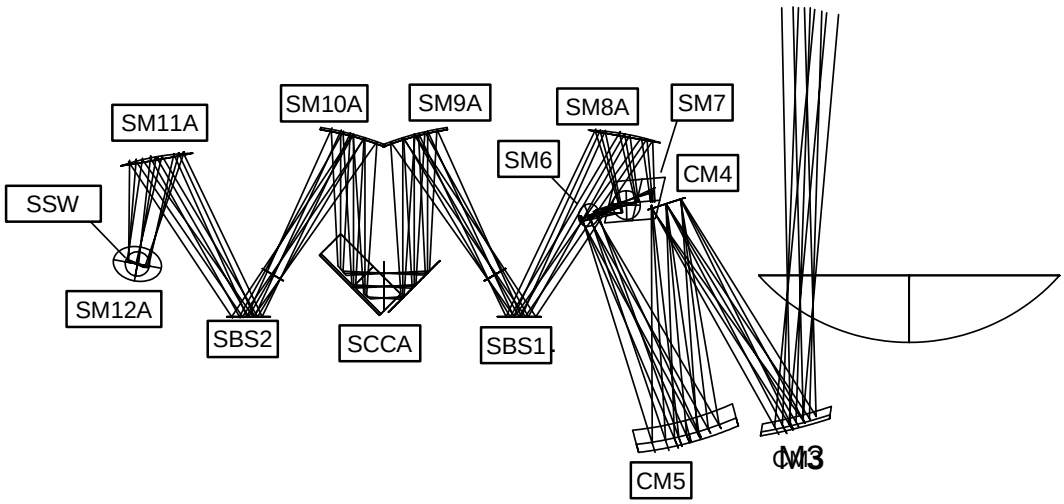

Figure 2-8 - Optical design of the spectrometer.

The FTS design is optimised for the 200-400 μm band. The wavelength coverage is extended to 15 cm^{-1} (670 μm) to give access to the astrophysically important 609-μm line of CI in our own and nearby galaxies, and to increase the range over which the spectral energy distribution of sources can be measured in the FTS low-resolution mode. A filtering scheme similar to the one employed for the photometer channel is used to restrict the passband of the instrument. Filters on the bolometer arrays themselves define the passband for each array.

2.3.2.2 Spectrometer detector arrays

The field of view of the FTS is approximately 2.6 arcminutes in diameter, and is covered by 37 hexagonally close-packed detectors in a short-wavelength array and 19 in a long-wavelength array. The detector modules will be similar to those used for the photometer, with a mechanical interface to the wall of the 2-K enclosure.

The two FTS arrays cover the 200-300 and 300-670 μm bands. The detectors and feedhorns for the short wavelength band are similar to those for the photometer 250-μm channel. The long wavelength band is

optimised for the 300-400 μm range. There is a degradation in point source coupling efficiency at wavelengths beyond around 400 μm due to the decreasing aperture size relative to the wavelength. The waveguide coupling the horn to the bolometer must also have a diameter large enough to transmit at 670-μm, and so is overmoded at the shorter wavelengths within the band. This results in an increase in background radiation on the detectors and a broadening of the beam by about 20% compared to the diffraction limit at the lower end of the band (Caldwell *et al.* 2000).

The layout of the FTS arrays is shown in Figure 2-9. The detectors on the periphery of the arrays are partly vignetted by the 2.6-arcminute field of view admitted by the instrument optics (indicated by the large circles in Figure 2-9.). The short-wavelength array feedhorns are sized to give 2Fλ pixels at 225 μm and the long-wavelength horns to give 2Fλ pixels at 389 μm. This arrangement, although slightly non-optimal from the point of view of point source sensitivity at the central wavelengths of the two arrays, has the advantage that there are numerous co-aligned pixels in the combined field of view. This maximises the observing efficiency for measuring a point source spectrum together with its surrounding sky background and also provides redundancy to the spectrometer in the case of failure of a single pixel within one array.

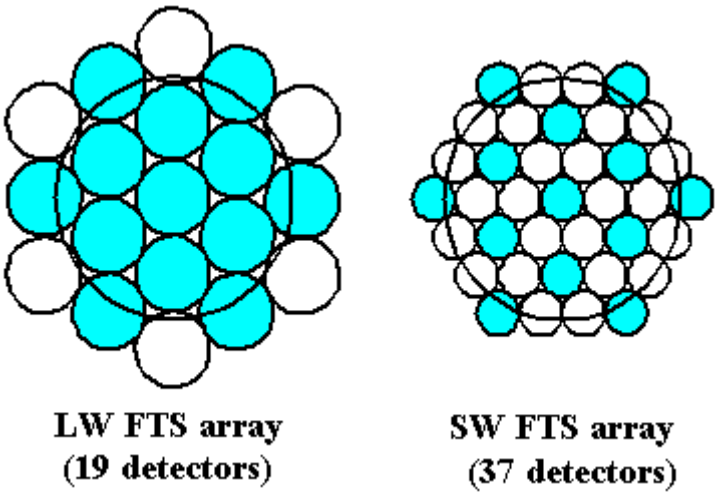

Figure 2-9 Layout of spectrometer detector arrays

2.3.2.3 Spectrometer observing modes

The FTS will be operated in continuous scan mode with the mirrors moving at a constant speed of up to 0.1 cm^{-1}, corresponding to a signal frequency range of 6 - 20 Hz. The spectral resolution can be adjusted between 0.04 and 2 cm^{-1} ($\lambda/\Delta\lambda$ = 20 - 1000 at 250 μm). The maximum scan length is 3.5 cm (taking 35 seconds or more and giving an optical path difference of 14 cm). To ensure that mechanism jitter noise is well below the photon noise level, a relative accuracy of 0.1 μm is required for the mirror position. The FTS calibration source will be on continuously while the spectrometer is operating, with a peak power of no more than 5 mW. For spectral mapping of extended sources, the beam steering mirror will be used to provide the necessary pointing changes between scans. The scanning mirror control system uses a digital feedback loop to provide a constant speed over the scan length, with an accuracy requirement of 1% (goal 0.5%). The position readout uses a Heidenhain Moiré fringe sensing system. The detectors are read out asynchronously with the samples time-stamped to match them to the corresponding mirror locations. No on-board processing will be done - the raw interferograms will be telemetered to the ground. The number of detectors and the available telemetry rate are compatible with an oversampling factor of two with respect to the Nyquist sampling rate of 40 Hz (sampling at approx. 80 Hz per detector). An oversampling factor somewhat greater than this is desirable - options to achieve this include increasing the data rate, decreasing the mirror speed, sampling only a fraction of the detectors in some cases (e.g., point source observations), or a combination of these.

2.3.3 Helium-3 cooler

The ^{3}He cooler (Duband 1997) uses porous material to adsorb or release a gas when cooled or heated. This type of refrigerator is well-suited to a space environment. Gas-gap heat switches (Duband 1995) are used the control the refrigerator and there are no moving parts. It can be recycled indefinitely with over 95% duty cycle efficiency and the lifetime is only limited by that of the cold stage from which it is run (in this case, the lifetime of the Herschel cryostat). The evaporation of ^{3}He naturally provides a very stable operating temperature under constant heat load over the entire cycle. The cooler requires no mechanical or vacuum connections and only low-current electrical leads for its operation, making the mechanical and electrical interfaces very simple. For operation in a zero-g environment two aspects of the design of a ^{3}He refrigerator have been addressed: the liquid confinement and the structural strength required for the launch. The confinement within the evaporator is provided by a porous material which holds the liquid by capillary attraction. For the thermal isolation and structural support of the refrigerator elements, a suspension system using Kevlar wires has been designed to support the cooler firmly during launch whilst minimising the parasitic heat load on the system. The base-line SPIRE cooler contains 6 STP litres of ^{3}He, fits in a 200 x 100 x 100 mm envelope and weighs about 1.6 kg. Its performance has been analysed using the same methods that successfully predicted the performance of the IRTS cooler on orbit. When operated from a 1.8-K heat sink it achieves a temperature of 287 mK at the evaporator with a 10 μW heat load, a hold time of at least 46 hours and a duty cycle efficiency of 96%. The energy input to the helium tank during recycling of the fridge is about 700 Joules. The ^{3}He cooler is a potential single point failure for the instrument. Its reliability and redundancy are under analysis, and an option with double parallel heat switches is being considered. Figure 2-10 is a photograph of a development model cooler which is similar to the SPIRE design.

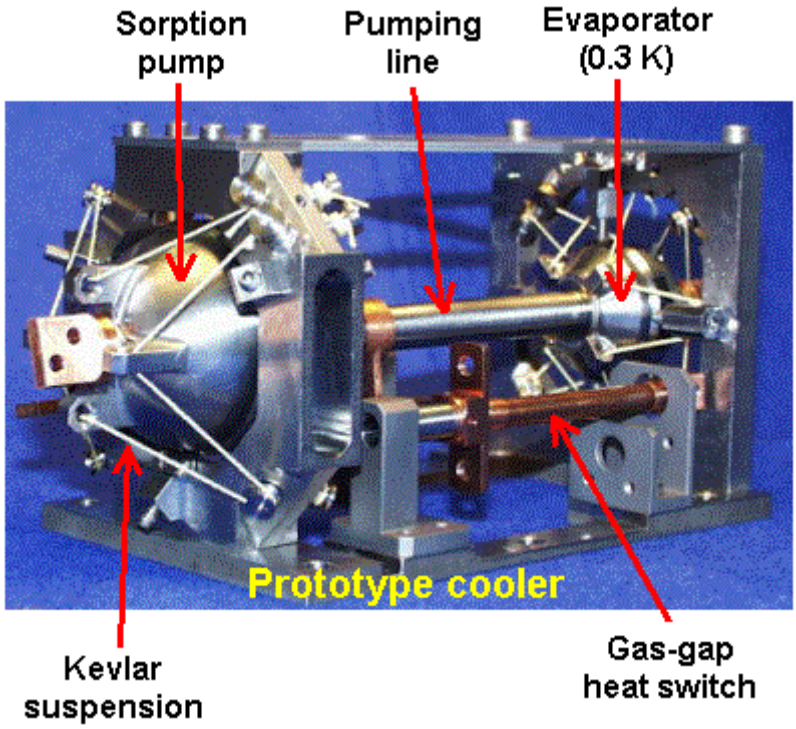

Figure 2-10 Prototype ^{3}He cooler

3. INSTRUMENT SYSTEM DESIGN

In this section the SPIRE instrument is described in terms of its systems level implementation. First an overview is given of the SPIRE instrument subsystem implementation, then the instrument is described as a number interacting systems. Finally a more detailed description is given of the systems design approach taken in the critical areas of structural design; optical design; thermal design; electrical design and EMI protection.

3.1 SPIRE subsystems

The SPIRE instrument can be divided into two separate sections, the cryogenic subsystems located on the Herschel Optical Bench (HOB) inside the Cryostat Vacuum Vessel (CVV) and the Warm Electronics (WE) which are located outside the CVV on the Herschel Service Module SVM below the CVV. A schematic diagram of the SPIRE subsystems inside the CVV is shown in Figure 3-1. The following features are illustrated in this Figure.

- The Herschel Optical Bench (HOB) upon which SPIRE, PACS and HIFI are mounted is shown with black hatching.
- The thermal straps between the various stages of the cryostat, cryocooler and the detector boxes are shown as blue hatching
- The Photometer and spectrometer Detector Boxes which are kept at 2 K are shown are indicated by blue crosses.
- The 4-K FPU is indicated by green crosshatching. This unit is sealed to prevent the ingress of against EM radiation and/or stray light. .
- Internal stay light baffles are indicated by black hatching.
- Indicative harness routing is shown by magenta.
- The light rays from the telescope is shown by red lines.

The only interface between the SPIRE subsystems inside the CVV and the WE on the SVM is via the 13 bulkhead connectors (and associated harnesses) shown at the top of Figure 3-1. The SPIRE harnesses that connect to the outside of the CVV connect to the WE on the left hand side of Figure 3-2. This schematic shows the Detector Readout and Control Unit (DRCU), which consists of two sub-units; the Focal-Plane Control Unit (FCU) and the Digital Control Unit (DCU), together with the electrical interfaces to the Herschel spacecraft.

Figure 3-3 shows a view of the FPU on the Herschel Optical Bench. Figure 3-4 and Figure 3-5 show views of the photometer and the spectrometer with the physical locations of the various subsystems. Table 3-1 lists and describes the sub-systems and gives the unit names used in the IID-B. A detailed description of the design of all the SPIRE subsystems is given in §4.

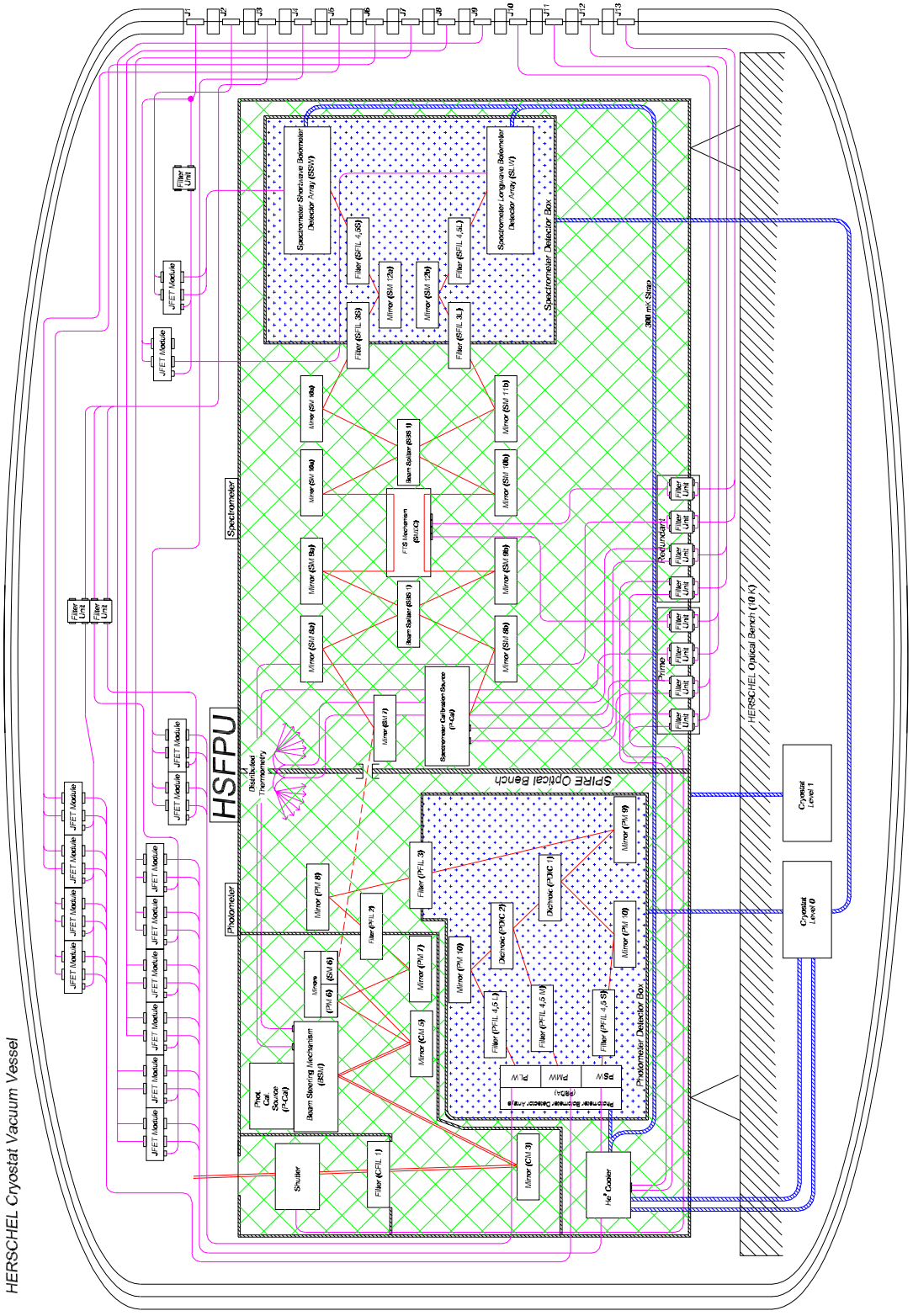

Figure 3-1 Schematic diagram of the sub systems of SPIRE contained within the Herschel CVV.

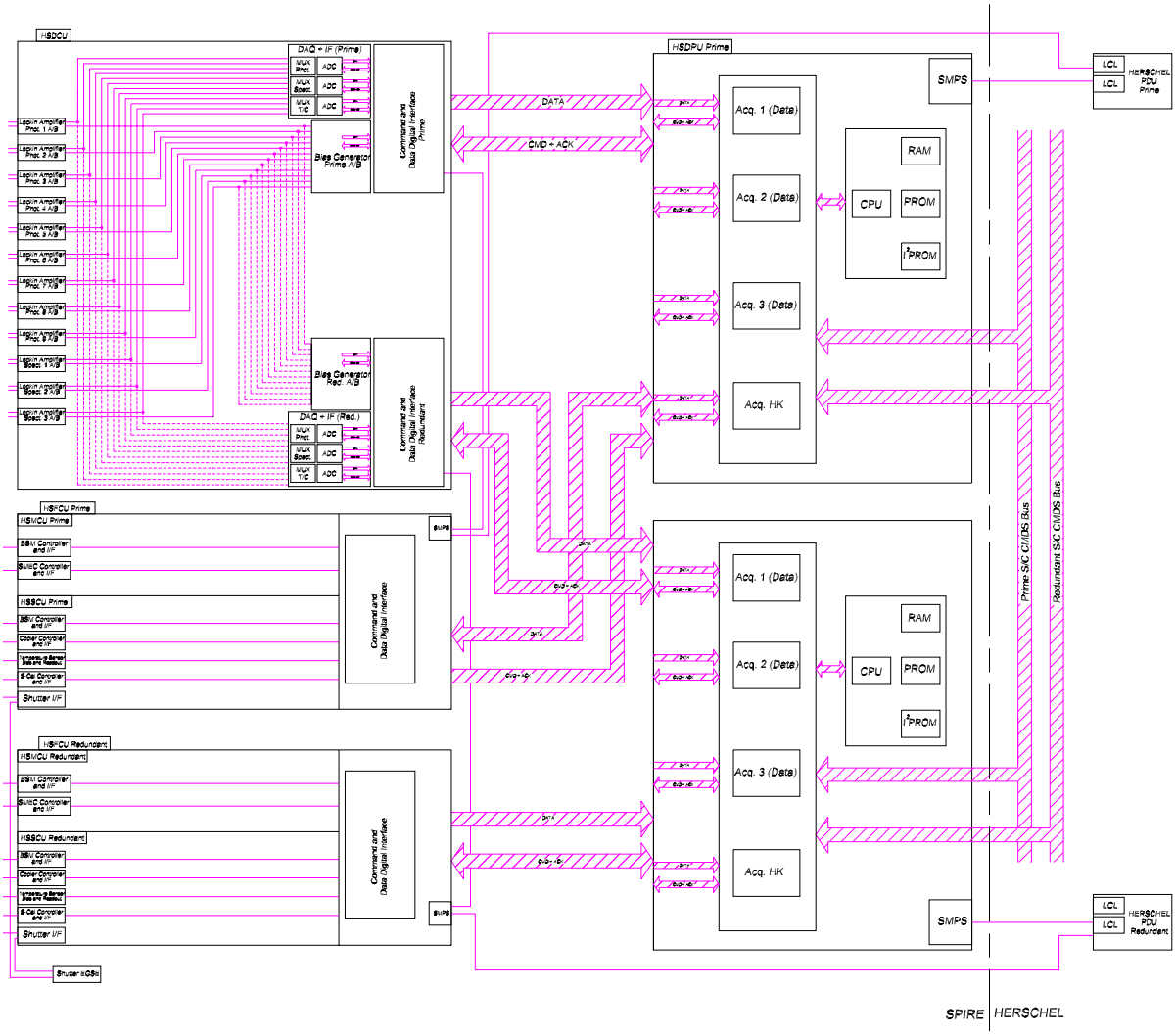

Figure 3-2 Schematic diagram of the sub-systems of SPIRE contained on the Herschel SVM.

The only interface between the SPIRE subsystems inside the CVV and the WE on the SVM is via the 13 bulk head connectors (and associated harnesses) shown at the top of Figure 3-1. The SPIRE harnesses that connect to the outside of the CVV connect to the WE on the left hand side of Figure 3-2. This schematic shows the Detector Readout and Control Unit (DRCU), the Focal-Plane Control Unit (FCU), the Digital Control Unit (DCU) and the electrical interfaces with the Herschel spacecraft.

Figure 3-3 shows a view of the FPU on the Herschel Optical Bench. Figure 3-4 and Figure 3-5 show views of the photometer and the spectrometer with the various subsystems. A detailed description of the design of all the systems of SPIRE is given in §4.

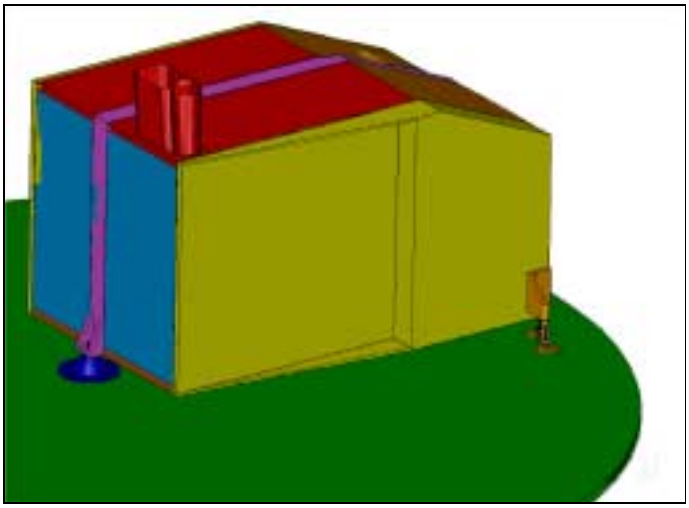

Figure 3-3 External view of the SPIRE FPU on the Herschel Optical Bench c/w with photometer and spectrometer beam envelopes.

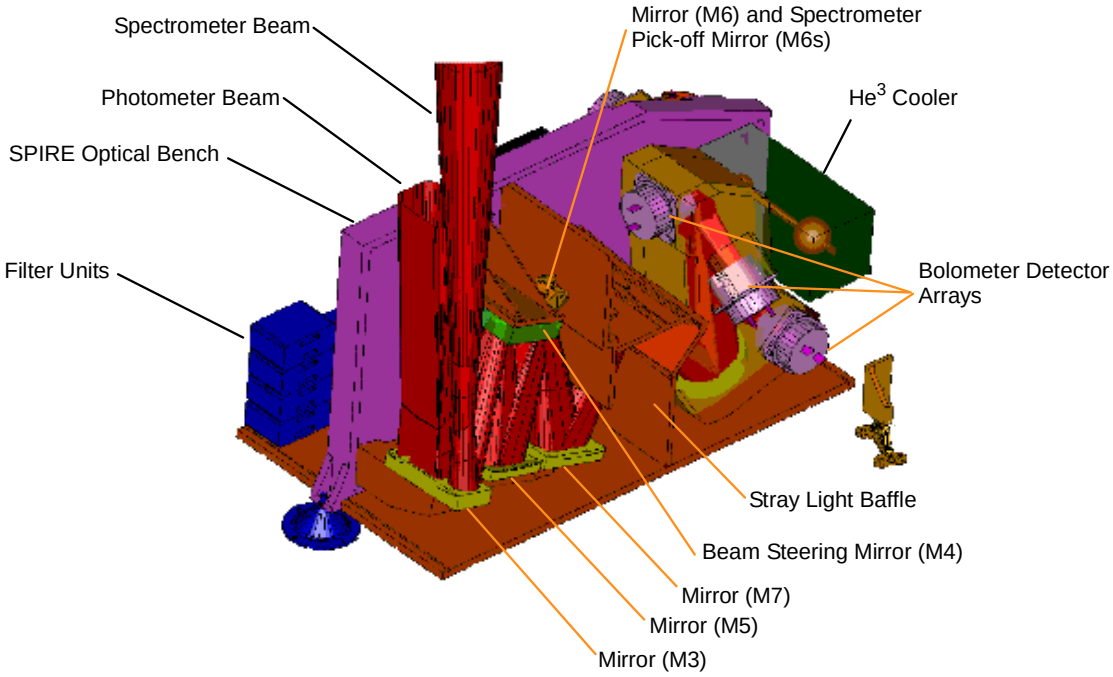

Figure 3-4 View of photometer side of the instrument with the FPU outer cover removed.

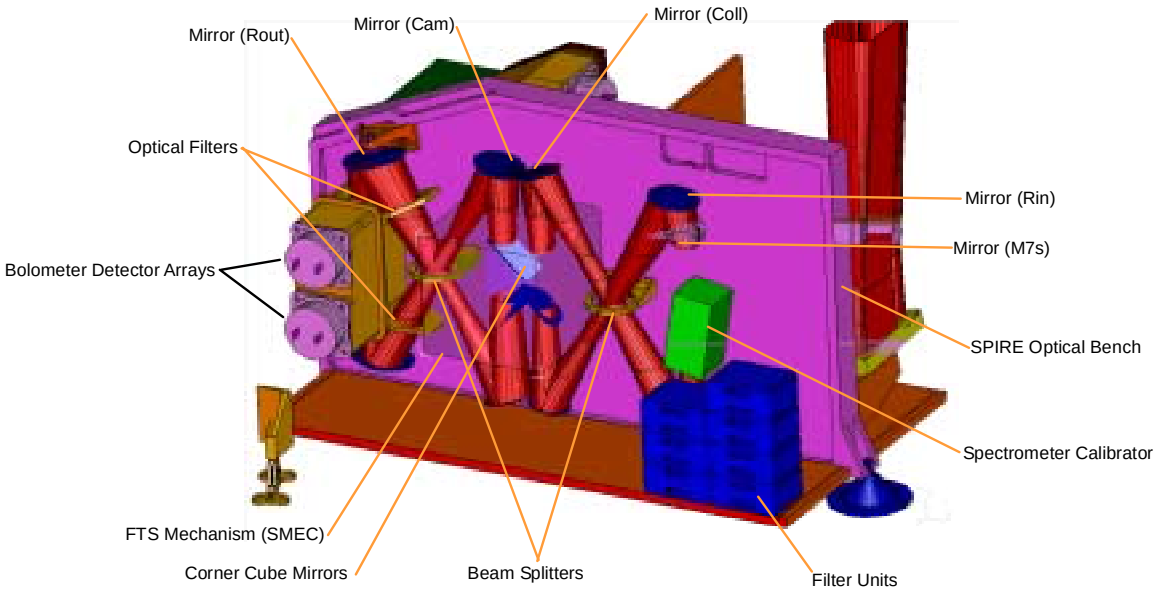

Figure 3-5 View of the spectrometer side of the FPU with the outer cover removed.

A complete list of the description of the design of all the sub systems of SPIRE is given in §4.

Table 3-1 - List of the SPIRE sub-systems.

Subsystem Name	**Description**	**Unit**	**Redundancy**
Structure	Focal plane unit structure to hold all cold sub-systems in the focal unit. This includes all thermometers necessary to monitor the instrument during cool down and operation.	HSFPU	No redundancy
Optics	All mirrors for the photometer and spectrometer channels	HSFPU	No redundancy
Filters	All filters; beam splitters and dichroics for the photometer and spectrometer channels The requirements on these are included with those for the optics.	HSFPU	No redundancy
Baffles	Straylight control baffles for the photometer and spectrometer channels	HSFPU	No redundancy
Cooler	^{3}He cooler unit cools the photometer and spectrometer detector arrays to 300 mK	HSFPU	No redundancy on hardware, full redundancy on control system and harnessing
Bolometer Detector Arrays (BDAs)	Bolometer array modules for the photometer and spectrometer	HSFPU	No redundancy. Loss of a single bolometer element is a soft failure mechanism but several hard failure mechanisms exist

Subsystem Name	Description	Unit	Redundancy
Beam Steering Mechanism (BSM)	This mechanism allows the photometer and spectrometer fields of view to be stepped or chopped across the sky.	HSFPU	No redundancy in the structure, mirror or flexure pivots. Redundancy in instrumentation, actuation and harnessing.
FTS Mechanism (SMECm)	The FTS moving mirrors drive mechanism and position measurement system. SMECm designates the mechanism and position encoder	HSFPU	No redundancy in the structure, mirror or flexure pivots. Redundancy in instrumentation, actuation and harnessing.
FTS encoder amplifier (SMECp)	SMECp the cold pre-amplifier for the position encoder detectors.	HSFPU	Fully redundant
Shutter Mechanism	A shutter is required in the instrument for ground test to allow the detectors to see the correct radiation environment.	HSFPU	No redundancy as not a flight item.
Photometer Calibration Source	Calibration source for photometer	HSFPU	No redundancy on light guide and reference source. Full redundancy on electronics and harnesses.
Spectrometer Calibration Source (SCAL)	Calibration source for the spectrometer	HSFPU	Redundancy on reference source heater and thermometer. Full redundancy on electronics, heater and harnesses.
RF Filter Modules	Each sub-system harness into the cold FPU must have an electrical RF filter to prevent EMI problems with the bolometers. These will be mounted in standard RF filter modules on the wall of the FPU box.	HSFPU	Fully redundant
Photometer JFET Box	JFET pre-amplifiers for photometer NTD germanium bolometers.	HSFTBp	No redundancy. Failure of single JFET amplifier is a soft failure mechanism
Spectrometer JFET Box	JFET pre-amplifiers for spectrometer NTD germanium bolometers.	HSFTBs	No redundancy. Loss of a single JFET amplifier is a soft failure mechanism
Detector Read-out & Control Unit (DRCU)	Detector amplifier and digitisation chain and instrument control electronics. Conceptually this is a single unit however for accomodation reasons it will be split into two phyiscal units	HSDRC	See below
FPU Control Unit (FCU)	Contains the electronics for the power conversion and distribution to the DRCU; for the control and read-out of the thermometers; cooler; calibration sources and the cold mechanisms	HSFCU	Full redundancy

Subsystem Name	Description	Unit	Redundancy
Detector Control Unit (DCU)	Contains the bias conditioning electronics for the bolometers arrays and JFET units and the lock in amplifiers and readout electronics for all the detector arrays.	HSDCU	No redundancy on the Lock-in Amplifiers. Full redundancy on DAQ. Full redundancy on Bias Generators
Digital Processing Unit (DPU)	Instrument on board computer – forms interface to CDMS	HSDPU	Full redundancy
Warm Interconnect Harness	Harnesses between warm boxes	HSWIH	Full redundancy
On Board Software (OBS)	All on board software that controls the function of the instrument. This is all contained in the DPU	HSOBS	N.A.
FPU Simulator	A set of electronic components, either passive or active, that mimics the analogue response of the FPU sub-systems to the warm electronics.	HSFPS	No redundancy as not a flight item
DRCU Simulator	A set of interface hardware and computer software that mimics the response of the DRCU and FPU to the DPU and on board software.	HSDRS	No redundancy as not a flight item

3.2 The SPIRE instrument as a system

SPIRE can be viewed not just as a series of physical sub-systems but also as a series of interacting systems. Figure 3-6 is a system topology of the SPIRE instrument that attempts to divide it into a number of systems areas with over lapping areas of interest. Table 3-2 expands on Figure 3-6 and gives details of what each system area represents; the issues to be addressed under each system area; the physical components that can be associated with each system and what methods of analysis and verification we intend using to ensure that each area is properly considered in the implementation of the instrument

Although Figure 3-6 and Table 3-2 are a very much-simplified view of the systems interactions in the instrument, they do serve to illustrate some important points about the system level design of SPIRE:

The Radiation Detection System – going from the cold detector arrays through to the digitised signals from the DRCU, is at the very heart of the instrument. All systems issues ultimately come back to ensuring that the detection system can operate correctly and without undue interference.

The Electrical System and Structure System can be seen as the “glue” that bonds the instrument together into a single unit.

The EMC/EMI Protection System touches on virtually every aspect of the instrument design. The issues raised by consideration of the EMC/EMI must always be taken into account in design and implementation of virtually every physical sub-system in the instrument

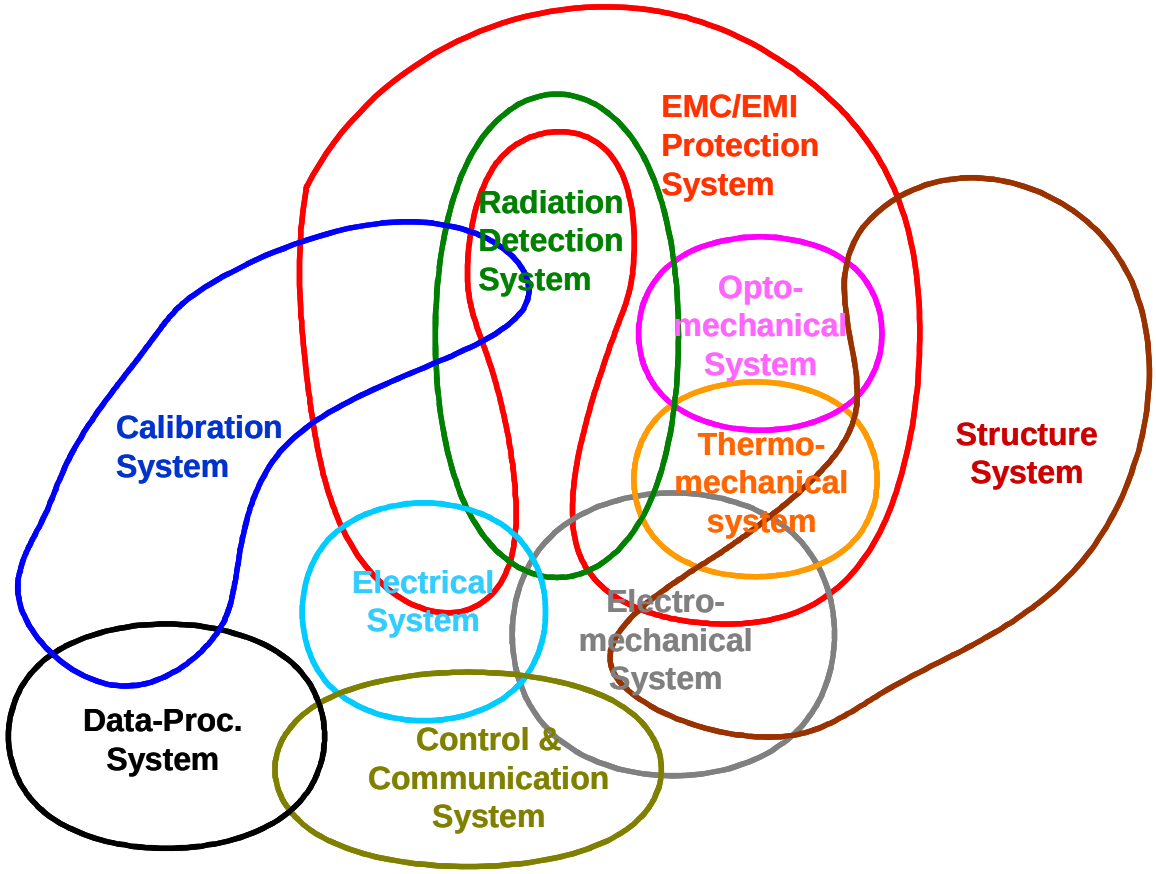

Figure 3-6 – Simplified view of the SPIRE instrument as broken into "systems."

Table 3-2 - Description of the SPIRE systems

System	Description/Issues	Sub-systems	Design analysis Tools	Design verification methods
Structural	To ensure that the SPIRE instrument is mechanically compatible with the Herschel system and capable of withstanding the launch environment Mechanical frequency response Ability to withstand launch environment Mechanical interface with Herschel system Instrument level integration Sub-system mechanical interfaces	Primarily instrument Structure and JFET enclosures Interfaces to all cold FPU sub-systems	CAD FEM	Prototype material testing STM/CQM instrument model vibration tests CQM system level integration

System	Description/Issues	Sub-systems	Design analysis Tools	Design verification methods
Opto-mechanical	To ensure that only the legitimate optical radiation reaches the radiation detection system and does so in a manner that fulfils the instrument requirements Optical design Optical interface to Herschel system Straylight Instrument optical performance Integration and alignment Sub-system optical interfaces	Structure Optics Filters Calibration Sources Detector Arrays Baffles SMEC BSM	Synopsis ASAP APART Feedhorn model (Gaussian Mode analysis; HFSS)	Component testing (filters etc) Optical alignment Instrument level tests
Thermo-mechanical	To ensure that the different parts of the instrument run at the correct temperature and that the instrument functions at the correct temperature according to requirements for all defined instrument operating and environmental conditions Thermal performance under all operating conditions Thermal interface to Herschel system Sub-system thermal interfaces Sub-system thermal control	Structure Cooler Thermometry Temperature Control JFET Amplifiers JFET Enclosure Filters Thermal straps SCU	ESATAN model Other computer models	Prototype sub-system tests (cooler; cooler plus strap etc) STM/CQM sub-system cold tests Instrument level STM cold tests Instrument level CQM cold tests System level CQM cold tests
Electro-mechanical	To ensure that the moving parts of the instrument meet the instrument requirements; do not unduly influence the operation of other parts of the instrument and that the instrument can operate according to requirements in the micro-vibration environment expected in the Herschel satellite Micro-vibration environment Mechanism control Harness mechanical frequency response and routing	FPU Harnesses Detector arrays SMEC BSM Shutter JFET Amplifiers Cryostat cold harness Cryostat warm harness MCU Shutter electronics	Dynamical analysis model (DSPACE?) at sub-system level only	Prototype sub-system tests Instrument level STM cold tests Instrument level CQM cold tests System level CQM cold tests

System	Description/Issues	Sub-systems	Design analysis Tools	Design verification methods
Radiation Detection	To ensure that the radiation transmitted by the opto-mechanical system is efficiently detected and converted into digital signals without excess noise or contamination from other electrical signals. Detector performance versus environment (temperature; photon background; micro-vibration; EMC) JFET Amplifier performance versus environment (*ditto)* Harness performance Detector sub-system interface compatibility – thermal; electrical; mechanical End-to-end system performance	Detector Arrays Thermal Straps Temperature Control Cooler FPU Harnesses RF Filters JFET Amplifiers Cryostat cold harness Cryostat warm Harness DCU	Mathcad Models System analysis	Prototype cold units in representative environment with representative electronics STM sub-system cold units for thermal and environmental test CQM sub-system end to end test CQM instrument level end to end test CQM system level end to end test
EMI/EMC protoection	To ensure that no radiofrequency EM radiation enters the radiation detection system from any source within the Herschel system. Also that the SPIRE instrument does not emit any radiofrequency EM radiation that might influence the operation of any part of the Herschel system EMC susceptibility and emission – radiated/conducted Electrical grounding Faraday cage integrity and performance RF filter performance Harness performance Power supply cleanliness Digital/analogue separation	Structure FPU Harness RF Filters JFET Box (FSFTB) Cryostat cold harness Cryostat warm harness DRCU (FSDRC)	Systems Analysis SPICE model	EM and QM electronics units as sub-system with simulator and EMC tested CQM instrument level testing CQM system level testing
Electrical	To ensure that the SPIRE instrument is electrically compatible with the Herschel system and that the different parts of the instrument are mutually electrically consistent with each other Electrical interface to Herschel system Power supply distribution and control Sub-system electrical interfaces Wiring tables Analogue to digital interfaces Digital to digital interfaces	DRCU (FSDRC) SPIRE Warm harness (FSWIH) DPU (FSDPU) S/C PDU S/C Warm harness DRCU Simulator FPU Simulator	Systems analysis	EM and QM electronics units tested as sub-system with simulator(s) CQM Instrument level testing AVM and CQM system level testing

System	Description/Issues	Sub-systems	Design analysis Tools	Design verification methods
Instrument control and communication	To ensure that the SPIRE instrument communicates with the Herschel system; that the different parts of the SPIRE instrument are mutually consistent with the operations concept and that the instrument operates safely and to requirements in all operational modes Data interface to Herschel system Operating mode definition Instrument commanding definition On board software definition Sub-system operational and control interfaces Sub-system data interfaces	DRCU (FSDRC) SPIRE warm harness (FSWIH) DPU (FSDPU) S/C CDMS FPU Simulator DRCU Simulator	Systems analysis Software simulators	EM and QM electronics units tested as sub-system with simulator(s) CQM Instrument level testing AVM and CQM system level testing
Instrument data processing	To ensure that the data produced by the SPIRE instrument are compatible with the requirements of the Herschel system and are processed into the required data products Interfaces to the ICC Data product definition Data processing definition Sub-system data processing interfaces Observing mode data processing interfaces	DPU (FSDPU) DRCU Simulator FPU Simulator ICC	Systems analysis Software simulators	Data sets produced by simulators EM and QM electronics units tested as sub-system with simulator(s) produces data sets Instrument level CQM tests for observation verification and producing data sets System level AVM and CQM tests for end to end verification

System	Description/Issues	Sub-systems	Design analysis Tools	Design verification methods
Calibration	To ensure that the data produced by the instrument can be converted into meaningful physical units to allow the correct operation of the instrument in all modes and the processing of the instrument data into the required data products Observing mode calibration definition Ground commissioning and calibration plan Flight commissioning and calibration plan Instrument to ground facility interfaces Ground facility definition Ground based observing programme definition	Photometer Calibrator Spectrometer Calibrator DPU (FSDPU) ICC	Systems analysis Instrument performanc e models	Prototype sub-system tests CQM instrument level performance verification Ground based observing programme

3.3 Structural design and FPU integration

We have already discussed the need to have various temperature zones with the SPIRE FPU. This, combined with the need for two essentially separate instruments in the SPIRE instrument, has dictated the design approach to be taken for the SPIRE structural design. Figure 3-7 shows the conceptual design of the FPU structure. A single stiff optical bench is used to mount all the subsystems and optical components, including two detector boxes that are thermally isolated from the optical bench on stiff space frames. On one side of the bench the components for the common entrance optics and the photometer channel are mounted, and on the other the components for the spectrometer channel. Each side of the optical bench has a cover that forms a structural “monocoque” element in the design. The integrated instrument box is mounted from the Herschel optical bench via three thermally isolating supports. One of these is directly mounted from the SPIRE optical bench and forms a fixed reference point, the other two are mounted from the two covers and are bipods with flexibility in one direction to allow for any differential thermal contraction during system cool down.

The FPU covers also form both a straylight shield to protect the instrument from the ambient thermal radiation environment in the Herschel cryostat and an RF shield to protect the detectors from any radiated EMI. All sub-system wiring entering the instrument box must pass through passive RF filters mounted in boxes from the SPIRE Optical Bench on the spectrometer side. When the cover is integrated with the optical bench the RF filter boxes will be sealed to the cover. The exception to this are the harnesses for the detectors themselves that connect the bolometer arrays to the externally mounted JFET units. These are filtered within the JFET units and then pass to the instrument box via a drilled plate hard mounted to the SPIRE Optical Bench. The wiring harnesses therefore form part of the RF shield therefore and careful attention must be paid their electrical shielding.

In addition to sealing the instrument box against RF, it must also be sealed against the possibility of stray optical radiation entering via routs other than the legitimate path defined by the telescope and SPIRE optical elements. To this end the thermal straps that must broach the covers to connect the sorption cooler and the detector boxes directly to the Herschel helium tank at 1.7 K must pass through light baffles.

The outline integration sequence for the SPIRE instrument FPU is as follows (see the *SPIRE AIV Plan* for more details):

(i) the 300-mK thermal bus bars (see section on thermal design below) are fitted into the detector boxes;
(ii) the optical elements that go into the detector boxes are fitted and their alignment verified (see Figure 3-1 for which elements are fitted into the boxes);
(iii) the detectors are fitted in to the detector boxes and connected to the 300-mK busbar;
(iv) the "baseplates" of the detector boxes and the detector harnesses are fitted to the optical bench panel;
(v) the mirror and filter mounts are fitted to the optical bench panel;
(vi) the positions of the interfaces between the mounts and the optical elements are verified by 3-D mechanical metrology (see section on optical alignment below);
(vii) the optical elements are fitted and the detector boxes are fitted to their baseplates;
(viii) the rest of the subsystems that mount to the optical bench are fitted together with their harnesses;
(ix) the covers are placed onto the optical bench panel;
(x) the instrument FPU can be fitted to the Herschel optical bench (or the test cryostat cold plate);
(xi) the JFET units are fitted to the Herschel optical bench (or cryostat cold plate) and the harnesses from the detectors connected.

Because the instrument FPU does not stand alone before the covers are fitted some MGSE is envisaged that will hold the optical bench panel and allow access to all sides during integration.

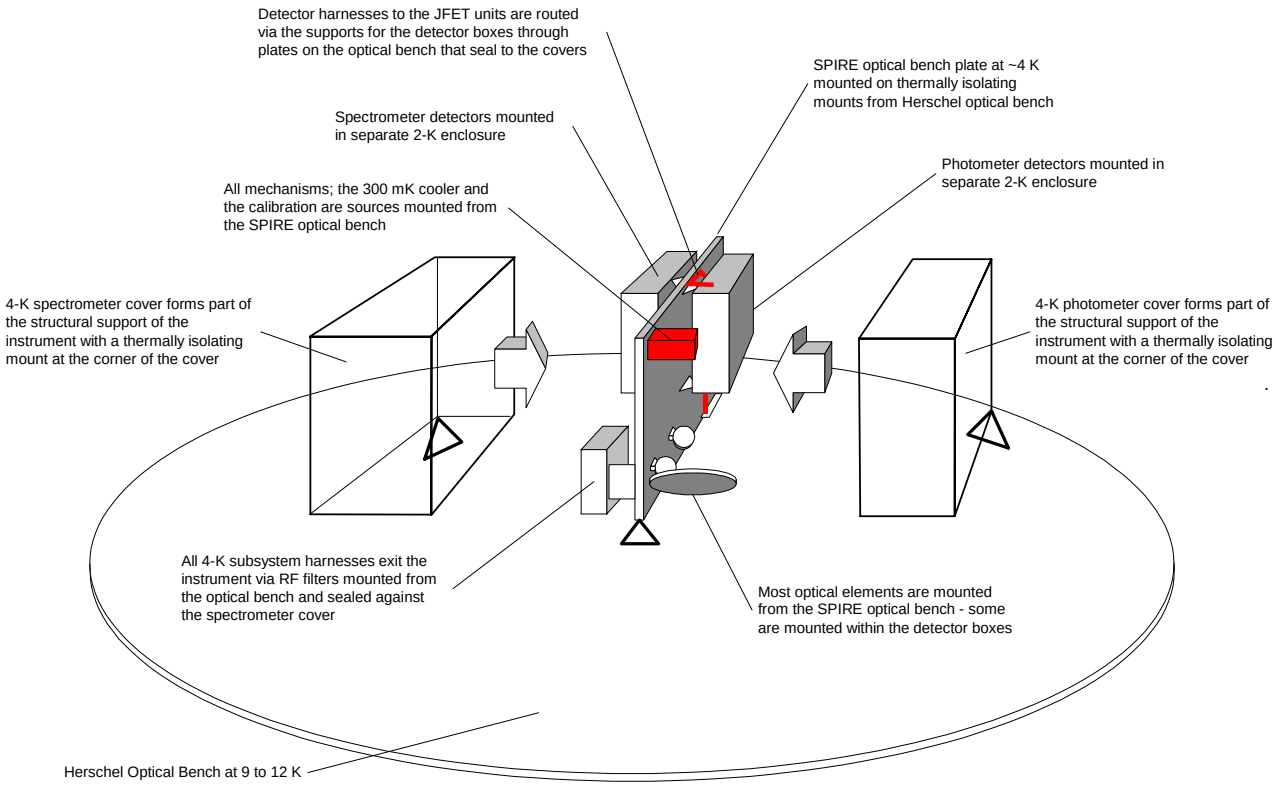

Figure 3-7 - Conceptual design of the SPIRE instrument structure. Once the 4-K covers are integrated the instrument box forms a straylight and RF shield

3.4 Optical Design

3.4.1 Common optics and photometer optics

The 3.5 m Herschel telescope will be either a Cassegrain or Richey- Chrétien system. In either case it will provide a well-corrected image at a focal ratio of f/8.68 (IID-A). The low focal ratio of the primary mirror (f/0.5) causes the telescope focal surface to be highly curved. SPIRE uses an off-axis part of the telescope FOV and its object surface is therefore tilted with respect to the central (gut) ray (c.f. Table 3-3). Figure 3-8 shows a scaled drawing of the telescope and SPIRE photometer.

Table 3-3 - Alignment of the SPIRE photometer and spectrometer gut rays w.r.t. the Herschel bore sight.

	x-y plane	**x-z plane**
Photometer	0º 0’ 0”	0º 10’ 59”
Spectrometer	0º 7’ 23”	0º 10’ 59”

At an early stage in the design process several decisions were taken on the system design of the instrument that were to be design drivers for the optical design:

i. the spectrometer and photometer are to have separate fields of view on the sky and no beam switching mechanism is to be used;
ii. the largest field of view available to SPIRE should be used for the photometer channel – this is 4x 8 arcmin rectangular;
iii. whatever is left should be available for the spectrometer – this is 2.6 arcmin circular;
iv. an ability to steer the beam around the sky to allow chopping and spatial sub-sampling is required;
v. the beam steering mechanism is to be available for both the photometer and spectrometer channels – i.e. it is to be placed ahead of any division of the fields into the separate instrument channels;
vi. the secondary of the telescope is to be used as the final exit pupil of the instrument and a cold aperture stop close to the detectors is required;
vii. no compromise is made in the photometer optical design to accommodate the spectrometer channel;
viii. imaging in the Spectrometer is not a key requirement; the primary science driver is for point sources viewed on axis.

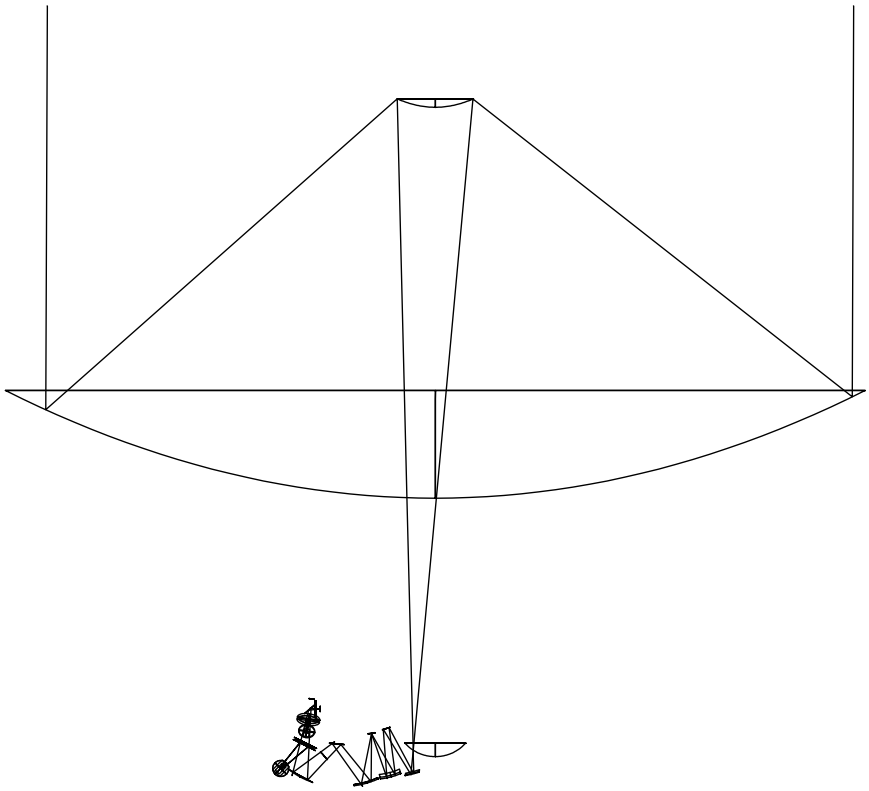

Figure 3-8 Ray diagram of the Herschel telescope with the SPIRE optics to the same scale. The primary mirror has a diameter of 3.5 m and the SPIRE FPU is about 500 mm wide.

The SPIRE optics are therefore divided into a common portion followed by the photometer and spectrometer optical chains. The common optics form an image of the secondary at the location of the beam steering mirror and provide a well corrected intermediate focus to allow the separation of the spectrometer and photometer beams into different parts of the instrument box

In addition the combination of the common optics and the rest of the photometer optical train has to provide:

(i) a well-corrected, flat focal surface, perpendicular to the gut ray, at f/5 at the proposed location of the detector arrays – i.e. correction for the highly tilted focal plane of the telescope;

(ii) sufficient back-focal length (BFL) to allow separation of the photometer beam into three spectral bands using dichroics;

(iii) a non-aberrated image of the telescope secondary at a physical location as close to the photometer detectors as possible and physically accessible to allow a real stop to be placed there.

All these functions are assured by the SPIRE common and photometer optical design as shown in Figure 3-9. CM3 is an off-axis ellipsoid projecting an image of the telescope secondary (CM2) onto CM4. This image is well-corrected and in focus at the centre of the CM4 so that the pupil image at the cold stop stays fixed during chopping and beam steering. CM4 is a flat mirror whose orientation is adjustable in flight to permit ±2 arcminutes chopping in the sagittal plane, allowing off-field chopping for a 4 x 4 arcminute sub-field, and ±30 arcminutes beam steering motion in both the tangential and sagittal planes to obtain fully Nyquist sampled images. The toric CM5 mirror reimages the focal plane onto PM6 and converts the focal ratio of the beam from f/8.68 to f/5. While CM3 and CM4 are common for both photometer and spectrometer, the two systems separate at PM6. The photometer PM6 is toric and sends the beam into an Offner-type relay system consisting of three spherical mirrors: PM7 (concave), PM8 (convex), and PM9 (concave). The tilt angles, separations and curvatures of these mirrors provide enough free variables to satisfy the need for well corrected flat image planes; a long back focal length and an image of the telescope secondary mirror close to the detectors. In particular, an easily accessible pupil image is provided between PM8 and PM9 in which the cold stop is located. The physical separation between the 4-K cavity and the 2-K cavity (detector box) into which the detectors are mounted, is made here so that the entrance to the cold

environment containing the detectors is as small as possible to restrict the possibility of straylight hitting the detector arrays.

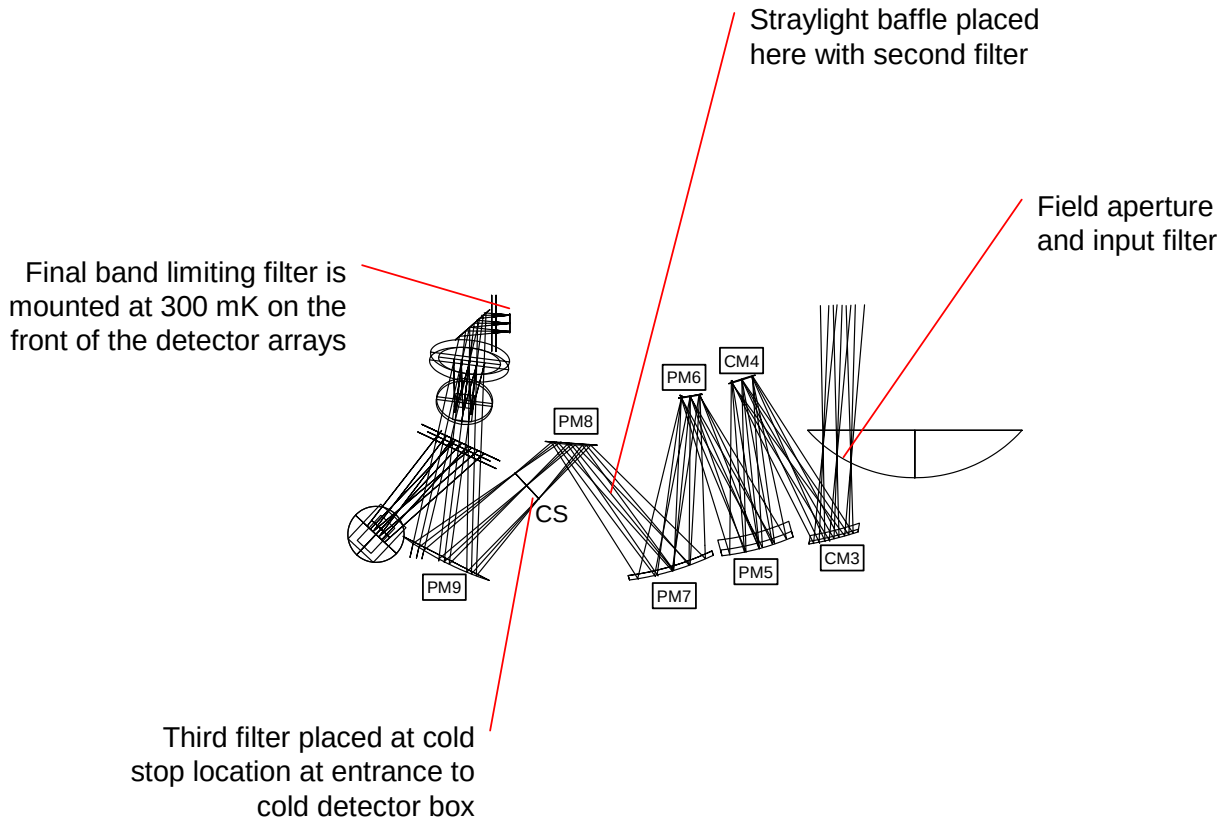

Figure 3-9 - Ray diagram of the SPIRE photometer showing the ray paths for three points in the tangential plane, centre and extremes of the FOV (±2 arc minutes). Also shown here are the locations of the straylight baffles and optical bandpass filters.

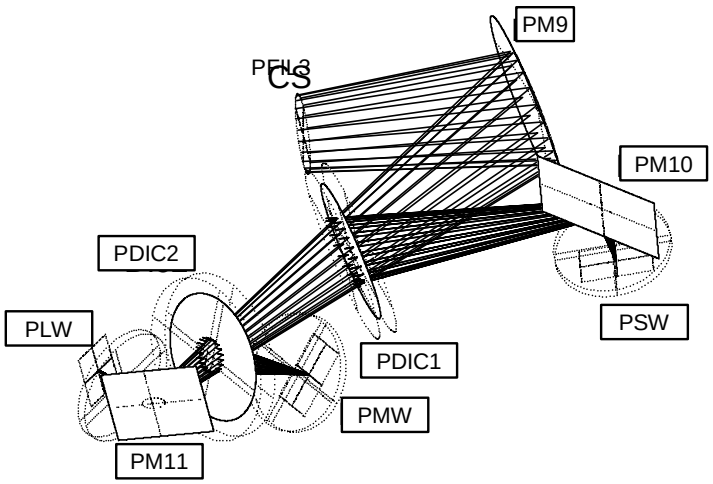

Figure 3-10 - The beam folding within the photometer detector box. The dichroics are low pass devices so PSW is the shortest wavelength array; PMW the medium wavelength array and PLW the long wavelength array.

The detector box contains PM9, the last powered mirror of the optical train, and dichroics and beam folding mirrors distributing the light between three detector arrays, covering the short (200-300 µm), medium (300-400 µm) and long (400-670 µm) wavelength bands. An edge filter at the cold stop minimizes stray radiation entering the cold box and band-pass filters in front of each detector array ensures the spectral limitation of each band. Figure 3-10 shows a 3-D view of the photometer detector box optics.

Figure 3-11 shows geometrical spot diagrams across the photometer FOV. The final focal surface is flat and perpendicular to the gut ray, and the exit pupil is close to telecentric. With a theoretical Strehl ratio better than 0.986 at 250 µm the system leaves headroom for manufacturing tolerances and the field distortion is below 1.1%.

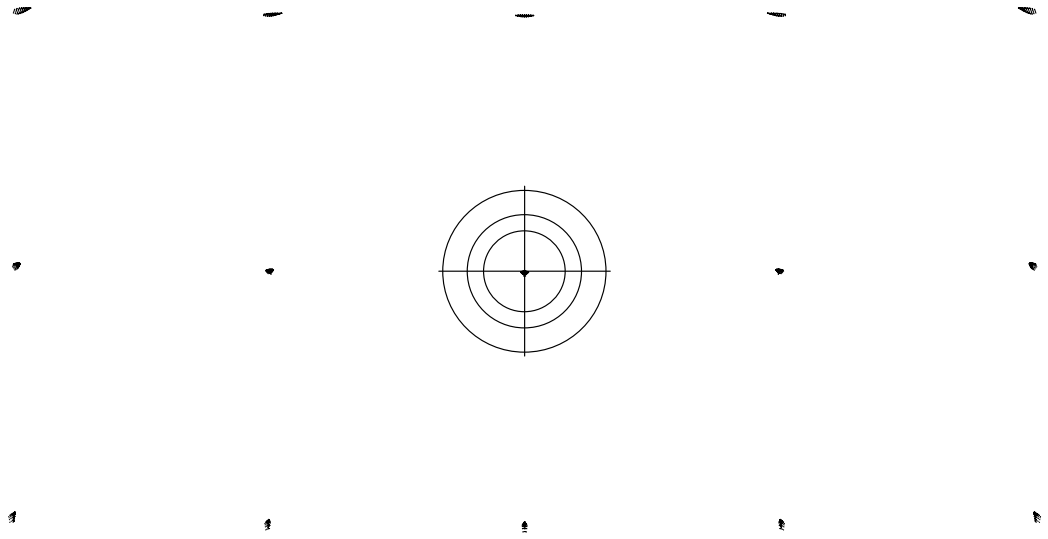

Figure 3-11 - Geometric spot diagrams across the 4′ x 8′ SPIRE photometer FOV. The spots are plotted in their actual positions and to scale. The concentric circles around the central spot have diameters 3.0, 4.3, and 6.1 mm and indicate the Airy disk size at 250, 350, and 500 µm, respectively. With a maximum RMS wavefront error of 4.7 µm, the theoretical Strehl ratio is better than 0.99 anywhere in the FOV at 250 µm. A slight distortion is observed, corresponding to 6′ or 1.1% of the FOV diagonal. The average focal ratio is f/4.9.

3.4.2 Spectrometer optical design

An imaging FTS has been chosen for SPIRE rather than a grating-based solutions because of its superior imaging capability, lower stray-light sensitivity, and variable spectral resolution. Among a large number of possible interferometer concepts, three were chosen for a final comparison, see Figure 3-12. In each case, two separate, band-limited detector arrays are required to divide the 200-670 µm band into two sub-bands: 200-300 µm, and 300-670 µm. Covering the entire spectrum with a single array would be too constraining with respect to spatial sampling and detection efficiency.

The Martin-Puplett interferometer (Figure 3-12a) offers a good and robust solution to this problem. Based on the use of three polarisers, components which can provide excellent efficiency over a broad band in the far infrared region, and roof-top mirrors, it provides two input and two output ports with a minimum of complexity. When the polarisers are properly oriented, the roof-top mirrors switch the polarisation of the beams so that 100% of the light incident upon P2 is transmitted towards the detectors. One polarisation of the incident light is lost at P1 however, reducing the optimal efficiency of this concept to 50%. P3 is required to analyse the interfering beams, sending complementary interferograms towards the two detectors. Usually, both detectors would see the entire band, hence detecting all the light incident onto P3, but in our case the spectrum would have to be divided into two by band-pass filtering each detector. This loses another 50%, reducing the theoretical efficiency to 25%.

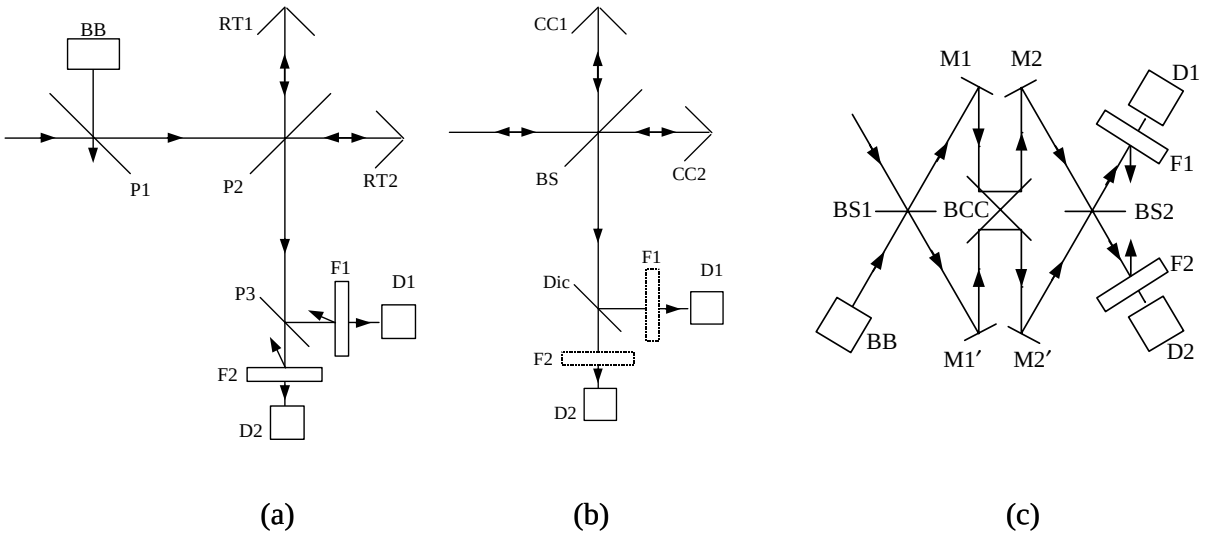

Figure 3-12 Three possible interferometer concepts for the SPIRE spectrometer: (a) Martin-Puplett polarising interferometer, (b) classical Michelson interferometer, and (c) Mach-Zehnder type dual beam interferometer. BB: blackbody source, RT: roof-top mirror, P: polariser, F: filter, D: detector, CC: corner-cube reflector (could also me mirrors or roof-tops), BS: beamsplitter, Dic: dichroic beam splitter, M: mirror, BCC: back-to-back corner cubes (or roof-tops).

As a second option, we considered a simple Michelson interferometer as shown in Figure 3-12b. This option was made possible thanks to a new development of 50/50 beamsplitters, (Ade *et. al*. 1999), providing greater than 90% efficiency (4RT) over the entire SPIRE band. No output polariser is required in this case and it can be replaced with a dichroic beam splitter, offering a theoretically loss-less channel separation. There is of course a 50% loss at the beamsplitter since half the incident radiation is sent back out through the telescope. This configuration is still twice as efficient as the previous one. Its main drawback is the lack of a second input port, required for balancing off the telescope background radiation.

The preferred solution is shown in Figure 3-12c. Rather more complex than the former options, it provides both a second input ports and a 50% theoretical efficiency. The concept is based on a Mach-Zehnder interferometer with its arms folded in order to avoid beam shearing during scanning of the optical path difference (OPD) and uses two 50/50 beamsplitters. If the detectors could be used over the entire spectral range, this concept would provide 100% efficiency, but the requirement for two separate bands imposes a 50% channel separation loss as in the Martin-Puplett case. The folding allows the optical path of both arms to be changed simultaneously with a single scanning mechanism, hence doubling the available resolving power for a given mirror-moving mechanism. A resolving power of 1000 at 250 µm, requiring a maximum OPD of 125 mm, is therefore obtained with a lopsided movement from -3 mm to +31 mm. The lowest resolving power, R = 20, is achieved using a double sided scanning of ±0.6 mm.

One of the difficulties encountered in the optical design of the interferometer concept of Figure 3-12c was the long distance between separation (at BS1) and recombination (at BS2) of the beams. Due to the FOV dependent beam spread, the size of the beam splitters and collimating and camera optics became prohibitive. Also, it was difficult to find space for the scanning mechanism. To improve the situation it was decided to move collimator and camera optics to within the interferometer by making the four mirrors M1, M2, M1′, and M2′ of Figure 3-12c powered. This is not without disadvantages, since at non-zero OPD, the two arms do not see the same optical system. A differential aberration analysis is therefore necessary. Keeping to a strict scheme of symmetry ensures minimal aberrations in the system, and the only residual aberration of some concern is differential distortion giving a lateral separation between the images of a point source at the

edge of the FOV. The induced contrast reduction is not negligible but small compared with other sources, notably alignment tolerances.

Figure 3-13 shows the ray diagram of the upper half of the spectrometer. The lower half has the same optical design. After reflection from the common mirrors CM3, CM4, and CM5, the spectrometer beam is picked off by the toric SM6 and sent out of the plane of the photometer system. The flat SM7 redirects it into a parallel plane, separated by 170 mm from the photometer plane. The input relay mirror (SM8) focuses the beam to an intermediate image plane located just after the first beam splitter, after which the beam is collimated (SM9) and sent vertically towards the corner cube assembly. The corner cube, modelled by non-sequential raytracing, shifts the beam and sends it up towards the camera mirror (SM10). Symmetrical with the collimator, the camera focuses the beam to an image plane just before the output beam splitter. The output relay mirror (SM11) focuses the beam onto the detector arrays. To accommodate the components within the available volume, a fold mirror is needed to take the beam out of the plane again. The input and output relays are toric in order to control astigmatism and image anamorphism. A slight asymmetry in the input and output relays is introduced in order to adjust the final focal ratio. The collimator and camera mirrors are spherical.

A pupil image is located near the final fold mirror, making this a convenient place for the entrance hole in the 2-K enclosure. This pupil moves as the OPD changes, however, so it is not appropriate for a limiting cold stop. Instead, a limiting aperture is placed in another pupil image at 4 K located between SM6 and SM7.

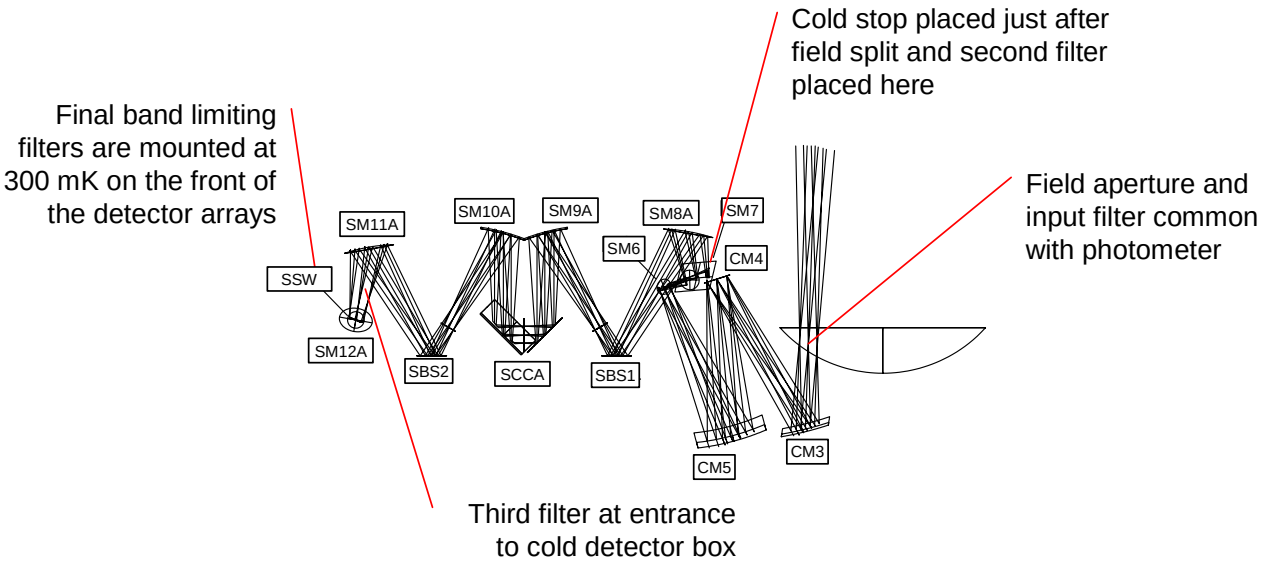

Figure 3-13 Raytracing diagram of the upper half of the SPIRE spectrometer. The symmetrical lower half is generated by reflection about the plane containing the two beam splitters. The location of the cold stop and the bandpass filters are also indicated.

Figure 3-14 shows spot diagrams for the spectrometer. Clearly the imaging performance is not quite as good as that of the photometer, the spots reflect the image quality in the intermediate focal plane at SM6. Since the planar symmetry is lost, it is very difficult to improve on this. However, the astigmatism has been brought to zero at the centre of the FOV and a good balance of aberrations over the rest of the FOV has been achieved by introducing a 3.8° rotation of the output relay mirror around its normal. The worst RMS wavefront error is 6.6 microns, giving a Strehl ratio at 250µm of 0.97. Apart from a slight rotation, the image suffers from a distortion of up to 9″, corresponding to 6% of the FOV diameter.

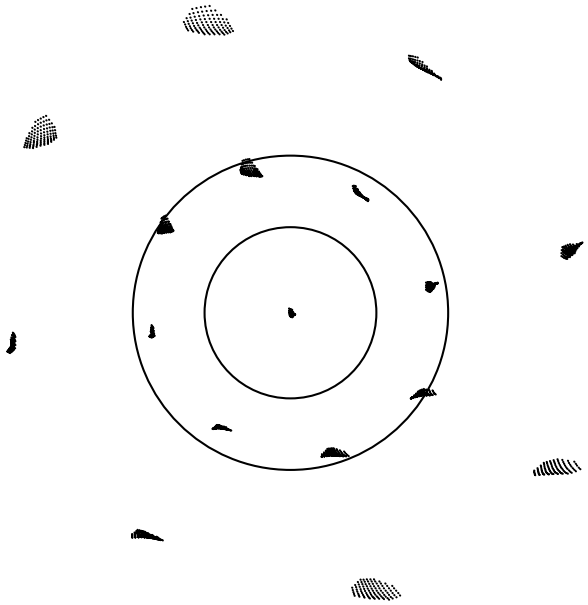

Figure 3-14 - Geometric spot diagrams at the centre, half field, and full field of the 2.6′ diameter spectrometer FOV. The spots are plotted in their actual positions and to scale. The concentric circles around the central spot have diameters 3.7 and 6.7 mm indicating the Airy disk size at 300 and 550 µm, respectively. With a maximum RMS wavefront error of 6.6 µm, the theoretical Strehl ratio is better than 0.97 anywhere in the FOV at 250 µm. Distortion corresponding to 9″ or 6% of the FOV diameter is observed. The average focal ratio is f/4.9.

One feature of the optical design of the spectrometer is that the final re-imaging optics are non-telecentric – that is the beams at different parts of the field of view are not parallel (or nearly so), unlike in the photometer design. This feature is forced by the lack of physical space available to the instrument. Whilst with most detection systems this would not make very much impact, with the feedhorn arrays this causes some loss of signal as the detector “beams” only illuminate a portion of the pupil for off-axis detectors. Figure 3-15 illustrates the situation.

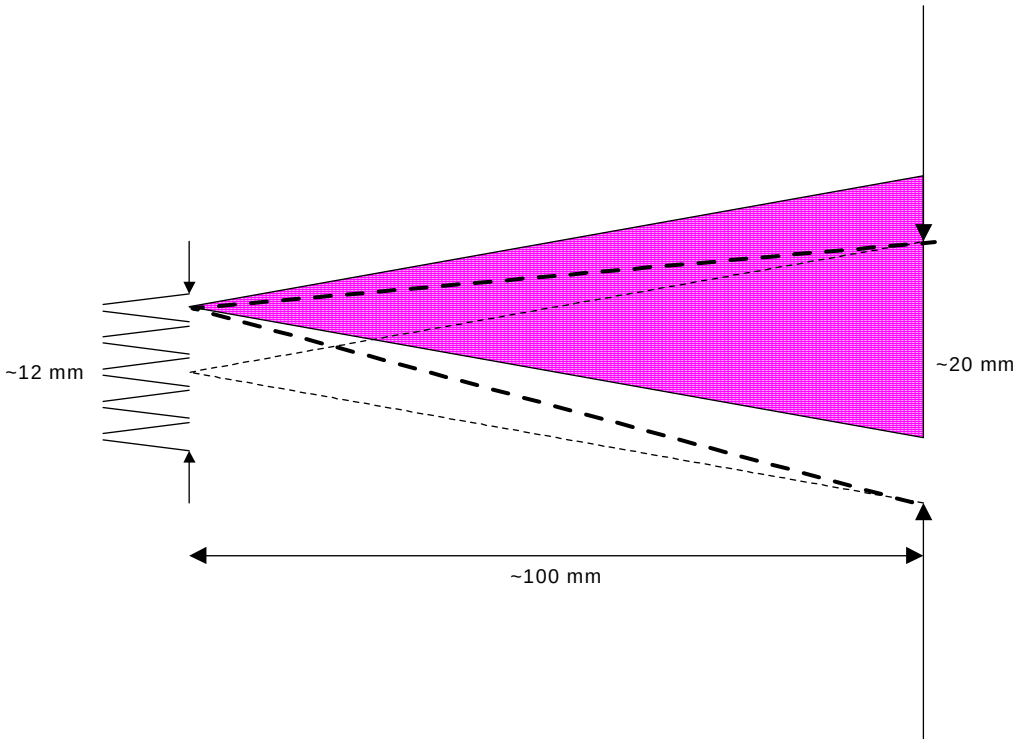

Figure 3-15 - Sketch of the final optical beams onto the spectrometer focal planes. There is a real pupil image of ~20 mm at about 119 mm from the focal plane which has a physical diameter of 23.8 mm. Off axis images therefore come onto the array at an angle of up to 3.5º – shown by the dashed line. The detectors themselves, because of the feedhorns, can only accept a certain range on input angles and, as they are configured to stare straight ahead, they only partially illuminate the pupil – shown in pink. Whilst this only causes a small loss of signal at the centre of the FTS mirror movement, at large mirror displacements the pupil images from the two interferometer arms shear past each other and the loss in fringe contrast will be greater.

3.5 Straylight control

Straylight control is defined as the reduction of any unwanted optical power falling onto the detectors in an instrument to as low as practically possible. This includes both the removal of out of spectral band optical power and the removal of in band optical power from sources outside of the field of view. These might be radiating surfaces within the structure of the instrument or satellite directly viewed by the detectors or seen via reflection or diffraction from other parts of the optical chain and structure.

3.5.1 Bandpass filtering

Any surface with a temperature greater than ~10-15 K will emit radiation in the detection band of the SPIRE instrument. The Herschel telescope will be at a temperature of about 70-80 K with an effective emissivity of 3-4%. There will, therefore, be a relatively large photon flux falling on the SPIRE instrument entrance aperture from the telescope alone. The bolometer detectors are sensitive to optical power at all wavelengths, therefore the first task in managing the amount of unwanted optical power falling on the detectors themselves is to limit the spectral band of the radiation falling on the detectors. This is achieved by a series of optical filters as described in the *SPIRE Filter Specification Document.* In practice a single passband filter does not have enough out of band rejection on its own and four filters are used strategically placed along the optical path to reduce the out of band radiation entering each part of the instrument structure. The overall passband provided by these filters is shown in Figure 3-16; the physical locations of the filters are shown in Figure 3-9 and Figure 3-13 above.

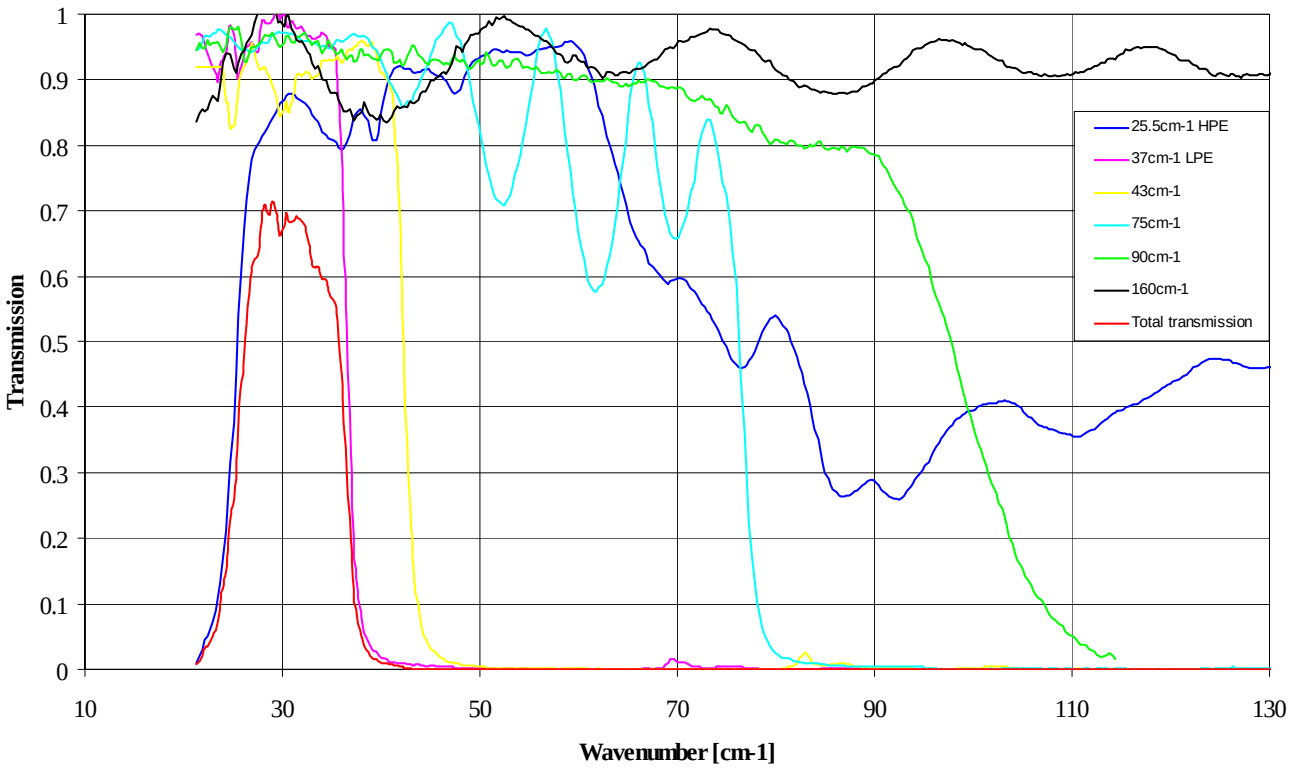

Figure 3-16 - Example showing the definition of a 350 micron photometer channel using real filters. The passband ($\lambda/\Delta\lambda$) in this case is ~3.

3.5.2 Baffling

Controlling unwanted optical power that is in the spectral band of the detectors is effected in the SPIRE instrument by having a series of compartments within the instrument separated by physical barriers or baffles. The overall concept for the photometer is shown in Figure 3-18 and for the spectrometer in Figure 3-19. The optical design, as described above, is arranged so that the entrance to the instrument itself is at the field plane of the Herschel telescope and a physical aperture plate is placed here together with an optical filter that rejects most of the out of band radiation. The aperture plate is made just large enough to allow the beams generated by the detectors to pass out of the instrument with the minimum vignetting. In fact the beams will be chopped and jiggled around the sky so the aperture plate is slightly oversized compared to the detector footprint on-axis – Figure 3-17 (also see *Definition of a combined focal plane plate for the SPIRE instruments*).

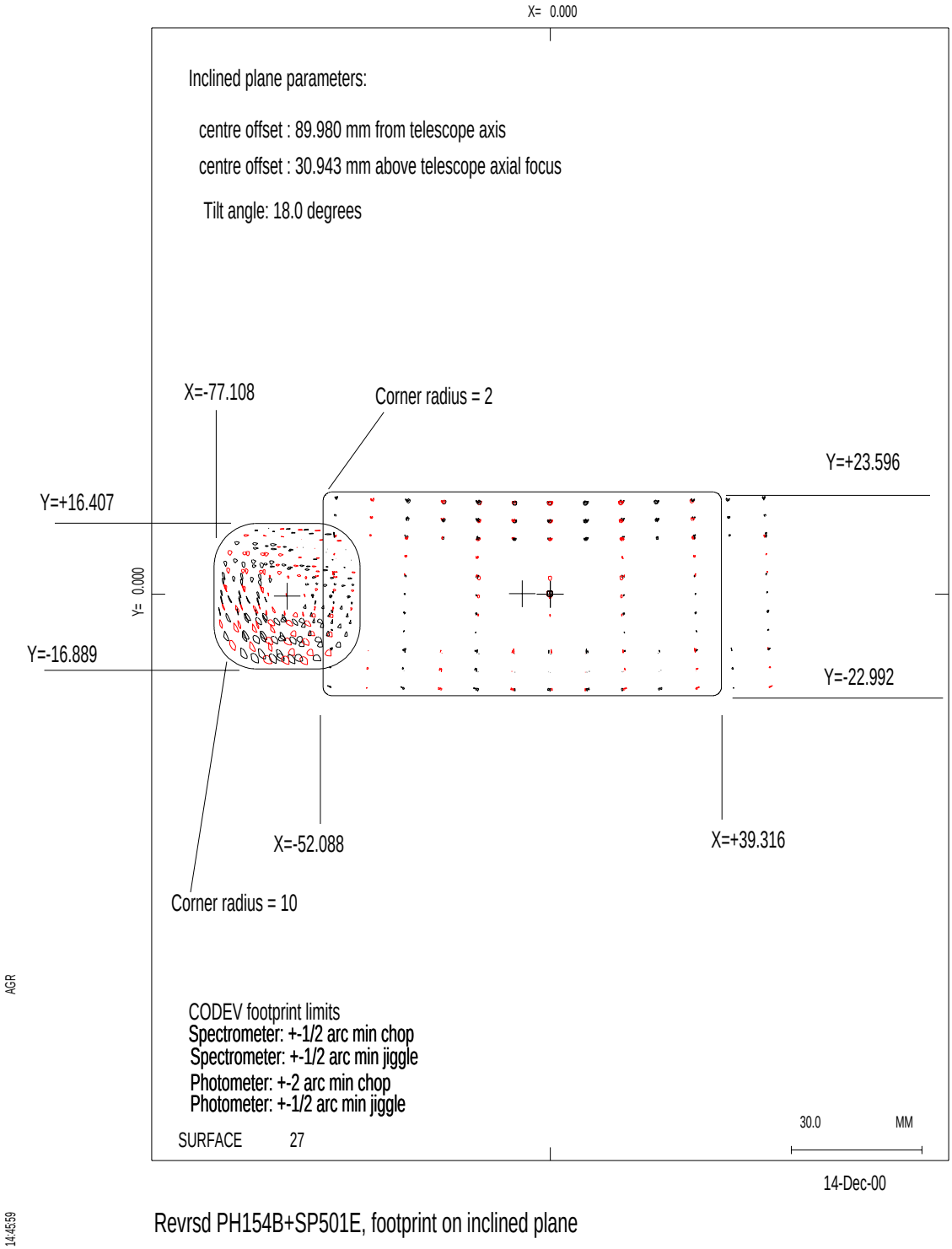

Figure 3-17 Chopped and jiggled footprints of the photometer and spectrometer arrays at the focal plane of the Herschel telescope. The solid line shows the boundary used to define the physical stop that will be placed at the entrance to the SPIRE FPU.

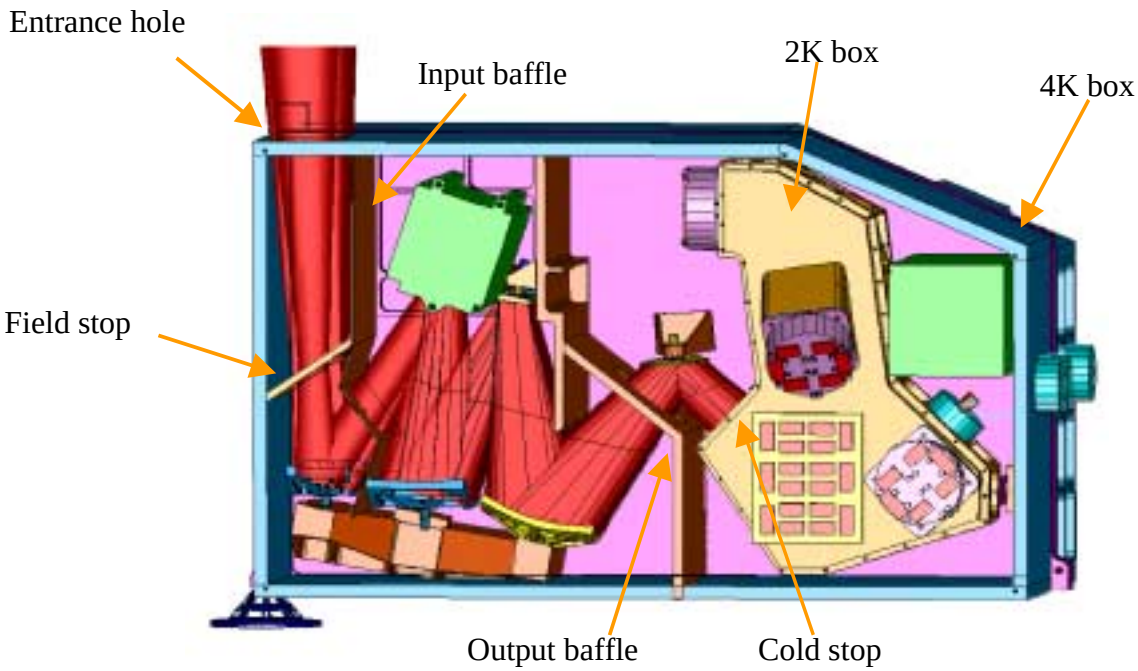

Figure 3-18 - Overview of the straylight baffling scheme for the photometer

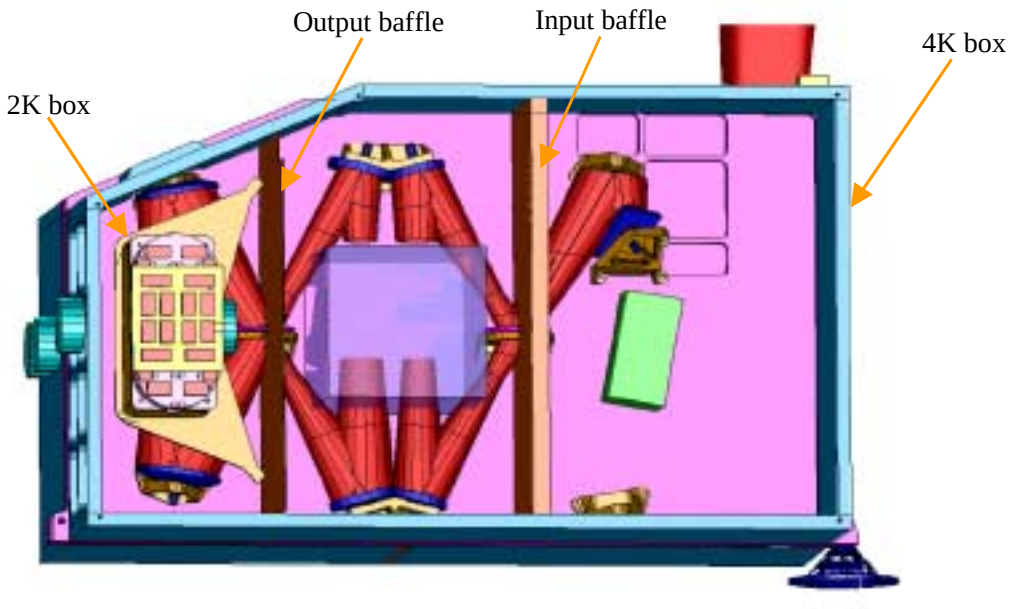

Figure 3-19 - Possible baffling scheme for the spectrometer

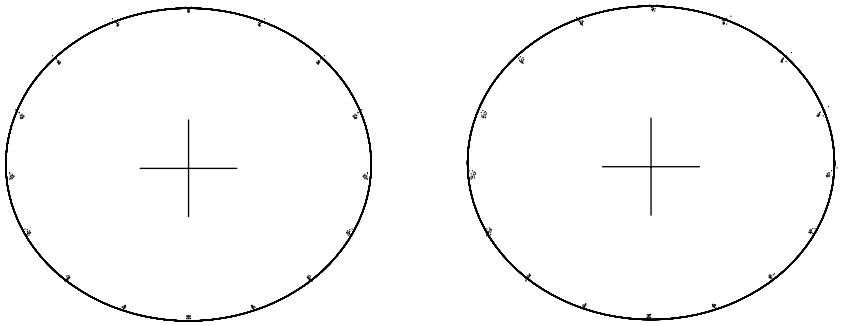

(a) (b)

Figure 3-20 - Pupil spot diagrams obtained by tracing rays from 15 positions in the FOV through 16 points along the rim of the telescope pupil to the cold stop

The photometer detectors are mounted to a sealed box that is kept below 2 K by directly strapping the detector box to the Herschel helium tank (Level 0). An image of the secondary mirror of the telescope is made at the entrance to this box and a physical aperture placed around at exactly the size of the image – see Figure 3-20. In Figure 3-20a the M4 beam-steering mirror is in its neutral position, in Figure 3-20b it is tilted by 2.17°, changing the instrument pointing by 2′ in the sagittal plane. Assuming the nominal M2 image to run through the centre of gravity of each spot, we may measure the radial pupil error ΔR for each point in the FOV at each point along the pupil edge. A useful measure of pupil aberration is relative pupil displacement $\Delta R/R$, found to be less than 5% both in the chopped and unchopped configuration. The good control of the geometric image of the telescope secondary means that the primary source of unwanted radiation from sources outside of the field of view from any part of the Herschel cryostat; telescope or sunshade is that passing into the instrument via reflection or diffraction from the telescope secondary mirror. Control of the straylight from such sources must carried out by the system level straylight control design. A further baffle is implemented in the photometer optical path between M7 and M8 to prevent the direct illumination of the cold box aperture by sources within the instrument box itself. The second bandpass filter is mounted at this point.

The straylight control within the spectrometer is more problematic than in the photometer as the moving mirror means that the final image of the telescope secondary mirror both shears and moves along the optical axis. Instead of placing the pupil at the entrance to the cold detector box, therefore, it is placed at an image of the secondary made by the Fabry mirror SM6 at the field plane where the spectrometer and photometer fields are separated. A physical stop is placed at this pupil image, which is at 4 K. A filter is also placed at the stop. As this stop is only ~25 mm diameter and, apart from holes for cables and thermal straps is the only aperture in the optical bench, the spectrometer part of the instrument box is very well baffled against radiation entering the instrument through the common entrance aperture. Two other baffles will be placed in spectrometer; one to prevent stray radiation from the calibrator reaching the detectors and one to prevent radiation from the mirror mechanism reaching the detectors – no filters will be placed on these baffles. The final baffle in the spectrometer is at the two entrances to the cold detector box where another filter will be placed as in the photometer.

The straylight model of the instrument has been constructed using the BRO APART code. A “reversed” Code V model has also been constructed to generated the optical paths from the detectors out through the system to space. These are the solid model beams shown in the general views of the instrument. By reversing the optical model one can determine more easily what it is possible for each part of the field of view to directly “see” within the Herschel system. The APART code is used to determine which straylight paths reach to detectors via multiple scattering and diffraction and what level of radiation falls onto the detectors from those paths given the physical construction; temperatures and scattering properties of the real system.

3.5.3 Diffraction limited optical analysis

One final aspect of the optical design that influences both the amount of straylight falling onto the detectors and the optical performance of the instrument in terms of both throughput and image quality, is the diffraction limited nature of the SPIRE optics. For SPIRE the sizes of the optical elements and stops within the system are significant compared to the longest wavelength radiation that has to pass through the system – $\lambda \sim 0.7$ mm compared to optical stops of 20-25 mm in some cases. Whilst use of the feedhorns on the detectors makes the diffraction limited nature of the optical design tractable by effectively acting as spatial filters and reducing sidelobes to a minimum, great care must still be exercised in the optical design to ensure that truncation of the beam from the detectors only occurs at the desired apertures. That is we wish to limit the effective throughput of the instrument only at the telescope secondary and its image within the instrument optical train. Some truncation at the edges of the field of view is inevitable at the field stop. All other optical components in the SPIRE instrument must be sufficiently oversized to allow the beams from the detectors to pass un-truncated at each and every point in the field of view.

The most basic rule of thumb that can be employed in taking into account the diffraction limited beam is to oversize all components by 20% of the geometrical footprint of the beam at the location of the element (see Figure 3-24). This is complicated by having a wide field of view as all beams from each detector must be amalgamated to make a single "instrument beam" before the oversizing is determined. This has been successfully done for all elements in the photometer optical train. In the spectrometer the situation is more difficult due to the moving mirror. The spectrometer components have been oversized to the physical limits possible but some truncation will still occur for some parts of the field of view at the limits of the mirror travel.

The BRO ASAP program has been used to ensure that the "20% rule" is indeed sufficient given the real Gaussian modes generated by the feedhorns and to determine what influence the truncation of the Gaussian modes has on the point spread function. Figure 3-21, Figure 3-22 and Figure 3-23 show the angular responses on the sky (i.e. the calculated point spread functions) for the long-wave, medium-wave and short-wave photometer detectors at the channel centre wavelengths. The following assumptions were made:

(i) the telescope mirrors is the JPL design;
(ii) the detector feed-horns designs are those described in the Diffraction analysis report (delta-PDR, June 2000).
(iii) the plots are calculated at the centre of the SPIRE FOV.

When these traces are compared with the theoretical Airy disc radii for the Herschel telescope quoted in the captions good agreement is seen.

One further aspect of the diffraction limited design of the SPIRE optics is the change optimum detector focal position with wavelength due to the quasi-optical nature of the relatively low frequency (long wavelength) radiation to be detected (*Goldsmith)*. This can be analysed using the ASAP code (Caldwell 2000*)* and the optimum detector positions found with respect to those given by the geometrical optical design. The detectors will be displaced along the optical axis at the position that gives the best coupling between the radiation field from the telescope and optics and the Gaussian mode generated by the feedhorns.

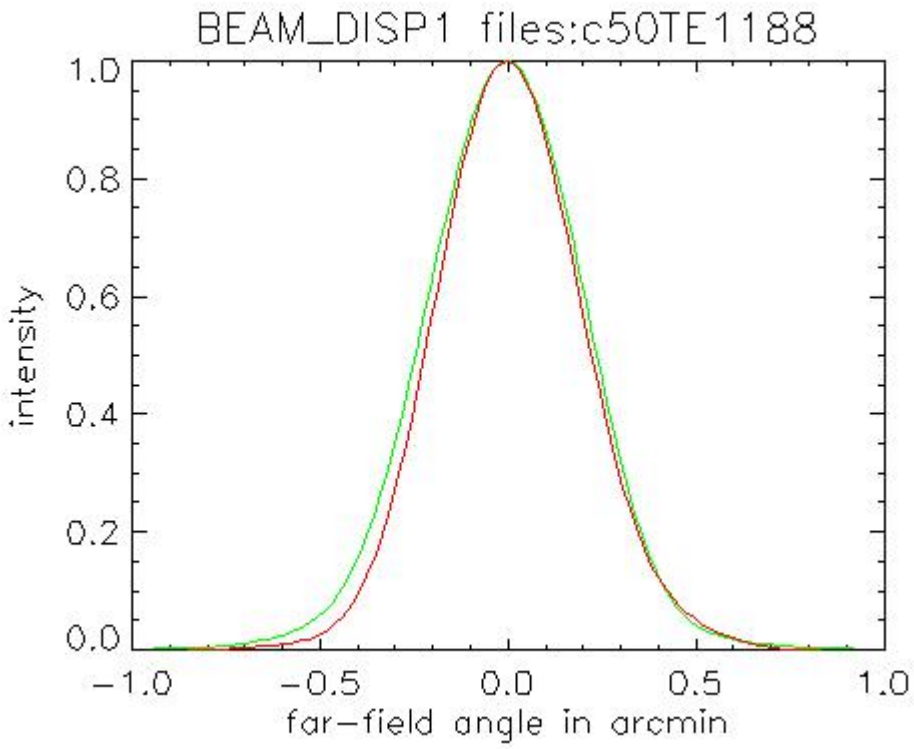

Figure 3-21 - PLW channel at λ = 500 μm, smooth-wall horn. The two profiles shown are principal sections of the response. Airy disc radius = 0.55 arcmin.

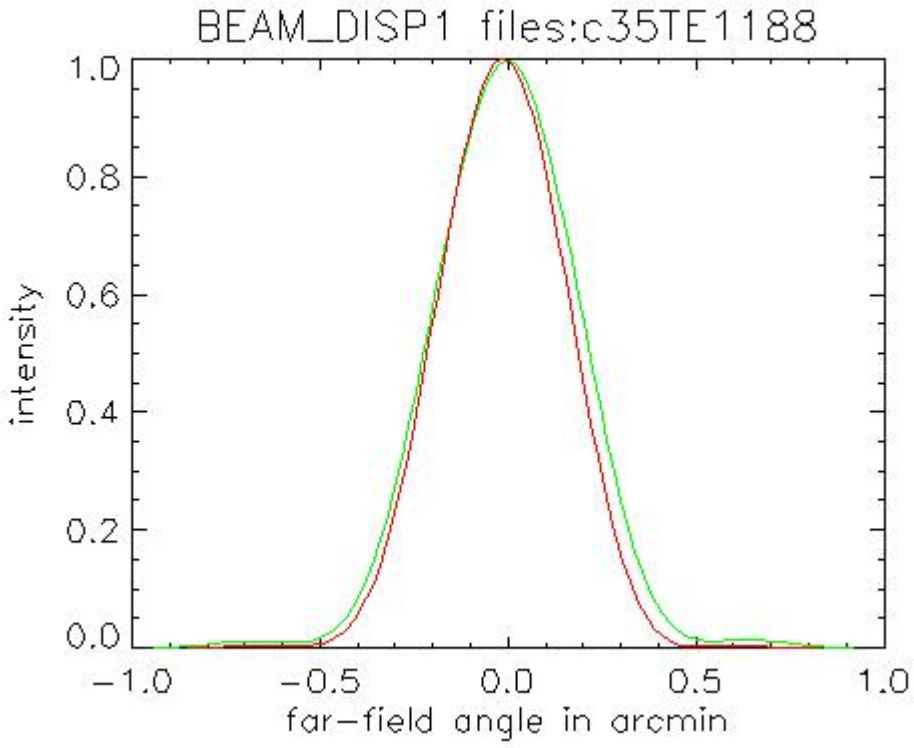

Figure 3-22 - PMW channel at λ = 35 μm, smooth-wall horn. The two profiles shown are principal sections of the response. Airy disc radius = 0.38 arcmin.

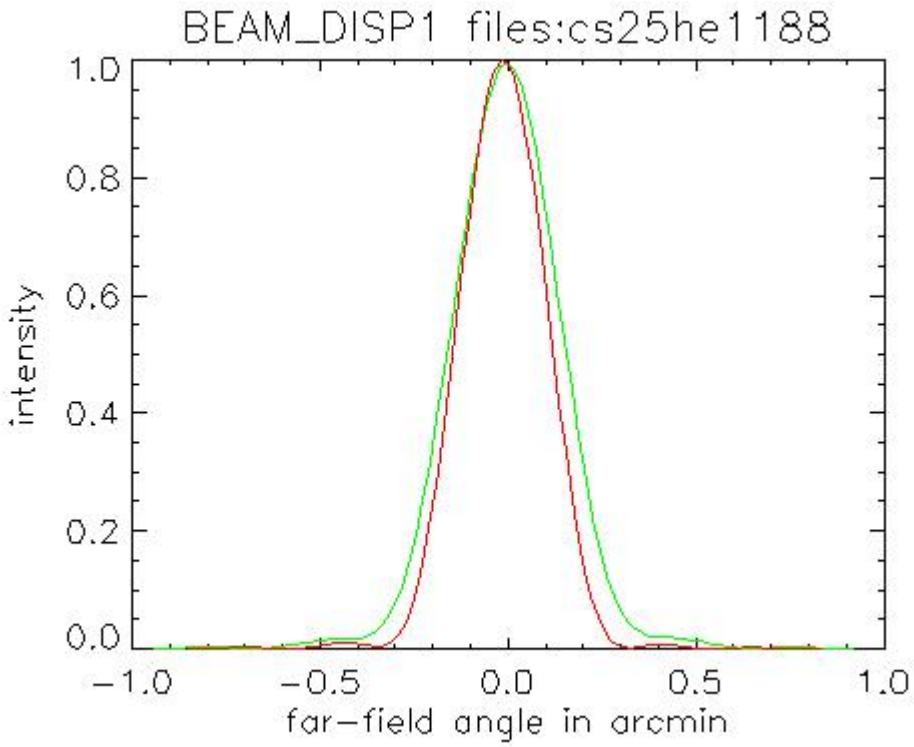

Figure 3-23 - PSW channel at λ = 250 μm, corrugated horn (smooth-wall case TBC). 2 profiles shown are principal sections of the response. Airy disc radius = 0.27 arcmin.

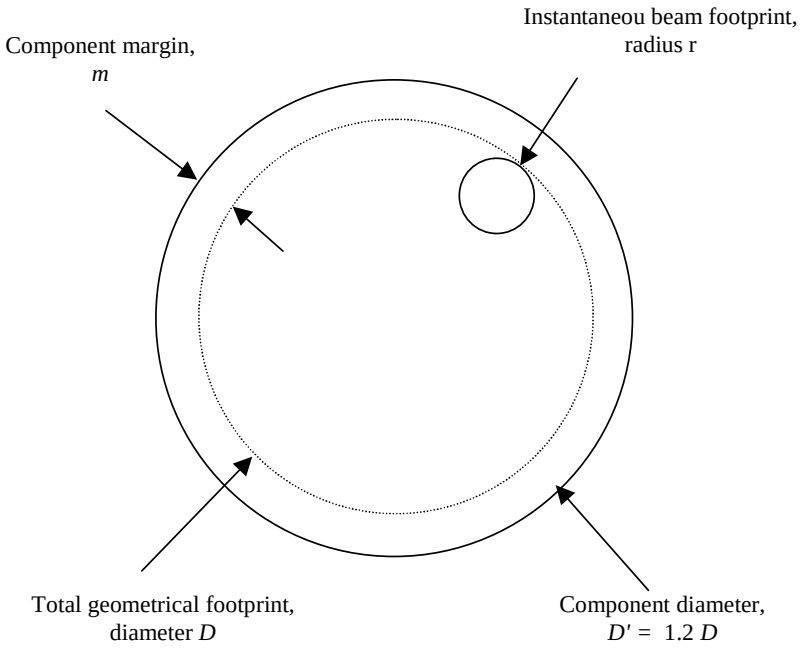

Figure 3-24 - Illustration of the 20% oversize rule and the comparison between component margin and instantaneous beam footprint.

3.5.4 Optical alignment

Alignment of the SPIRE FPU will be performed according to a philosophy based on high-precision machining and pre-assembly 3-D measurements and a program of optical alignment checks during and after assembly. Nominally no adjustments will be necessary but, if a serious misalignment is detected, its compensation will be possible by re-machining of the M6 mirror stand. Alignment of the instrument with respect to the telescope axis and pupil will be performed using a Herschel optical bench simulator consisting of a set of reference mirrors accurately located with respect to the instrument interface points. Verification of image quality and internal alignment stability will be effectuated using a set of alignment tools (sources, reticules, theodolites etc) mounted in strategic positions in the optical train (object plane, cold stop, image plane). The detailed alignment procedures are described in the *SPIRE Alignment Plan*. Details of the calculation of the optical alignment budget are given in the *SPIRE Optical Error* Budgets document, here we give an overview of the requirements on the alignment.

An optical sensitivity study shows that with an alignment tolerance of 0.1 mm and 1′ applied to all the mirrors in the photometer, the alignment-related relative pupil displacement will be less than $\Delta R/R_I = 4.1\%$. This compares favourably with the contribution from telescope alignment errors, budgeted to $\Delta R/R_T = 6\%$, and the theoretical design contribution of $\Delta R/R_D = 5\%$. The total instrument budget is estimated by square-summing of the random alignment errors and summing of the deterministic design error:

$$\Delta R / R = \sqrt{\Delta R / R_I{}^2 + \Delta R / R_T{}^2} + \Delta R / R_D ,$$

giving a total of 12.3%. For an exactly sized pupil this gives a loss of 8% in telescope transmission factor.

For the spectrometer, the predominant alignment criterion is interferometer contrast, calculated from the misalignment-induced lateral separation of the interfering images using the van Cittert-Zernike theorem. Note that this only concerns mounting tolerances of the fixed optical components within the interferometer (beamsplitters and collimator/camera mirrors) since the interferometer design with its back-to-back corner cube reflector leaves the interferogram contrast insensitive to errors in the scanning movement. Again, tolerances of 0.1 mm and 1′ have been found appropriate, offering a contrast in the interferogram of 87%. Including mirror surface quality and differential aberrations a total contrast greater than 80% is expected.

3.6 Thermal design

The thermal design of the SPIRE instrument is predicated on the following constraints:

(i) the need to reduce the temperature of the structure; mechanisms and optics to below a temperature where they can radiate significant optical power onto the detectors;
(ii) the need to get the bolometers to 300 mK or less and keep them at this temperature in a stable manner for all instrument observing modes;
(iii) the need to minimise the thermal load into the Herschel cryostat to make the mission last as long as possible given the amount of liquid helium available;

3.6.1 Instrument temperature levels

Given these drivers and the structural layout of the SPIRE instrument, three basic temperature levels have been defined within the SPIRE FPU. The various optical components (mirrors, filters, beam splitters etc.) and other instrument sub-systems (structure, mechanisms, harnesses etc.) must not be allowed to radiate significant IR power in these wavelengths. The temperature of all components that can either directly or indirectly (i.e. via multiple reflections) irradiate the detectors must therefore be below 5 K. The main

structure of the instrument and most of the optics are therefore held at 4 K (termed Level-1 of the cryostat); the structure that houses the detectors is held at 2 K (Level-0), and, in order to achieve a sensitivity matched to the photon noise limit from the telescope thermal background, the detectors must be at 300 mK – this temperature is generated internally by the sorption cooler which is mounted from the 4-K optical bench. The detector JFET amplifiers must run at a temperature of ~120 K so they are mounted on silicon nitride membranes which isolate them thermally from the surrounding structure. These membranes are then housed in a JFET units that is hard mounted to the Herschel optical bench at the cryostat Level-2 temperature of between 9 and 12 K.

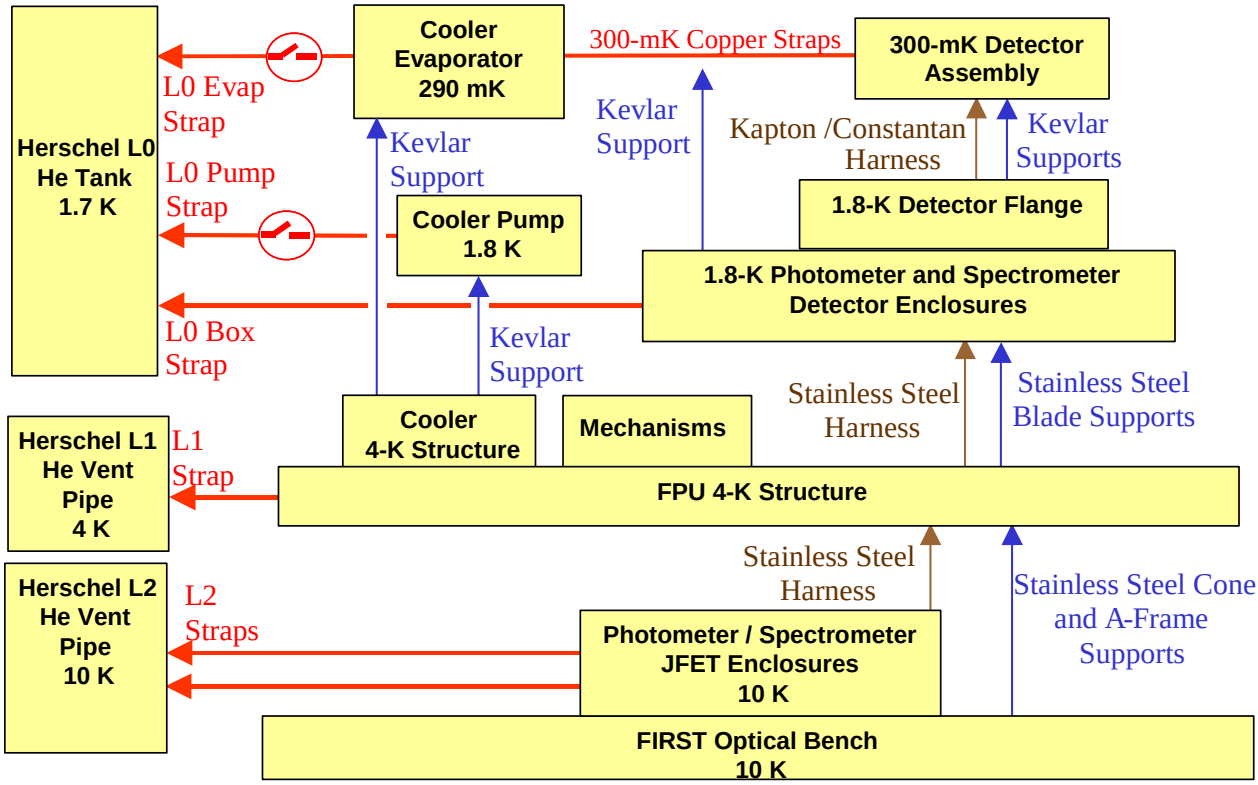

Figure 3-25 - Summary of the thermal analysis model for the subsystems within the CVV.

3.6.2 Cryogenic heat loads

To maximise the life of the mission and therefore the quantity of science data, the rate of consumption of helium must be minimised. This is done by (i) minimising the power dissipated in the various sections of the instrument, and (ii) by minimising the flow of heat from warmer stages to stages requiring lower operating temperatures. Stringent thermal budgets have been applied to all dissipating elements in the focal plane, and to the mechanical mounts that support the FPU from the Herschel optical bench; the mechanical mounts for detector cold boxes from the SPIRE optical bench and the support system for the various elements that have to be maintained at 300 mK. The electrical harnesses for the mechanisms and the detectors also contribute significantly to the thermal loads and these will have to be carefully designed to ensure that they meet both the electrical and thermal requirements placed upon them. The heat flows within the instrument are represented in an *ESATAN* model and shown schematically in Figure 3-25. A detailed description of the SPIRE thermal mathematical model is found in the *SPIRE Thermal Configuration Control Document.*

3.6.3 Temperature stability

The temperature of the bolometric detectors must be highly stable to achieve the required sensitivity, and there are corresponding requirements on the thermal stability of the instrument itself. A detailed analysis of the effects of temperature drift on the sensitivity of the instrument in various operating modes has been conducted (*Bock - Temperature Stability Requirements for SPIRE)* and shows that the detector temperature must have a stability of 0.6-1.2 $\mu K/Hz^{-1/2}$ in the detection band of the detectors and, further, must drift by no more than 1 mK per hour over the course of an observation. There is a very weak direct dependence on the temperature stability at the 1.7 K level and the corresponding figures for the 4-K level are, for the case of drift scanning to detect point sources, 5 $mK/Hz^{-1/2}$ and 0.3 K per hour.

3.7 EMC

Bolometric detectors are sensitive to any form of power input to the device. Unwanted electromagnetic radiation (from any part of the spectrum) absorbed by the detector will generate a spurious signal. Over and above this, any spurious RF power reaching the detector through conduction along the bias or signal wires will be dissipated through ohmic heating of the thermometer element, generating a spurious signal. It is critical therefore that bolometers be protected from EMI via an effective RF shield and a grounding scheme that prevents ground loops and protects the sensitive parts of the system from injected EMI.

3.7.1 Signal quality

The signal, gain and noise figures expected at each portion of the detection chain are shown schematically in Figure 3-26. The basic signal level is of order of a few mV at the detector and, after current amplification, at the output of the JFETs. The voltage equivalent noise at the detectors is of order 25 $nV/Hz^{-1/2}$ so all amplification and digitisation stages must contribute insignificant noise compared to this. The value of the basic detection noise also represents the sensitivity of the system to injected EMI.

3.7.2 Grounding and RF shield

In order to maintain the very low noise required at the detector it is necessary to create an RF shielded environment around the detectors and to filter all wiring entering the enclosure. In the SPIRE instrument the RF shielded enclosure is created using the FPU box and the JFET boxes together with harnesses running between them – this is shown in yellow in Figure 3-27. The only significant aperture into the RF shield will be the optical entrance aperture of the instrument itself. The RF rejection performance of real enclosures is difficult to model and predict as it is very sensitive to the detailed physical implementation and the necessary electromagnetic modelling is complex and computer-intensive. Whether there is sufficient attenuation of RF frequencies by the apertures along the optical path of the instrument remains to be seen. If tests prove that that further attenuation is required, a “chicken wire” type RF filter will be fitted to the instrument entrance aperture. At this location, the optical beam is defocused and the presence of a fine wire mesh in the beam would not cause significant distortion to the final image at the detector plane.

The grounding of the SPIRE electrical system is complex, even more complex than shown in Figure 3-27. The basic grounding scheme treats the two halves of the instrument, the photometer and spectrometer, as entirely separate electrical systems with their own power supplies and grounding. The analogues grounds of the two systems can be brought to a unipoint connection to the system ground through the thermal straps to the cooler – as shown in Figure 3-27. However, there is a separate ground and power supply for the digital part of the detector control electronics (not shown in Figure 3-27) which also has to be connected to system ground. There is some concern that this may lead to injection of noise into the analogue system via the system ground. Another possibility therefore is to isolate the RF shield at the cold end and connect to system ground in the warm electronics. Both these possibilities are open to us providing the mechanical structure of the FPU is electrically isolated from the cryostat. This will be implemented by electrical isolation washers

on the feet of the FPU mounts and sapphire plates on the thermal straps between SPIRE and the Herschel cryostat.

In order to study the relative effects of various noise injection and signal cross talk, a SPICE equivalent circuit of the detectors and the read out and AC biasing electronics has been developed. This model can be seen in Figure 3-28.

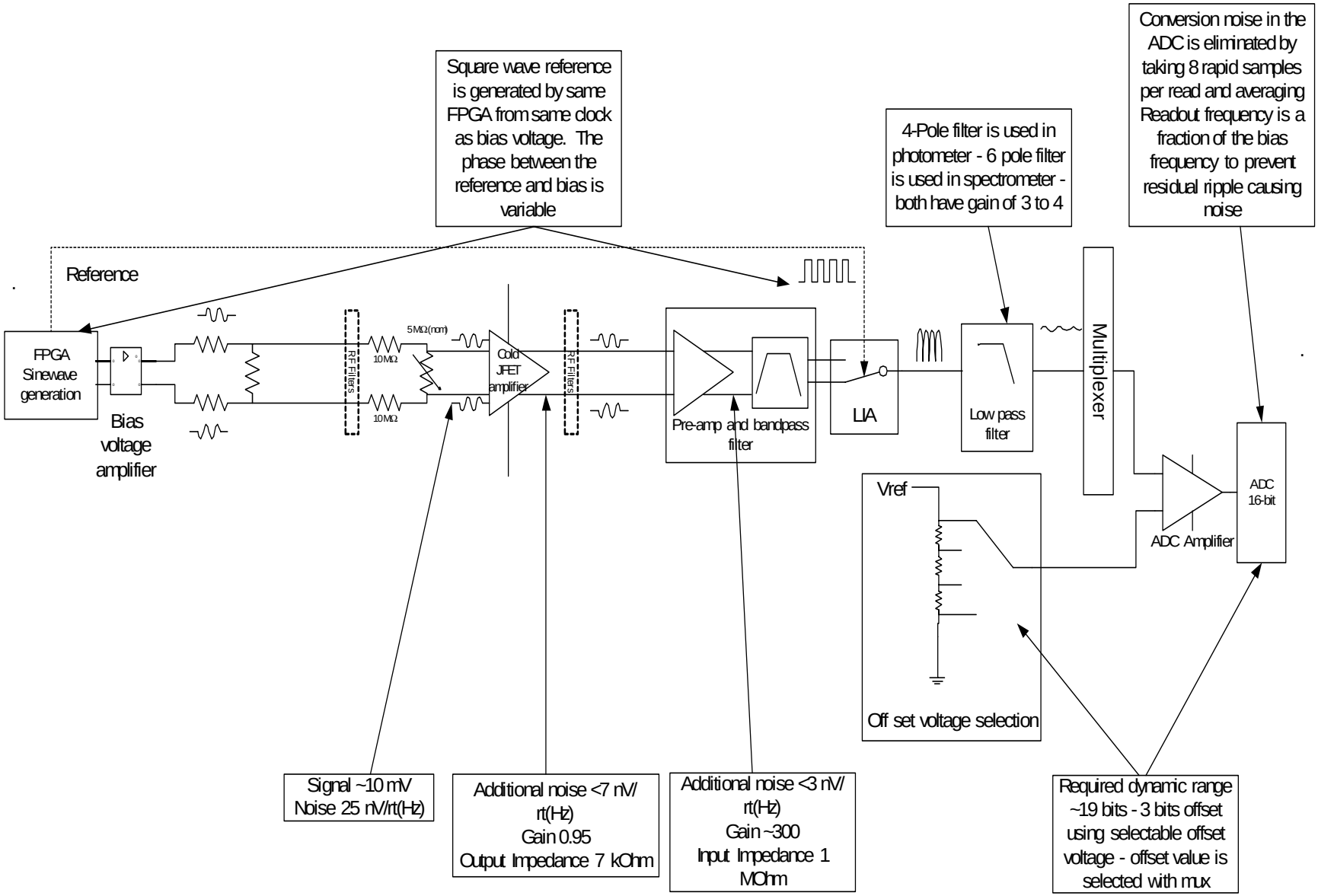

Figure 3-26 - Schematic representation of the SPIRE signal chain showing the noise sources and gains through the system

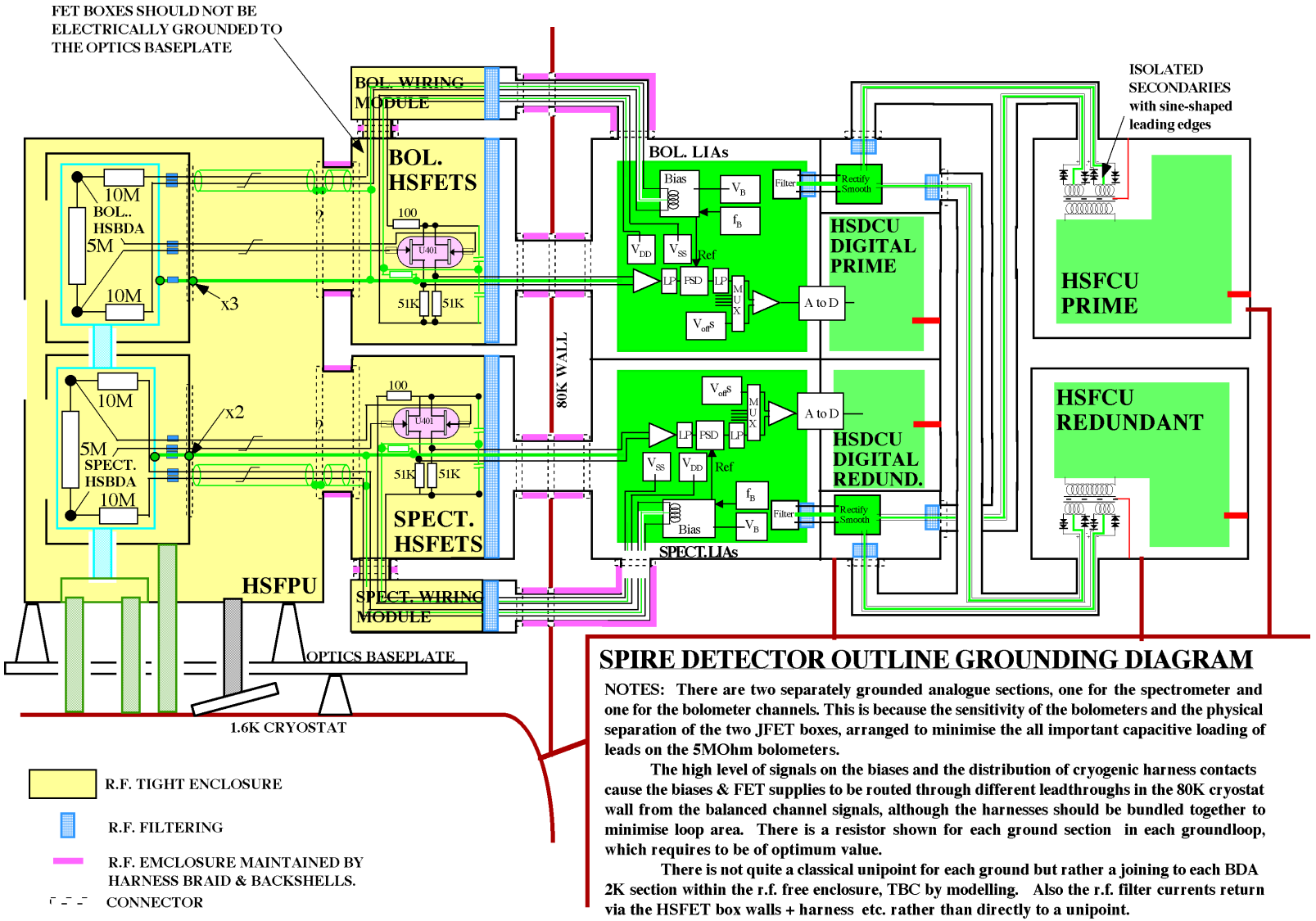

Figure 3-27 - Outline grounding diagram for the SPIRE instrument – this is subject to change and is shown for illustrative purposes only.

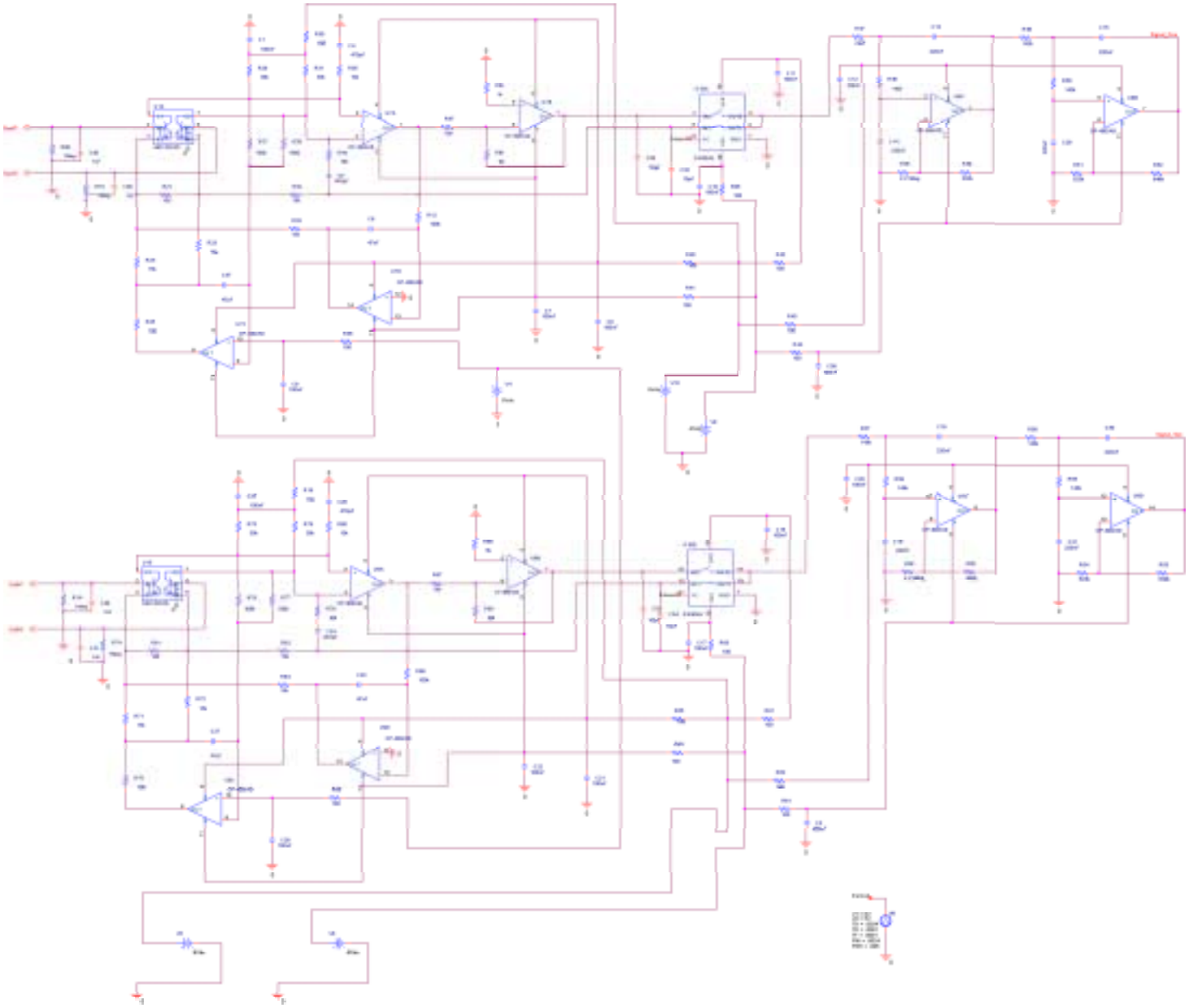

Figure 3-28 – SPICE model of the detector driving electronics used for EMC analysis.

3.7.3 Microphonics

The impedances of the NTD bolometer elements are on the order of 5 MΩ. This represents a compromise between high responsivity (which requires high impedance) and immunity to EMI and microphonic disturbance, which require a lower impedance). The JFETs located outside the FPU convert the impedance of the detection circuit to approximately 7 kΩ.

So-called microphonic effects are due to the physical motion of the detector wiring that result in either capacitative or inductive injection of voltages into the signal lines. The magnitude of microphonic induced noise increases with the magnitude of vibration of the harness and the support structure. With the low signal levels to be detected, very small vibrations of the wires cause a serious problem. Microphonic effects can be strongly suppressed by use of differential wiring. However, charge can build up due to the physical solicitation of asperities on the conductor and insulator interface.

As the harness connecting the bolometer elements to the JFET units represents the most vulnerable part of the detection system, it will be strapped down to the structure to give a minimum resonant frequency of any part of the harness of 1 kHz. In practice this means running the harnesses via the cold detector box supports, onto the optical bench and along the FPU covers. The harnesses will be strapped to the structure at intervals of approximately 1 cm. This routing is not optimum for the electrical requirements as the capacitance of the harness will be near to 100 pF, meaning that the bias frequency may have to be lower than initially desired to prevent roll off. However, the need to prevent induced noise from microphonics is felt to be an overriding concern as the bias frequency can be varied sufficiently in the electronics to optimise the performance of the detection system.

3.8 System-level criticality

A top-level analysis has been conducted into the effects of a failure or partial failure of one of the SPIRE subsystems (*Assessment of System Level Failure Effects for SPIRE,* Swinyard). In this analysis the following failures are shown to be mission critical – i.e. a failure of one of these sub-systems will cause major loss of scientific capability for the SPIRE instrument:

(i) total loss of the cooler;
(ii) Structural failure in the 300-mK system leading to thermal short;
(iii) total loss of the photometer long wavelength array;
(iv) total loss of either spectrometer array;
(v) total loss of the FTS mirror mechanism.

All other sub-system failures will lead to a greater or lesser degree of loss of performance and difficulty of operation, but they do not lead to a total failure of either the photometer or spectrometer scientific goals. The redundancy and reliability of these sub-systems will be addressed as a first priority.

For most sub-systems cold redundancy can be provided to ensure a high probability of avoiding total failure in any part of the sub-system implementation (see section 3.8.1). However in some cases this is not possible, for instance there will not be multiple detector arrays and only a single cooler will be fitted. In the case of the detectors reliability is achieved by having many pixels arranged in blocks for the purposes of power supplies and multiplexing into ADCs etc. In the case of the cooler, and the 300-mK thermal architecture, either large safety margins will be implemented backed up by testing or “soft” failure modes will be designed to prevent dead thermal shorts in the event of structural failure.

An additional method of providing operational reliability is to define backup operational modes for the sub-systems and instrument. The following instrument backup operating modes are required in event of sub-system or system failure:

(i) more frequent cooler recycling including the possibility of autonomous recycling under control of the DPU alone;
(ii) slow chop mode in the event of partial BSM failure;
(iii) open loop BSM control using commanded current to the actuators;
(iv) single axis BSM operation;
(v) slow scanning of FTS mirrors;
(vi) step and look operation of the FTS in conjunction with the BSM;
(vii) open loop operation of the FTS mechanism by commanding the current to the actuator;
(viii) DC operation of photometer calibrator this will allow V-I's on detectors under different loadings for calibration;
(ix) selection of smaller numbers of detectors from photometer arrays in event of telemetry bandwidth problems;
(x) selection of smaller number of spectrometer detectors in event of problems with telemetry bandwidth and/or loss of spectrometer calibrator.

3.9 Redundancy scheme

The general design philosophy of the instrument, as far as is possible, is that the total failure of a single sub-system will does not lead to the total loss of instrument operations. In order to achieve this, SPIRE has been designed with both a prime and a redundant side to the instrument. There is no electrical cross strapping between these two sides of the instrument, except at the SPIRE/Herschel data interface where both the Prime and Redundant HSDPU subsystems are *each* connected to the Prime and the Redundant Herschel MIL-STD-1553 data buses (See Figure 3-2). Normally, to switch between the prime and redundant sides of the instrument, the spacecraft sends appropriate commands on the MIL-STD-1553 bus to the HSDPU to firstly shut down the HSFCU and then to prepare itself for shut down. Once the HSDPU is ready, the two prime spacecraft level LCLs in the HPDU that power the HSDPU and HSMCU are unlatched and the Prime side is then shut down. The two redundant LCLs are then latched and the Redundant HSDPU and HSFCU are powered up. Due to impracticalities, some systems (for example, the ^{3}He Cooler) are not duplicated. In these cases, either the Prime or Redundant side of the instrument can control them. Importantly, in the signal detection subsystems, there is no redundancy in the detectors, the JFETs and the Lock-in Amplifiers. The specific redundancy scheme adopted for each sub-system is described in Table 3-1. Figure 3-2 illustrates the redundancy in the Warm Electronics. Figure 3-1 shows the redundancy in the FPU subsystems. It can be seen that the cryogenic bulkhead connectors J10 and J11 on the CVV wall are harnessed to the prime Filter Boxes (and from there the prime subsystems) Connectors J12 and J13 are connected to the redundant Filter Boxes and the redundant subsystems.

3.10 System budgets

A summary of the various budget allocations to SPIRE are summarised below in Table 3-4 .

Table 3-4 - SPIRE Budget allocations

Item	**Budget Allocation**	
Focal Plane Mass Budget	57.6kg	
SVM Mass Budget	30kg	
FPU ⇒ Stage 0 Thermal Load	10 mW average	100 mW peak
FPU ⇒ Stage 1 Thermal Load	25 mW average	100 mW peak
JFB ⇒ Stage 2 Thermal Load	33 mW average	200 mW peak
WE dissipation to SVM	86 W	
Data transmission from HSDPU to CMDS	100 kbps	

4. SUBSYSTEM DESIGN

4.1 Warm Electronics

The Warm Electronics are located on the Herschel SVM below the Cryostat. The temperature of the SVM is conditioned to remain between -15°C and +45°C during operation of the instrument. The principal function of these subsystems is to (i) act as the back end for the instrumentation contained in the CVV, and (ii) to interface SPIRE with the Herschel spacecraft. This is illustrated in Figure 4-1.

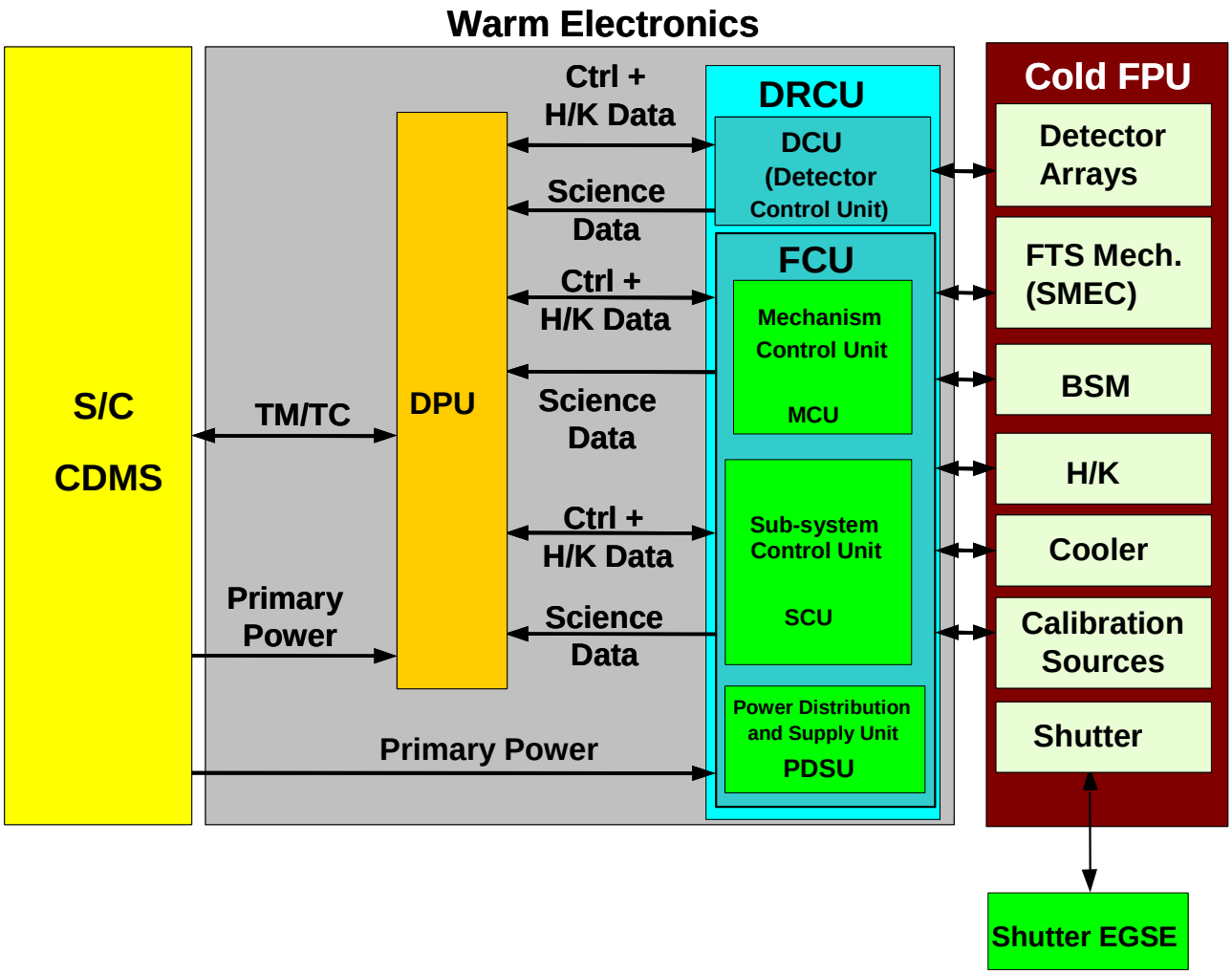

Figure 4-1 - Schematic representation of the Warm Electronics.

4.1.1 Digital Processing Unit (HSDPU)

The DPU interfaces with the Detector readout and Control Unit subsystem (DRCU) and with the spacecraft Command and Data Management System (CDMS) and power systems. Figure 4-2 is a high-level block diagram showing the electric and data interfaces of the DPU to the spacecraft and the DRCU. The interface with DRCU is composed of three high-speed data links for science data collection and one low speed, bi-directional serial bus with three output buffers, for command transmission and housekeeping data collection. The interface with the spacecraft has a baseline average 24 hour data rate of 100 kbps, with burst mode

transmission up to 350 kbps. This interface is compliant with the MIL-STD-1553B standard, with the DPU acting as a remote terminal and the spacecraft CDMS acting as the bus controller.

DC/DC Converter: The DC/DC converter is a SMPS running off a spacecraft level clock signal at 131.072 kHz that powers the DPU board. This clock signal synchronises all the SMPSs connected to the main power bus and avoids the generation of conducted EMI harmonics. The input voltage to the SMPS provided by the s/c power bus is at 28 V and the nominal output voltage to the CPU board is 5V. The average power delivered to the DPU is X W.

CPU Board: A schematic representation of the information flow within the DPU is shown in Figure 4-3. On the top left hand side of the Figure, the DPU "Command-handling" electronics receives and interprets commands from the CDMS. Upon successful receipt of these commands, a handshake/acknowledge message is sent back to the bus. The high level commands from the CDMS are processed by the DPU to provide digital driver commands to the DRCU (which acts as the analogue drive/read out electronics for the cryogenic part of the instrument) and are in general executed in real time. It is the task of the spacecraft to determine the sequence and absolute timing of the commands to be passed to SPIRE. These commands are passed to the DRCU via the "Commanding" block in the lower left hand corner of Figure 4-3. Science frames and housekeeping data from the instrument are passed to the "Data Collection" block via the high-speed data interfaces with the DRCU. The housekeeping data (such as instrument temperature, control currents etc.) are monitored by the "Autonomy" block. In the event of a fault condition in the DRCU or in the cryogenic section of the instrument, commands are passed to the DRCU to put the instrument into safe mode. Notification of a fault condition is also passed to the CDMS via the "Packetisation Block" in the top right corner of Figure 4-3. The CDMS then determines if the instrument should be turned off and unlatches the LCL for the DRCU and the DPU as necessary. All data passed from the DPU to the CDMS is formatted according to the ESA Packet Utilisation Standard.

The core microprocessor of the DPU is the TEMIC TSC 21020 which is the Analog Devices 21020 Digital Signal Processor adapted for space applications by TEMIC. The CPU board is based on this chip (20 MHz clock), with:

(i) an appropriate timer for time management and synchronisation purposes;
(ii) a watch-dog system that can be hardware disabled through jumper;
(iii) Radiation tolerant memories and components.

Figure 4-4 shows the block diagram for the CPU board. There are three high-speed, unidirectional synchronous serial 1355 links with a 1 MHz clock between the DRCU and the CPU board. These three links upload the science data from the DCU. Three serial synchronous buses are used to interface the control electronics of the focal plane unit subsystems: the bus will be used to transmit commands and receive responses or to control and receive housekeeping information. The baseline clock speed is 0.2 MHz. Figure 4-5 shows the memory organisation of the CPU and the interfaces between the DPU and the spacecraft and DRCU with the size of the various types of memories. The CPU directly accesses 1 MB of EEPROM memory, where the boot sequence software resides. It also accesses 2 MB of SRAM for program data.

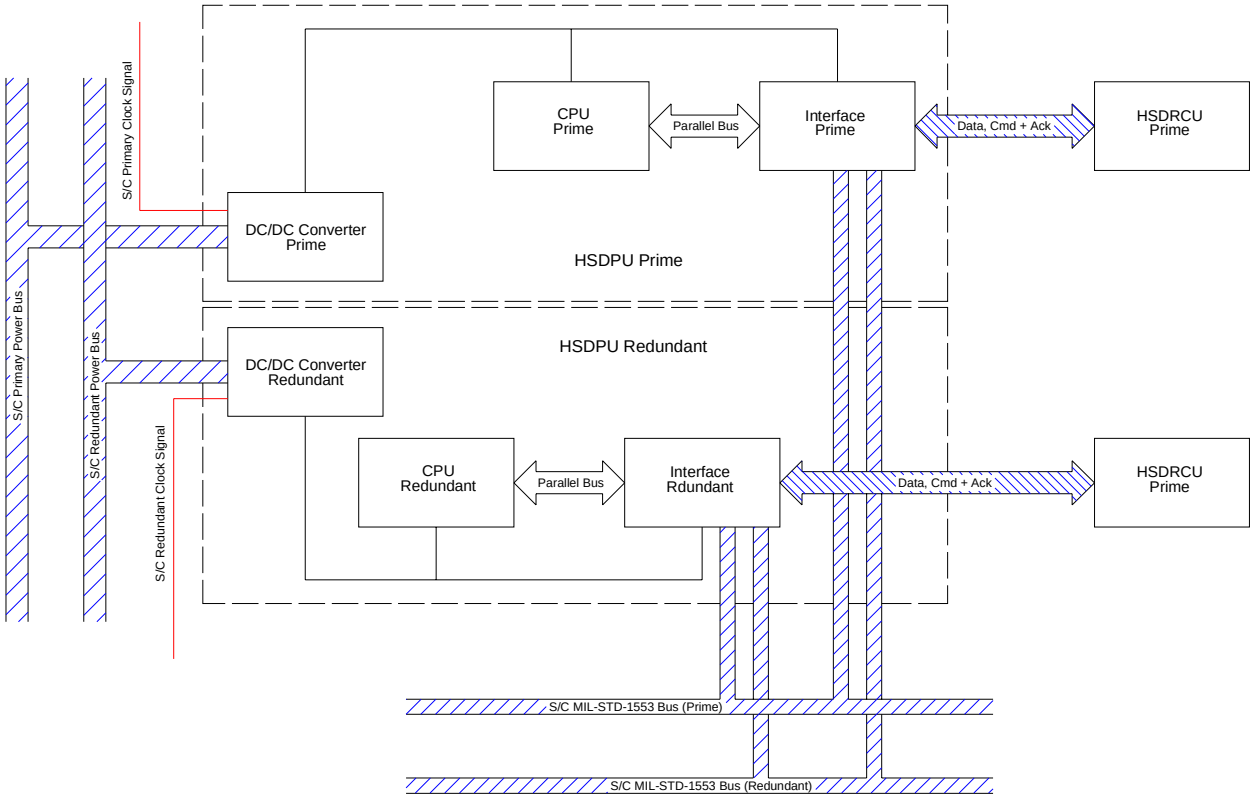

Figure 4-2 High level DPU block diagram.

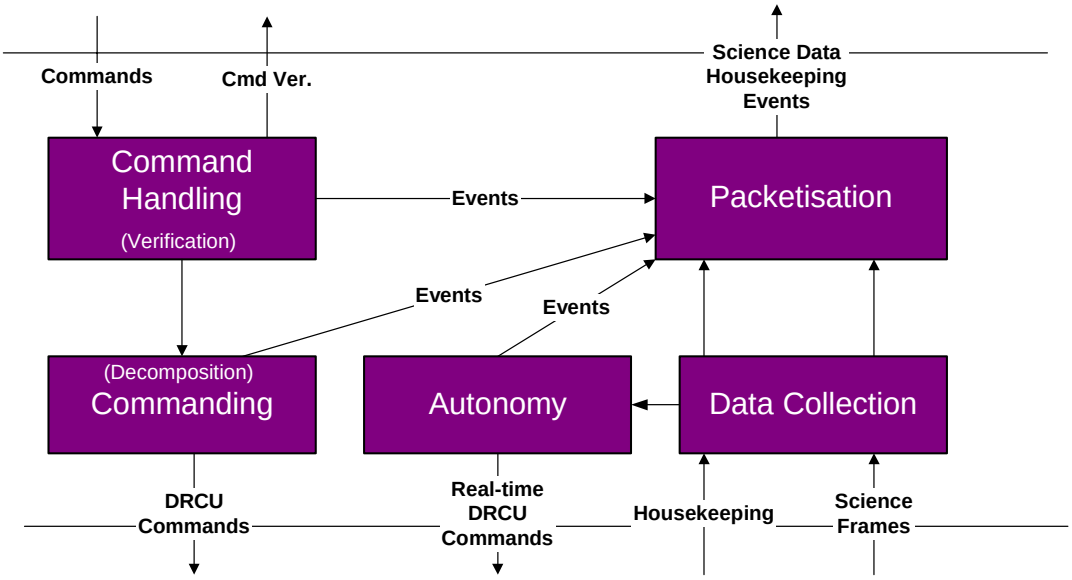

Figure 4-3 - Conceptual diagram showing the flow of information within the DPU

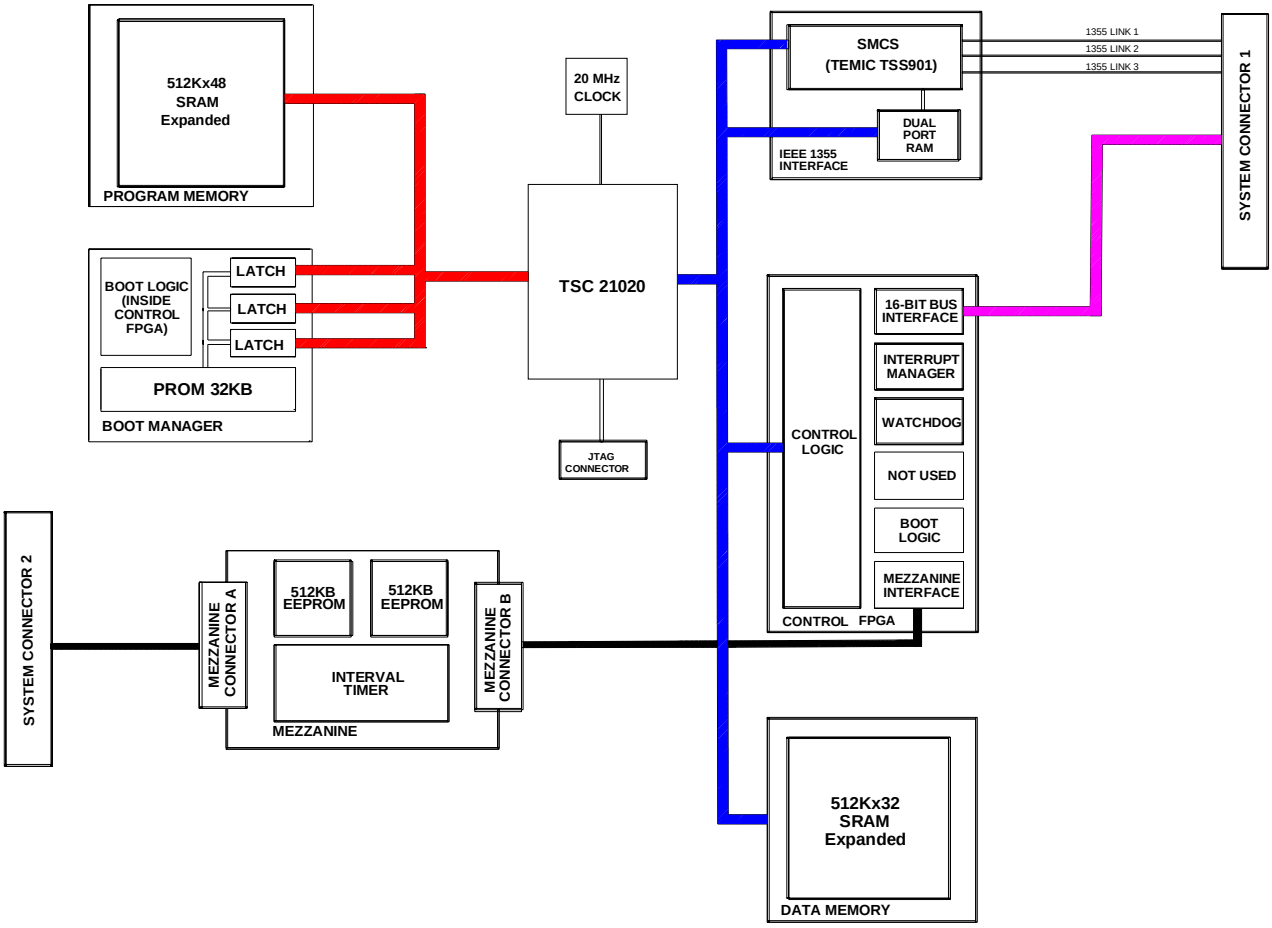

Figure 4-4 – CPU board block diagram.

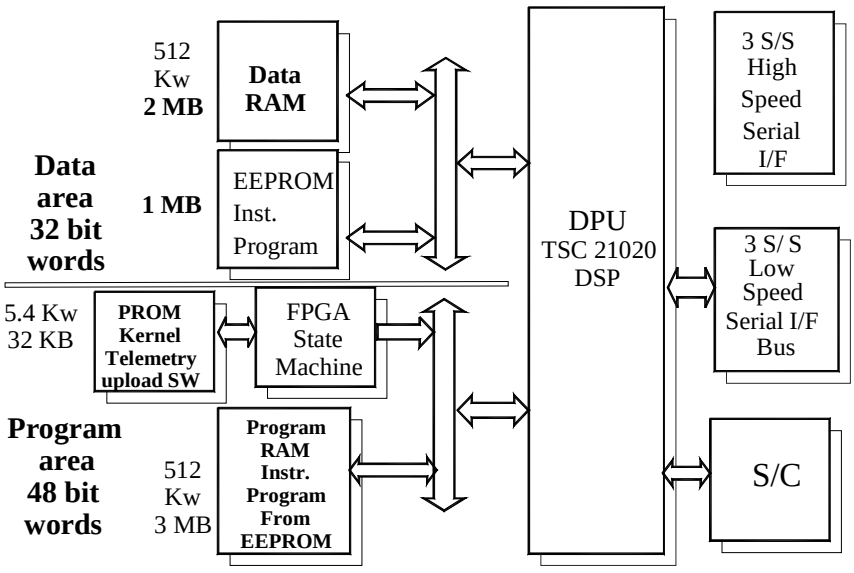

Figure 4-5 - DPU internal memory

Onboard Software: The CPU board carries in the PROM the basic software to drive and control the DPU. The tasks the OBS carries out are schematically shown in Figure 4-6.

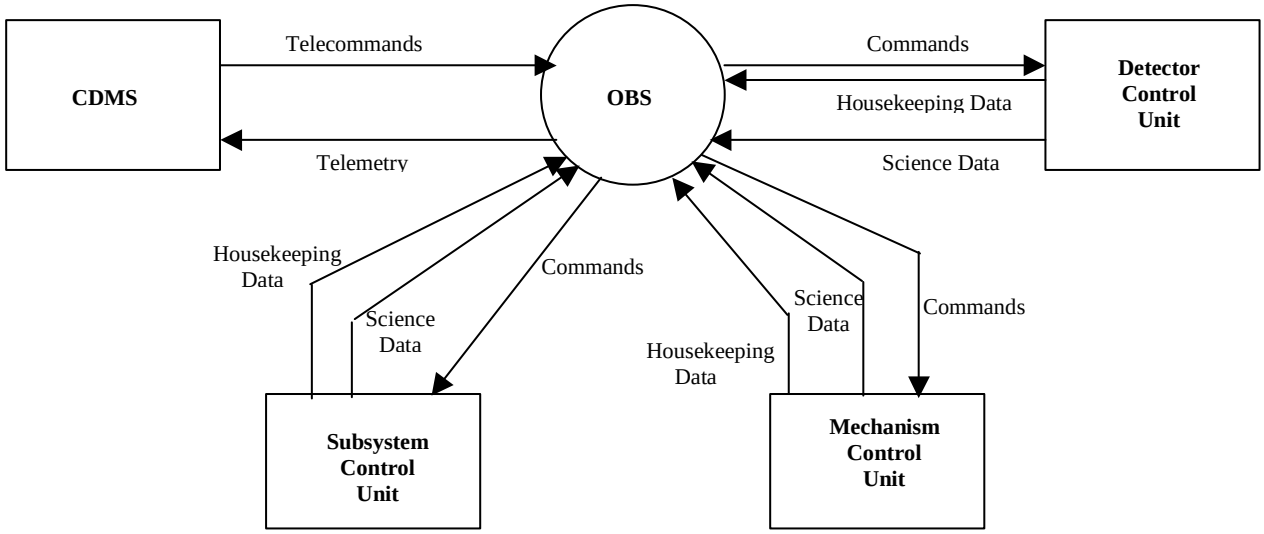

Figure 4-6 SPIRE DPU On Board Software Context Diagram

The main functions of the OBS are the:
(i) acceptance of instrument commands from CDMS;
(ii) execution of predefined commanding sequences;
(iii) instrument health/status monitoring;
(iv) implementation of pre-defined procedures on detection of instrument anomalies. When an anomaly occurs, the OBS either (i) adjusts the instrument operation parameters, and/or (ii) switches the operating mode and/or (iii) activates subsystem redundancy;
(v) science data acquisition and packetisation;
(vi) HK data packetisation;
(vii) transmission of data (science, HK, events and telecommand verification) from the instrument to the CDMS.

In addition, the OBS shall provide the following software oriented functions:
(i) the ability to load, via telecommands, replacement and/or additional software (patches, tables, command sequences);
(ii) self-test and software verification facilities;
(iii) the possibility to load and dump part of DPU/DCU memory;
(iv) the possibility to write and check EEPROM;
(v) the possibility to inhibit these functions during flight operations.

4.1.2 Detector Readout and Control Unit (HSDRCU)

The DRC is an electronic unit housed into two boxes: the FCU and the DCU, located between the FPU and the DPU. The DRCU includes the front-end electronics of the following sub-systems:
(i) BDAs,
(ii) SMEC,
(iii) Beam Steering Mirror,
(iv) Cooler,
(v) PCAL and SCAL,
(vi) Thermometry & Analog Housekeeping,

The DRCU comprises 4 physical sub-units:
(i) the DCU which includes the detector control, biasing, readout and digitization electronics;
(ii) the MCU includes the mechanisms' (FTS+BSM) control electronics;
(iii) the SCU includes the sub-system control electronics; and
(iv) the PSU which takes power from the spacecraft power bus and converts it to the required voltage for the other sub-units of the DRCU.

These components are schematically represented in Figure 4-7.

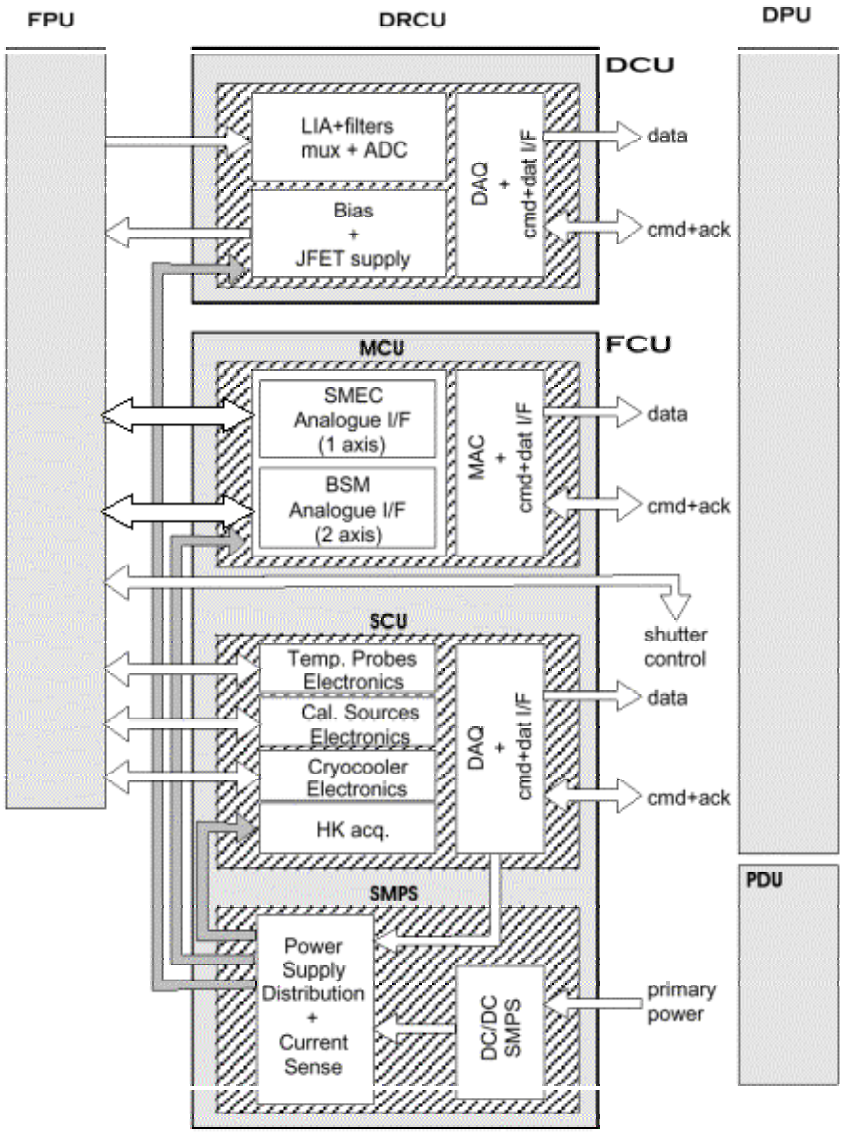

Figure 4-7 - Schematic block diagram of the DRCU including the interfaces to the DPU and the FPU.

4.1.2.1 Detector control unit (DCU)

The DCU acts as the interface between the analogue signals from the detectors and the digital DPU. A schematic drawing of the DCU together with the detector train components in the FPU and the interfaces with the DPU and FCU is shown in Figure 4-8. There are three basic board types used in the DCU; the Lock-in Amplifier (LIA) boards, the Bias Boards and the Data Acquisition and Interface (DAQ + I/F) boards. They are all connected by the motherboard, which forms the back plane for the other boards.

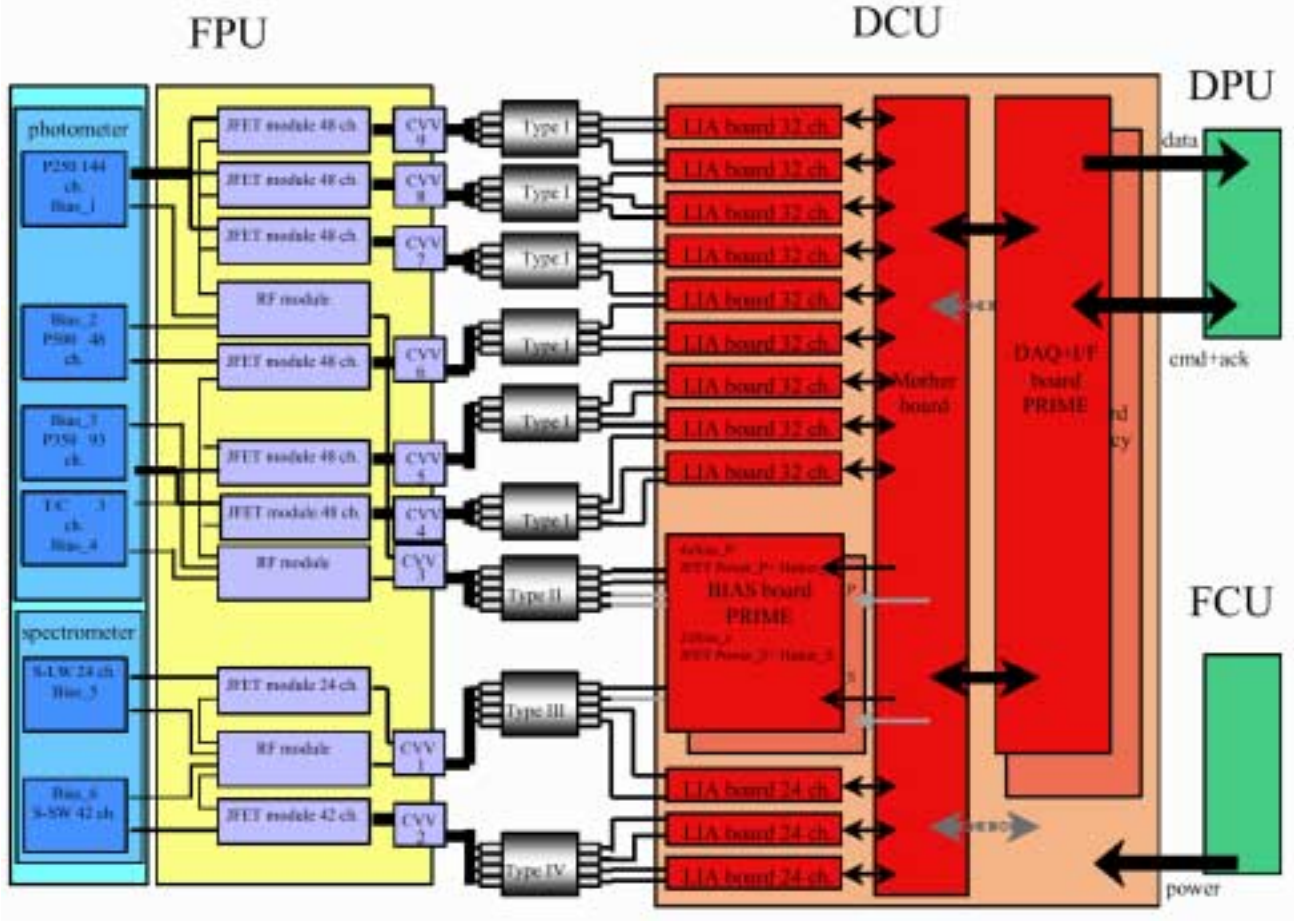

Figure 4-8 - Schematic representation of the DCU including it's interfaces with the FPU, DPU and FCU.

Detector Bias Generators: As described in §4.4.4, the detectors are differentially biased with an AC voltage, which is provided by the Bias Generator board. Due to the criticality of this component of the detector read out electronics, there is both a prime and redundant board for the bias signals. The amplitude, frequency and phase of the bias signals are all software commandable with the XC-4010-200 FPGA chip on the DAQ + I/F board. This FPGA generates a series of 12-bit words, which correspond to the amplitude of the bias signal. These words are loaded into Analog Devices AD7475A, 12-bit DAC chips that generate the analog bias signal. These signal are then amplified to the required amplitude with Analog Devices OP-400 operational amplifiers. The characteristics of the bias signal are summarized in Table TBD.

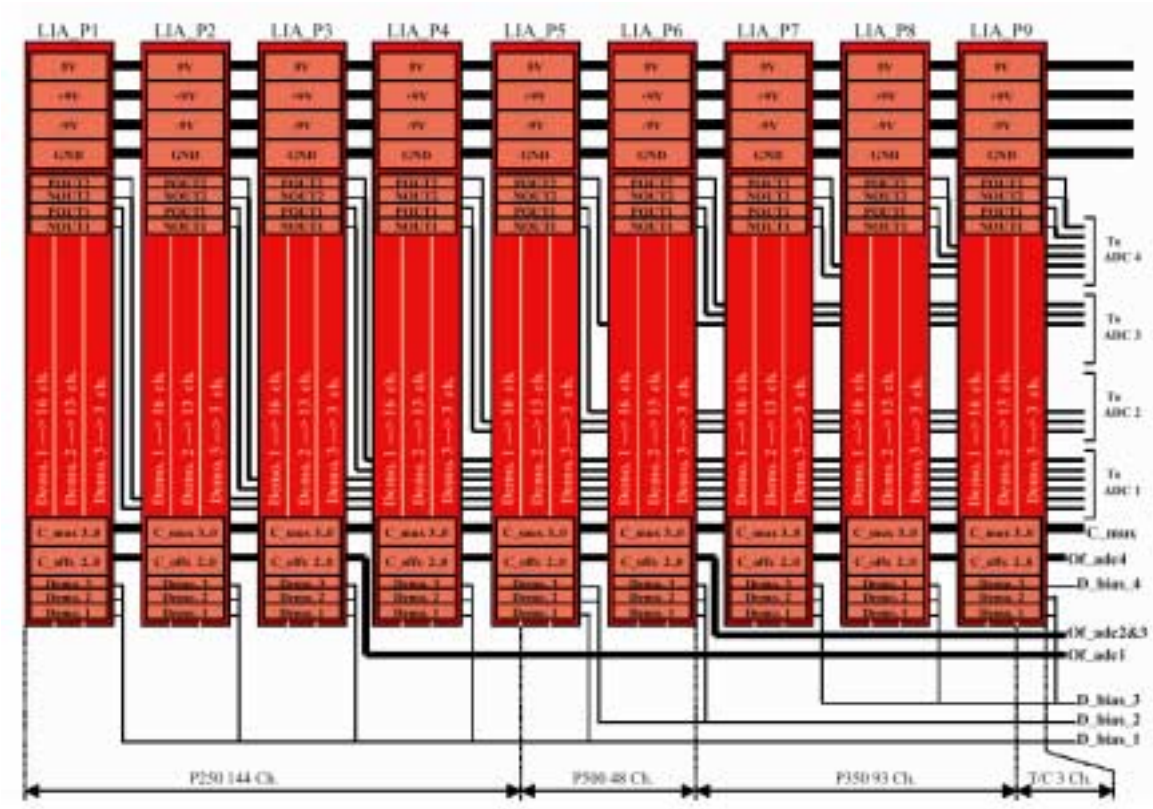

Figure 4-9 - Back plane connections to the photometer LIA cards. The spectrometer LIA boards are conceptually indentical.

LIA Amplifiers: The Lock-in Amplifiers are used to read out the AC signals from the detectors and convert them into DC. Each bolometer has a dedicated amplifier. The amplifiers are grouped together in groups of 32 on each LIA board. Figure 4-9 shows the interconnection between the LIA boards on the motherboard. The analogue output from each of the amplifiers is placed on a bus connected to the DAQ + I/F board.

Each individual amplifier has;

(i) a differential input pre-amplifer circuit that uses Analog Devices OP-400 operational amplifier;

(ii) an Intersil, DG303A digital switch. This takes the pre-amplified AC signal from the bolometer and full wave rectifies it using the signal from the bias generators. The switching is signal is phase commandable to compensate for any signal phase change that occurs between the detector and the digital switch in order to maximize the output from the switch;

(iii) an active post low pass filtering circuit that removes the bias frequency and bias harmonic components from the rectified signal. The low pass filter circuit uses two Analog Devices OP-400 operational amplifiers.

These three components are illustrated in Figure 3-26. There are a total of 12 LIA boards; with nine being used for the photometer and three used for the spectrometer.

The DAQ + I/F boards: There are a total of

In order to limit the mechanical properties of this unit it is now divided into two boxes which are respectively the DCU and the FCU including the MCU, the SCU and PSU.

The SCU function is manifold: it is in charge of interfacing FPU sub-systems such as the cooler heaters, the calibrators and the thermometry sensors plus housekeeping parameters with the DPU through digital interfaces. This function covers the sensors biasing, the signal amplification and the digitisation of the Analog parameters. The SCU is also in charge of providing all the sub-systems with secondary power supply lines from the S/C 28 V interface by means of the PSU (a set of DC/DC converters). This PSU is associated to a supply current

monitoring capability for safety purpose. As illustrated below the DRCU has electrical interfaces with:
• the FPU
• the DPU
• the PDU (S/C)
• the EGSE (for shutter ground test only)

The DRCU is composed of two subsystems; the Detector Control Unit (DCU) and the FPU Control Unit (FCU) which are both housed in a single box. Each system has analogue interfaces with the systems in the CVV and digital interfaces with the DPU for the transfer of scientific data, telemetry and commands/acknowledge packets. There is no electrical connection between the DCU and FCU.

A common SMPS (with several outputs) is part of the DRCU box. The secondary output lines of this SMPS supply the sub-systems via distribution electronics whose function it is to monitor the current consumption of each sub-system and enables switching off in case of over current.

Electrical interfaces with the FPU are located in the front cover of each board while interface with DPU are located in the rear cover of the DRCU box : this configuration minimizes wiring length and risk of cross-talk of sensitive analogue signals of the FPU/DRCU interface.

4.1.2.2 Mechanisms Control Unit MCU

The MCU controls and monitors the two mechanisms of the SPIRE instrument, viz.:
(i) the Spectrometer Mechanism (SMEC). The control is typically based on a scan at a configurable speed, but can be set-up on the basis of a step position control in case on use of the step and integrate mode of the instrument;
(ii) the chopper and jiggle axis of the Beam Steering Mirror subsystem . The control is a position step control pattern.

The position and rate control of the 3 axes is performed by an Analog Devices 21020 DSP chip using PID control architecture. The MCU software is based on a master scheduler using the principle of time sharing without a specific multi tasking kernel. The tasks to be performed shall be called on the basis of a software interrupt generated by the inner DSP timer. The software interrupt defines the global sampling time (ie the computation cycle) of the DSP tasks at a programmable rate of between 100 and 300 μs. During each cycle, the following tasks are performed :
(i) the SMEC control loop task
(ii) the BSM chop control loop task,
(iii) the BSM jiggle control loop task,
(iv) the communication with the command line and other various internal DSP tasks.

The scan parameters are put in memory for configuration purpose with a command bi-directional serial line.

The MCU receives commands from the DPU via a 32-bit, bi-directional serial interface. The MCU also sends three types of data back to the DPU:
(i) **H/K Data**: which consists of the readout of single variables read by the command line at a rate of about 1 Hz. The H/K variables readout by a get_parameter command from the DPU. The delay between transmission of a H/K readout request and the response is about 500 μs. Typical H/K variables include, mean SMEC scan speed, SMEC control status, SMEC encoder status, Chopper mean position, Jiggle mean position etc.
(ii) **Trace Data**: The trace data is a buffer in the DSP memory which contains a long data acquisition. The number of trace variables, the sampling time, the length of the data buffer are programmable. This buffer can be read off-line, i.e. when the DPU sends a dedicated command for each varaible. Typically, the trace data mode shall be used for the scanning of large number of samples for engineering purposes;

(iii) **Telemetry Data**: The telemetry data is the SMEC time counts between two encoder 2 micron positions and the BSM chop and jiggle positions The telemetry data is transmitted on a fast 16-bit, 1 MHz serial line. The telemetry line is independent of the DSP control and monitoring and is used for the delivery of data related to the detector signals , with a high level of synchronisation.

Physically, the MCU is composed of a motherboard which acts as the back-plane for the with two MAC (Multi-axis Controller) boards, the two SMEC boards a the single BSM board. All these boards have a prime and redundant side. Figure 4-10 shows the schematic block diagram for these boards. The MAC interfaces via two digital interfaces with the DPU. The first link is a bi-directional 32-bit serial interface for the transmission of telecommands from the DPU and the retransmission of acknowledge words back to the DPU. This interface is controlled by a FPGA chip. The commands are then passed to the DSP chip. During normal operation, the DSP cycles at a frequency between 10 kHz and 3.33 kHz through the following sequence:

(i) the SMEC digital PID control algorithm is updated;
(ii) the chop stage BSM digital PID control algorithm is updated;
(iii) the jiggle stage BSM digital PID control algorithm is updated;
(iv) the trace table is updated;
(v) any commands from the DPU are uploaded from the FPGA and the acknowledge reply is sent.

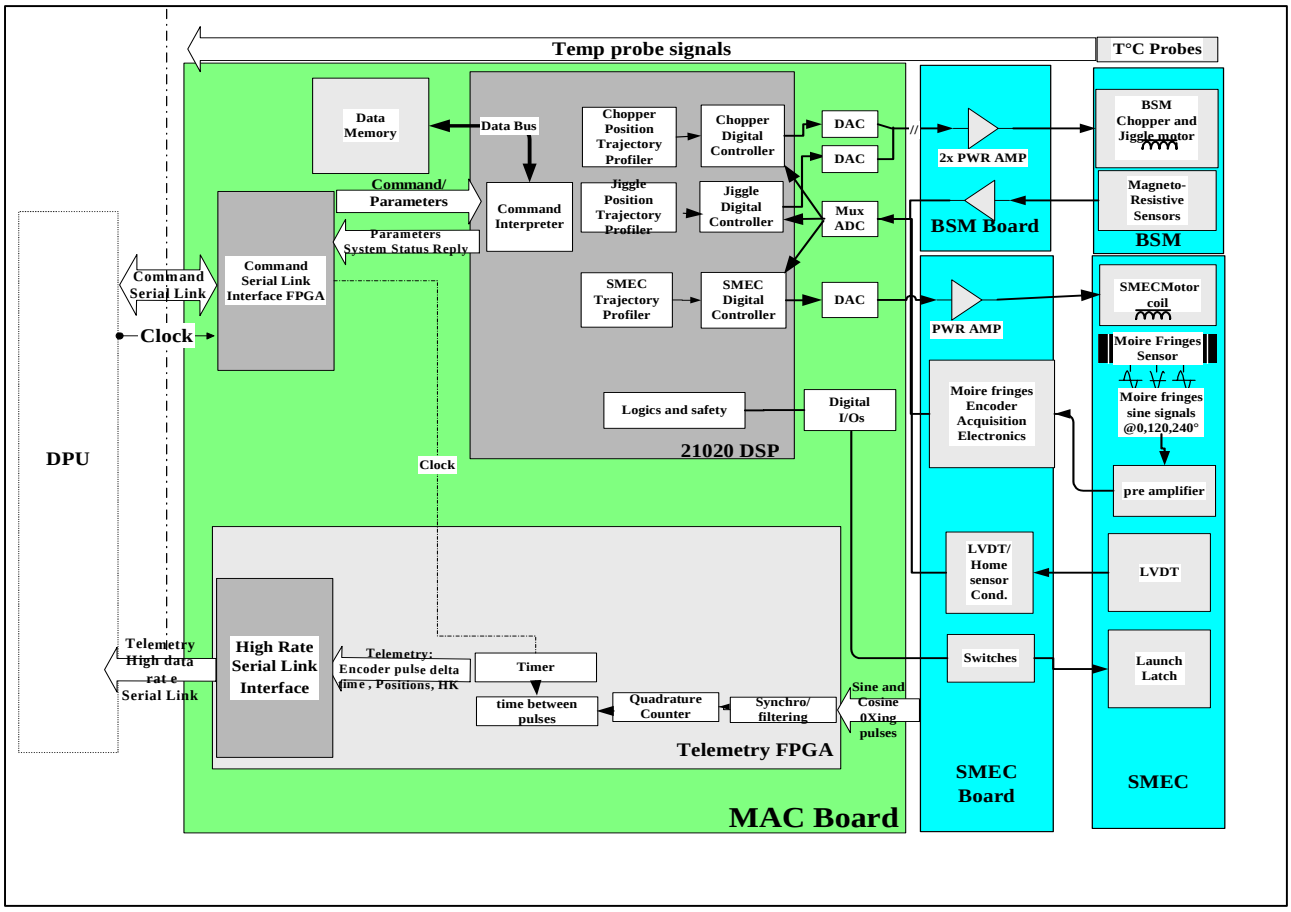

Figure 4-10 - Architecture of the MCU.

The PID algorithm is implemented in software using standard 21020 assembly language without the use of a specific off-the-shelf real time operating kernel. The assembly language is chosen because Analog Devices provides directly specific libraries to produce PID, filtering, arctan computation with a high efficiency and readability.

The SMEC is typically required follow a saw-tooth position profile as shown in Figure 4-11. The scan nominally starts from 3 mm before the Zero Path Difference (ZPD) position, through to 32 mm. The absolute position of the mirrors vs. time is required in order to be able to obtain a spectrum from the detector signals. This is done in a two step procedure.

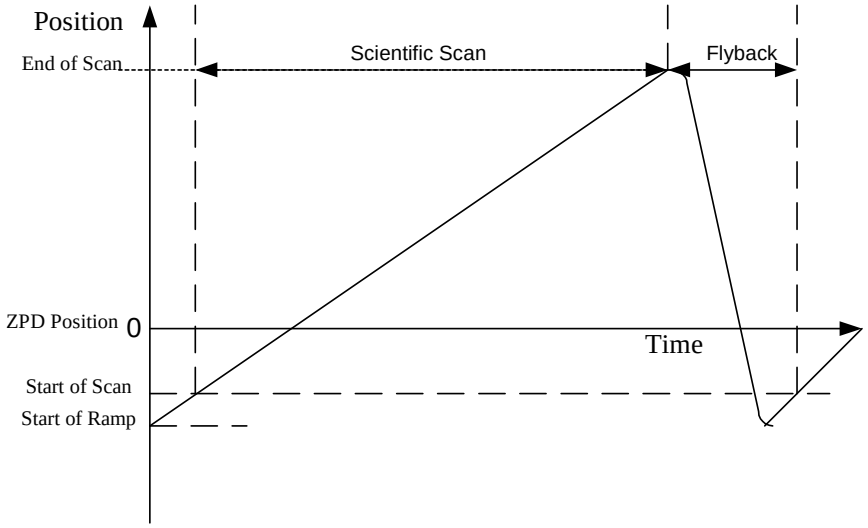

Figure 4-11 - SMEC Scan characteristics

BSM position sensing: The position of the BSM chop and jiggle stages is monitored via coil inductance. Along with magneto resistive sensing elements.

4.1.2.3 Subsystems Control Unit (SCU)

4.1.3 Detector Control Unit (HSDCU)

The Detector Control Unit controls the Detectors of the photometer and the spectrometer, provides the correct detector bias current, conditions the output from the detectors and converts the analogue signals into digital signals.

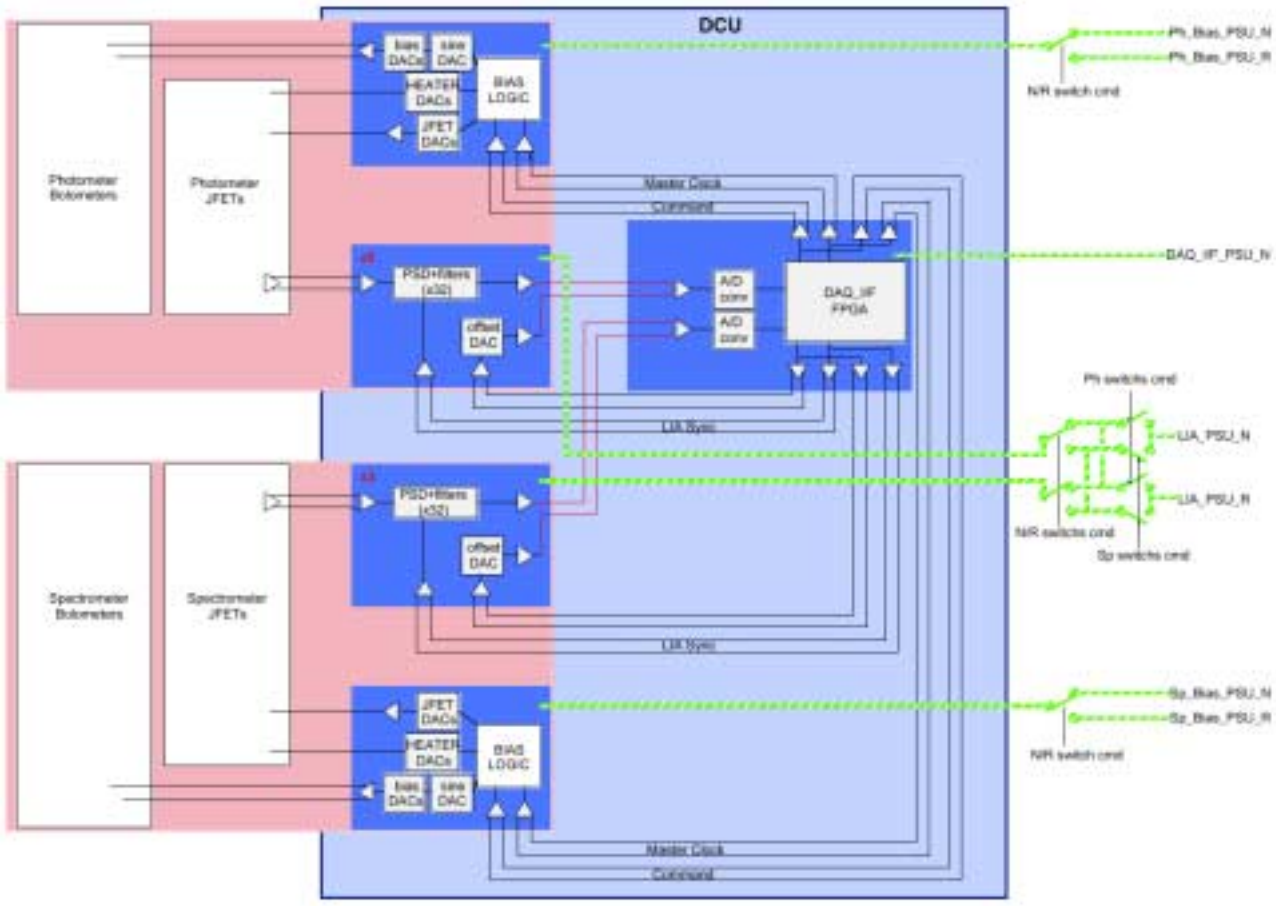

Figure 4-12 – Schematic block diagram of the detector

This is achieved with three different cards mounted in the DCU, viz. the LIA Card, DAQ+I/F Card and the Bias Card. Each LIA Card takes 32 differential signal inputs from the detectors and preamplifies the positive and negative signals with four OP-400 operational amplifiers. They are then fed into a DG303A CMOS Analogue switch

Table 4-1 – Detector driver electronics specifications.

Number of channels	48 96 144 24 48	PLW BDA PMW BDA PSW BDA SLW BDA SSW BDA
Signal AC amplitude	10 mV	Dark condition
Signal DC level	5 mV	JFET V_{Osmax}
Common mode offset	1 V	DC
Noise allocation	7 nV/Hz$^{1/2}$ 0.64 pA/Hz$^{1/2}$	0.05 to 25 Hz
Input capacitance	< 100 pF	
Input impedance	> 1 M	
Base band signal bandwidth	0.03 to 5 Hz 0.03 to 25 Hz 5 Hz	Photometer Spectrometer Thermometry
Input noise impedance	> 7kΩ	
Common mode rejection	- 60 dB	30–300 Hz

4.2 RF Filters

The bolometer detectors in the spectrometer and the photometer are sensitive to all frequencies of electromagnetic radiation. Although the BDA feedhorns act as effective high pass filters, it is essential that emissions from within the FPU unit be minimised to eliminate spurious sources of signal. The harnesses that pass from the WE on the SVM to the FPU can act as receiving antennas. The voltages received by the harnesses outside the cryostat could then possibly retransmit EM radiation within the FPU and corrupt the signals from the BDA.

To eliminate this possible source of noise on the detector signal, low pass RF filters protect all harnesses passing into the FPU. Three basic types of harnesses pass into the FPU; (i) bolometer signal wires, (ii) bolometer bias wires, and (iii) FPU sub-system drive and instrumentation wires (eg. Coil drive current wires, thermistor readout signals etc.). These three types of harnesses can be identified on the SPIRE system diagram, Figure 3-1. The bolometer signals are filtered within the JFET boxes and will described separately below in §4.3. The bolometer bias harnesses and the subsystem harnesses are conditioned by sets of filter boxes.

There are six filter boxes for the subsystems are located on the spectrometer side of the FPU (see Figure 3-5). They have two 37 way MDM socket connectors on the WE side of the box connected to two 37 way MDM plug connectors on the subsystems side of the box. Each pin on WE side of the box is connected to an equivalent pin on the detector side via a muRata VFM41R01C222N1C 3-terminal varistor-capacitor EMI filter. There are therefore 444 individual filters allocated to the subsystems. The filter requirement is that it rejects all frequencies from 500 MHz to 10 GHz at –60 dB. The filter operates by conducting high frequency noise signals to ground via the third terminal of the filter. The bode diagram showing the insertion losses for the filter *at room temperature and with a 50Ω source impedance* is shown in Figure 4-13.

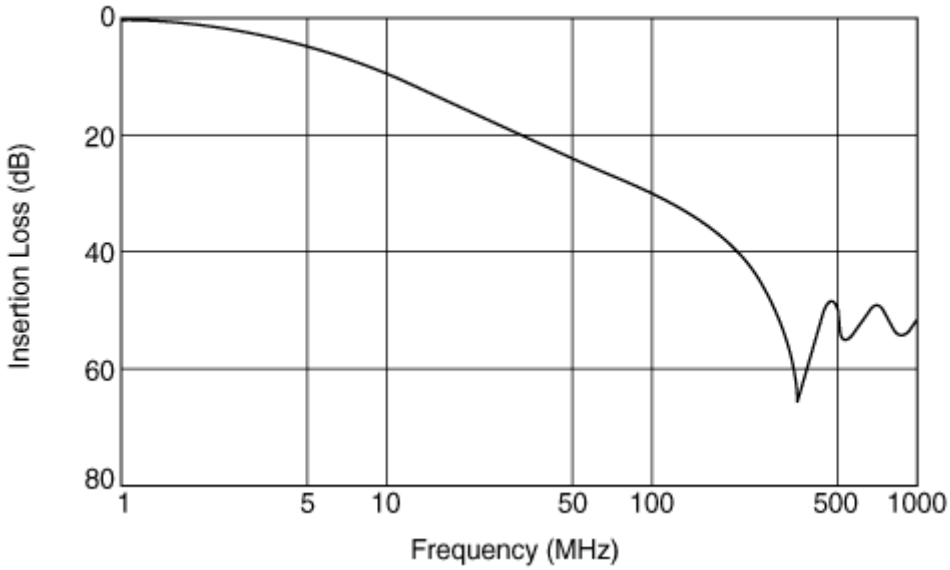

Figure 4-13 – Insertion losses for the muRata EMI filters.

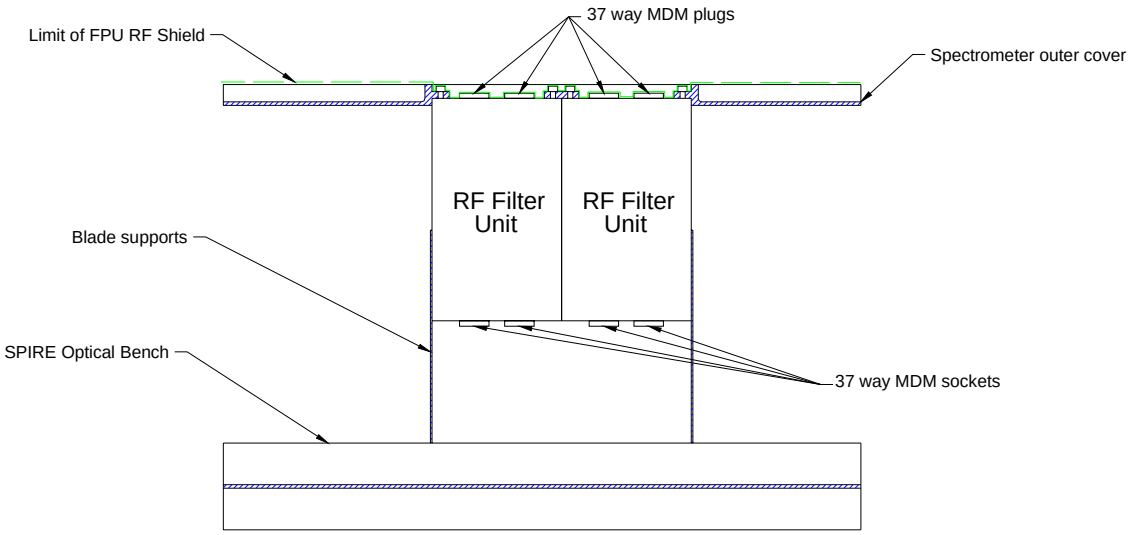

Figure 4-14 - Schematic representation of the Filter Box mounting technique showing effective limit of the FPU RF shield.

The filter units are attached to the SPIRE optical bench by a blade support structure as shown in Figure 4-14. As the spectrometer cover is placed over the SPIRE optical bench, the outer cover meets with the filter units. The filter boxes are then screwed tightly to the outer cover with a 30 mm bolt spacing and become a part of the RF tight FPU enclosure. The effective outer extent of the FPU RF tight enclosure is shown on Figure 4-14 by the green dashed line. The required mechanical rigidity of the filter boxes come from the bolts attaching them to the outer cover. The first natural frequency of the filter boxes is above the required 200 Hz.

4.3 JFET units

The functionality of the JFET in the read out electronics of the BDAs is adequately described in §4.4.4 below. The JFET boxes are described here as a sub-system in themselves. Electrically isolated

Model U401 Silicon JFETS are used to read out the SPIRE detectors, mounted in groups of 24 on silicon nitride membranes. The contract traces and JFET source resistors are lithographed on the membranes. The JFET modules for the photometer and spectrometer are mounted in separate enclosures (illustrated in Figure 4-15) on either side of the FPU.

There are two sets of JFET boxes, one set drives the signals from the photometer detectors and the other set drive the spectrometer detectors. To minimise the signal loss or phase distortion due to harness capacitance, the length of the harnesses between the JFETS and the bolometers needs to be minimised. Hence, the two groups of |JFETs are located on the Herschel optical bench as close to the FPU structure as is practical.

Thermal Design: To attain the required noise performance, the individual JFET devices need to operate at around 110K. This poses several challenges to the thermal design of the modules:

(i) the surrounding structure is at the same temperature as the Herschel optical bench. The thermal load from the JFETs to the JFET structure has to be minimised so as to minimise the power used to heat the JFETs. The nominal limit for all the JFETs in a single operating mode is 33 mW.;

(ii) the thermal load from the JFETs to the structure needs also to be limited to ensure that the heat load to the FPU through the detector harnesses is minimised.

High thermal impedance is therefore required between the JFETs and the rest of the structure. This requirement is achieved through the mounting of the devices on thin silicon nitride membranes and low cross section lithographed wires to the individual JFET terminals. The silicon nitride membrane also meets the functional requirement of providing a high resonant frequency.

As described above in §4.2, the length of harnesses from the SVM to the FPU provide a potential source of EMI within the FPU. Filters identical to the ones described above in §4.2 are inserted on all the inputs to the JFET boxes. Included in the structure of the JFET box is the provision of filter units identical to the ones used inside the FPU to filter the AC bias signals going to the detectors. All the harnesses passing from the JFET units to the FPU are shielded. This effectively enlarges the RF shielding provided by the FPU enclosure to include these shields. This identified as the yellow coloured section on Figure 3-27.

The structure is rigidly attached to the Herschel optical bench by four bolts. It is fabricated from aluminium in order not to generate thermal stresses at cryogenic temperatures. The first mode of vibration is above 100 Hz. The structure also has a thermal strap connecting it to Level-2 of the cryostat. The structure is electrically isolated from the Herschel optical bench by Vespel washers (TBC).

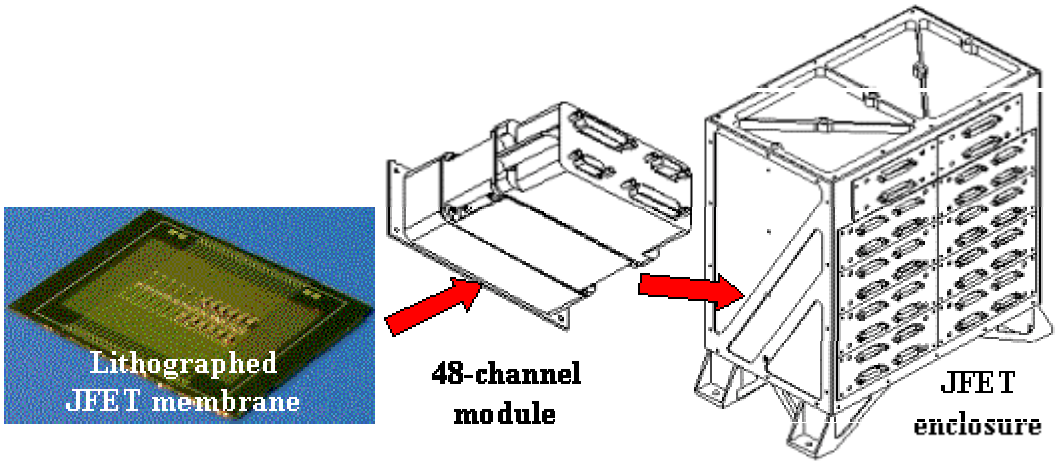

Figure 4-15 - SPIRE JFET module design showing the JFET modules and the filter modules.

4.4 Bolometric Detector Arrays

4.4.1 Principle of semiconductor bolometers

The SPIRE detectors are semiconductor bolometers. The basic principles of operation are illustrated in Figure 4-16.

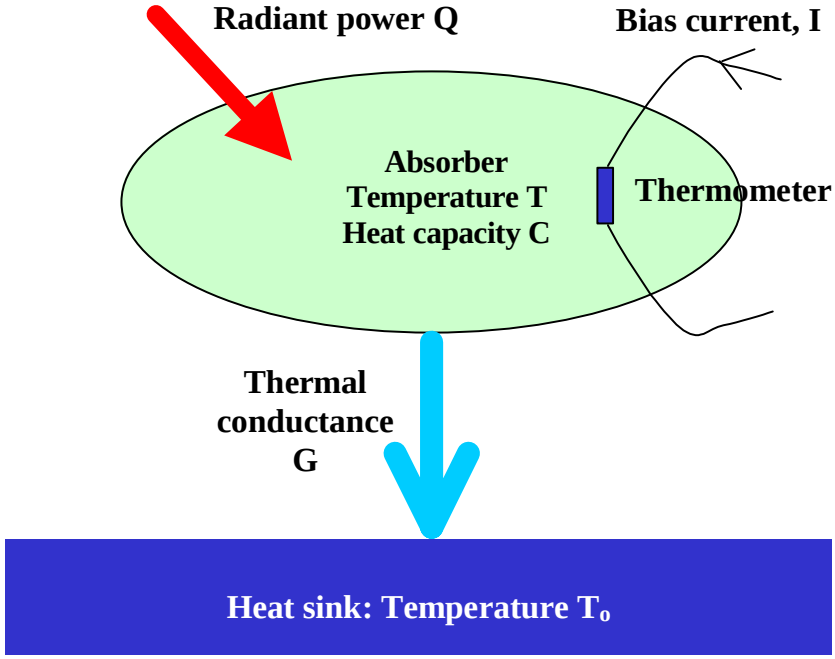

Figure 4-16 Principles of bolometer operation.

The bolometer comprises a low heat capacity absorber designed to absorb the incident submillimetre radiation. The absorber is coupled to a heat sink at a fixed temperature T_o by a thermal conductance, G. Absorbed radiant power, Q, is thermalised in the absorber resulting in an increase in temperature over the equilibrium value in the absence of illumination. A semiconductor thermometer is attached to the absorber. A bias current, I, is passed throughout the thermometer, and the corresponding voltage across the thermometer is measured. The bias current dissipates electrical power $P = I^2R$, which heats the bolometer to an operating temperature T, slightly higher than T_o. The main performance parameters for bolometric detectors are:

Responsivity:	$S = dV/dQ$
Noise Equivalent Power NEP:	$= a(4kT_o^2G)^{1/2}$ where k is Boltzmann's constant and a is a constant of order 1.
Time constant:	$\tau \sim C/G$ where C is the heat capacity of the bolometer.

For a full account of the theory and practice of semiconductor bolometers, see, for example, Mather (1982), Griffin & Holland (1988), Richards (1998).

4.4.2 SPIRE bolometer performance requirements

The combination of good sensitivity and speed of response requires low-temperature operation. The ultimate limit to the sensitivity of the SPIRE instrument is determined by the thermal background power from the telescope. The background power incident on a SPIRE detector is typically a few pW , almost all of which is

from the telescope. This corresponds to a background photon rate of ~ 10^{10} photons per second. Note that this is enormously larger than in the case of optical observations. The accurate subtraction of this thermal background is essential if the much fainter astronomical signals are to be measurable. Furthermore, statistical fluctuation in the arrival rate of these background photons creates a fluctuating noise power which represents a fundamental thermodynamic limitation to the sensitivity. For SPIRE, the associated photon-noise limited NEP, NEP_{ph}, is a few x 10^{-17} W $Hz^{-1/2}$. In order to achieve photon noise-limited performance, the inherent NEP of the detector system must be comparable to or lower than this. The noise of the bolometer itself is a combination of Johnson noise and phonon noise (due to the quantised flow of thermal energy from the bolometer to the heat sink).

The instrument performance models described in §6 contain detailed calculations of the background power levels and sensitivity for SPIRE. In addition, the operating modes require time constants of 30 ms for the photometer and 16 ms for the FTS. With current bolometer technology, these sensitivity and time constant requirements can be met by detectors operating at a temperature of around 0.3 K, cooled by a ^{3}He refrigerator.

4.4.3 SPIRE bolometer design and specifications

SPIRE will use arrays of semiconductor bolometers developed at Caltech/JPL. Figure 4-17 illustrates the basic detector design. The absorber is a "spider-web" of metallised silicon nitride. This appears as a filled planar absorber to the submillimetre radiation which has a wavelength much longer than the grid spacing. The spider-web structure has high mechanical strength and a low filling, factor providing low heat capacity and immunity to glitches that can be caused by ionising radiation. The diameter of the spider-web is typically a few times the wavelength to be detected. The thermometer is a small (20 x 100 x 300 μm) crystal of Neutron Transmutation Doped (NTD) germanium. This material is highly suited for use in low temperature bolometers as its thermal behaviour closely approaches that of an ideal thermal device, the material displays very low 1/f noise, and the manufacturing processes are highly repeatable and reliable. A wide range of NTD materials is available to tailor the impedance of the device to the desired range for the chosen operating temperature. Large arrays of bolometers can now be made, as illustrated by the array wafer shown in Figure 4-17.

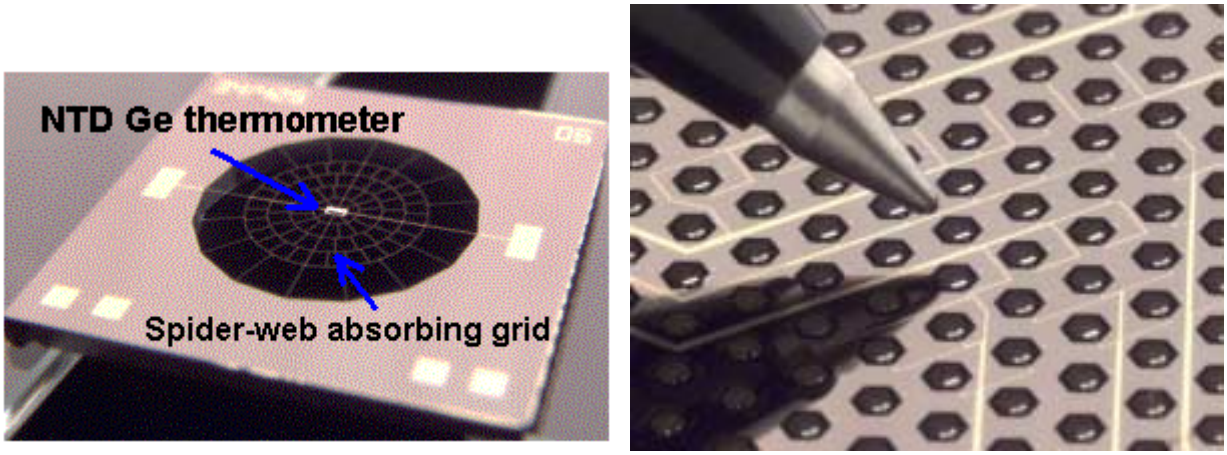

Figure 4-17 - Left: individual spider-web bolometer. Right: large-format array wafer used as a 350-μm SPIRE prototype array. The absorbers have a 0.725 mm diameter with a grid spacing of 72.5 μm. The filling factor is 8%. The absorber is suspended by five 5-μm wide, 240-μm long support legs. The thermistors are placed to one side of the absorber and read out with two leads deposited on a single, 18-μm wide support member.

4.4.4 Bolometer readout electronics

The resistance of the detector at the operating point is typically 5 MΩ. Lower values make it difficult to avoid being preamplifier noise limited while higher values can pose problems with electromagnetic pick-up

and sensitivity to microphonic disturbance. The detector noise is typically 10-20 nV/Hz$^{-1/2}$, and the noise of the readout amplifier must be of this order or less. With current transistor technology, this requires the use of silicon JFETs, which must operate at a temperature of around 100 K, and must also be located as close as possible to the detectors. This is why SPIRE employs JFET amplifier modules as part of its cold FPU. The essential features of the readout electronics are shown in Figure 3-26. The bolometer is biased (heated to its optimum operating temperature of around 1.3T_o) by a sinusoidal current bias at a frequency of at least 100 Hz, applied via the 10-MΩ load resistors. The bias excitation is much faster than the thermal time constant, so that bias itself does not produce a temperature modulation. This is preferred over DC bias as it up-converts the signal information to the bias frequency, getting well above the 1/f noise knee of the JFET readout amplifiers. With this arrangement, because of the inherently low 1/f noise of the bolometers, the1/f noise knee of the system can be very low (less than 0.1 Hz).

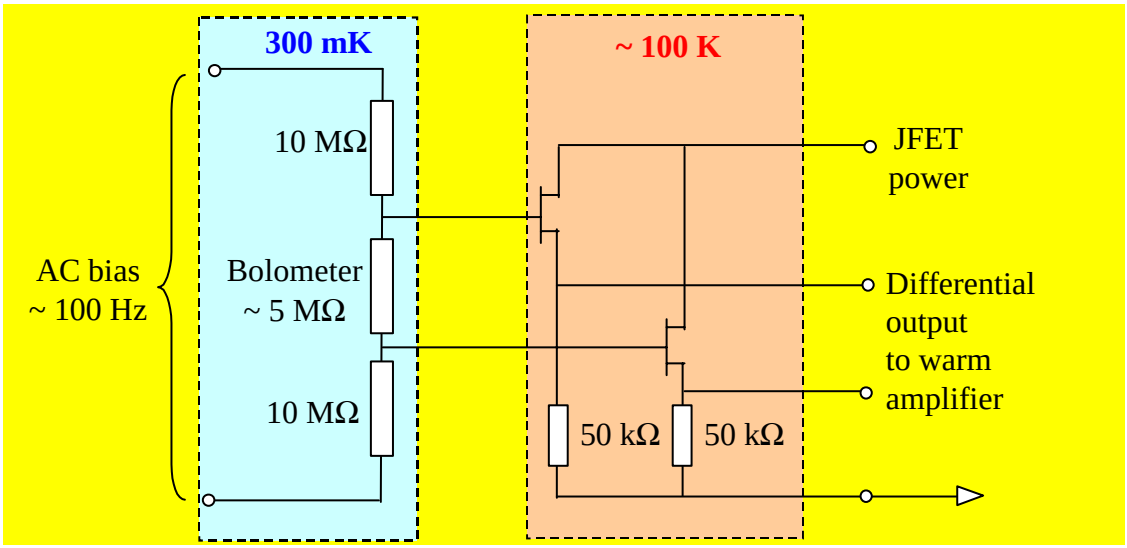

Figure 4-18 Bolometer bias and cold readout circuit

4.4.5 Feedhorns and bolometer cavities

The size of a composite bolometer (typically mm diameter) is small compared to the telescope diffraction spot (in the case of SPIRE, with f/5 final optics, the spot size is 2.44λF = 12.2 mm at 500 μm) and the first-pass absorption efficiency of the absorber is only ~ 50%. In order to couple the telescope beam onto the detectors in the array, conical feedhorns are used, with a short section of waveguide at the end of the horn to feed the radiation into a cavity containing the bolometer, as shown schematically in Figure 4-19. The waveguide acts as a low-pass filter as it does not propagate radiation of free space wavelength > 3.4a where a is the radius. For high efficiency, the absorber is located in the centre of the cylindrical cavity with λ/4 spacing between the front of the cavity and a reflecting back-short at the back. The feedhorns are packed in a hexagonal arrangement in the focal plane to fit as many as possible into the area available.

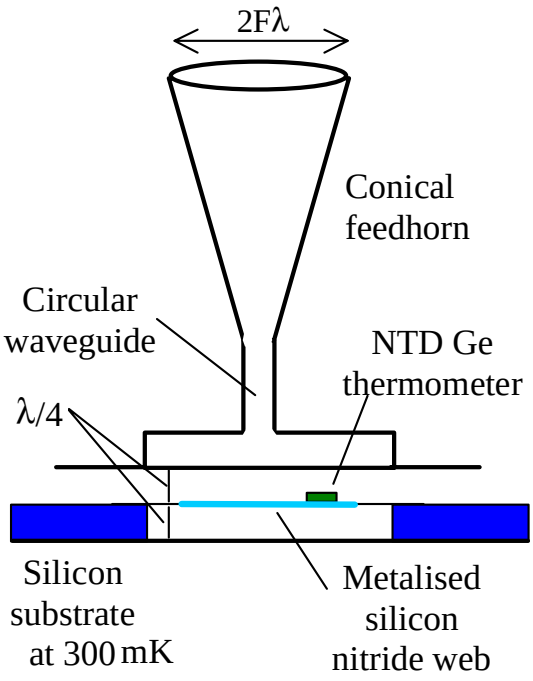

Figure 4-19 - Feedhorn and cavity design

Maximum feedhorn aperture efficiency of 70-80% is achieved for a horn diameter close to 2Fλ (e.g., Griffin 2000), corresponding to a beam spacing on the sky ~ 2λ/D, where D is the telescope diameter. The horn restricts the detector field of view, giving a tapered (near Gaussian) illumination of the telescope primary mirror (with an edge taper of approximately 8 dB in the case of SPIRE). Whilst the horns are close-packed in the focal plane, their beams on the sky do not fully sample the image unless the horn diameter is = 0.5Fλ. Several separate telescope pointings are therefore needed to create a fully-sampled image. For the 2Fλ horns 16 pointings are required in principle, as illustrated in Figure 4-20. In the case of SPIRE, the step size is dictated by the shortest wavelength channel (250 μm) and the number of steps is dictated by the longest wavelength channel (500 μm) so that a 64 point jiggle map is needed to achieve simultaneous full spatial sampling in all photometer bands.

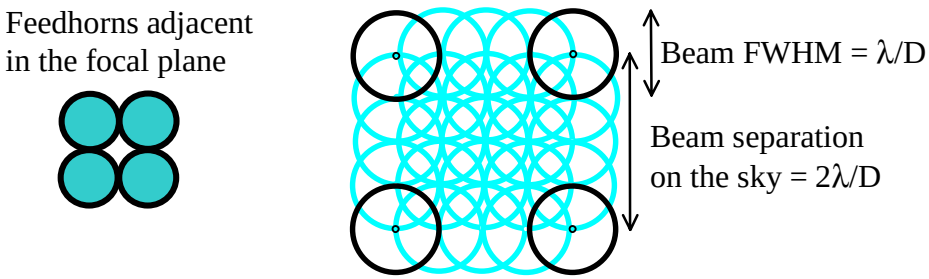

Figure 4-20 A 16-point "jiggle pattern" is needed to achieve a fully sampled map with 2Fλ feedhorns (for hexagonal packing the jiggle pattern is slightly different but 16 steps are still required).

The main advantages of feedhorn arrays are:

(i) maximum efficiency for detection of a point source with known position;
(ii) well understood horn properties, allowing good control of the beam and reliable design;
(iii) good stray light rejection - the bolometer field of view is restricted to the telescope;
(iv) good rejection of EM interference - the horn plus integrating cavity act as a Faraday enclosure;
(v) minimum number of detectors for a given total field size.

The main disadvantages are that the observing modes are complicated (jiggling or scanning) and that the efficiency for mapping is a less than the ideal (Griffin, 2000). This means that the full collecting area of the telescope is not used with maximum efficiency.

In order to collect the radiation from a point source with good efficiency, the detector through put must be of the order of λ^2. The diffraction-limited beamsize of a telescope of diameter D is approximately $\theta \approx 1.2\lambda/D$. The corresponding solid angle on the sky is $\Omega_{sky} = \pi(\theta/2)^2$. The throughput (the product of area and solid angle, which is conserved in an ideal optical system) is therefore

$$A_{tel}\Omega_{sky} \approx [\pi D^2/4][\pi(1.2\lambda/2D)^2] \approx \lambda^2.$$

The SPIRE photometer uses smooth wall, single-mode feedhorns - the circular waveguide section allows propagation of only one mode (TE_{11}). The corresponding throughput (defined as the area-solid angle product) is exactly λ^2. The spectrometer uses multi-mode feedhorns that pass both TE and TM modes.

4.4.6 Bolometer array thermal-mechanical design

The design of the SPIRE array units (called Bolometer Detector Arrays, BDA's) is illustrated in

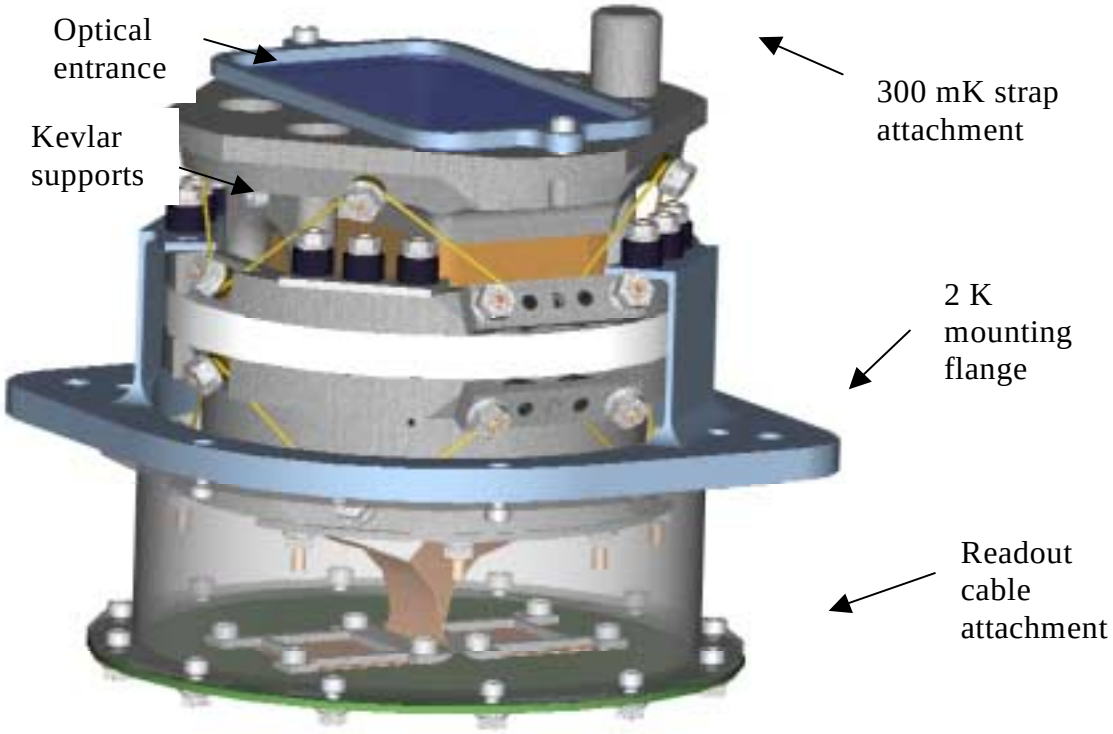

Figure 4-21. Each BDA unit is split into a 2-K and a 300-mK section. The 300-mK section contains the feedhorns, waveguides, bolometer array wafer and the supporting structure. The 2-K detector structure forms the mechanical interface between the 300-mK structure and the photometer or spectrometer 2-K enclosures. The enclosures are connected via thermal straps to the 1.7-K stage of the Herschel cryostat. The heat load from the 2-K structure to the 300-mK structure of the BDA is minimised by suspending the 300-mK section from the 2-K structure with two pre-tensioned 3000-denier Kevlar cords. Kevlar has high mechanical strength in tension and a very low thermal conductivity at this temperature, and forms gives good thermal isolation between the assemblies. The estimated heat load is less than 1.6 μW per array. The high mechanical rigidity of the Kevlar cord yields a high resonant frequency (> 200Hz).

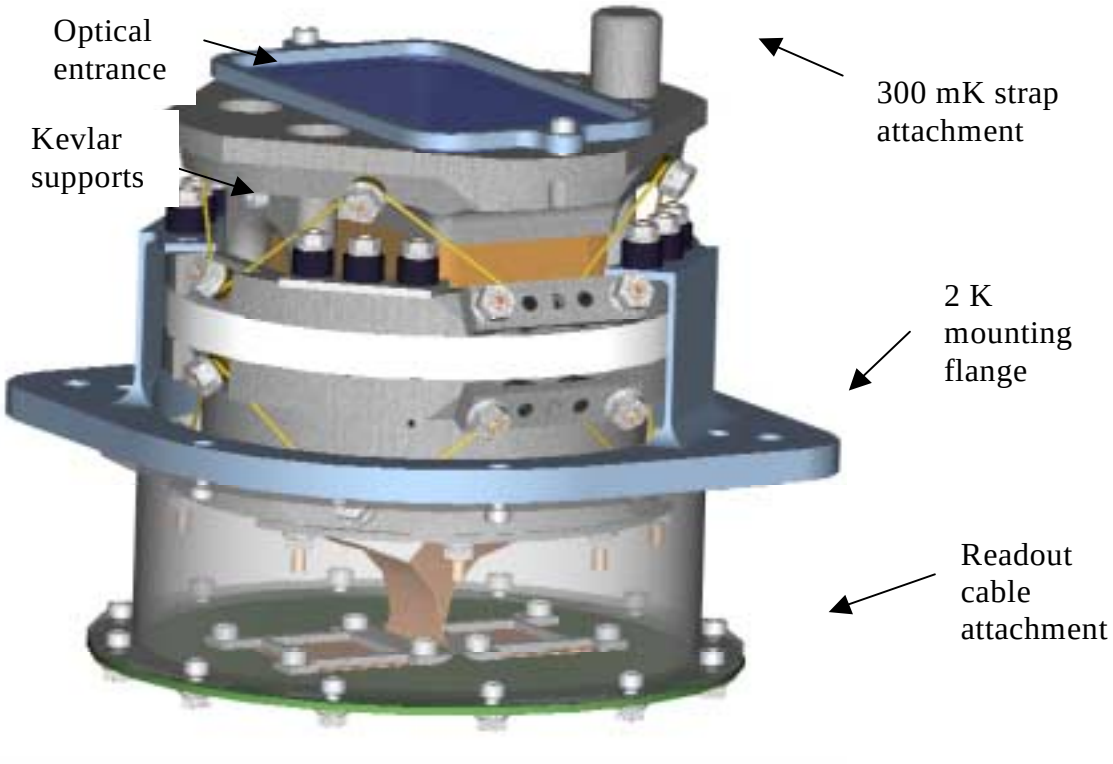

Figure 4-21 Bolometer Detector Array module

Table 4-2 lists the main design and performance parameters for the SPIRE detectors (update from SSSD):

Table 4-2 main design and performance parameters for the SPIRE detectors

Yield	> 90%
Operating Resistance	~ 5 MΩ
Time constant	< 30 ms (photometer) < 16 ms (spectrometer)
Responsivity	0.4 GV W^{-1}
Detector noise	14 nV $Hz^{-1/2}$
Efficiency of bolometer-cavity-feedhorn combination	> 0.6
BDA mass budget	0.5 kg
BDA heat load budget on ^{3}He cooler	1.6 μW

4.5 Mirrors

The basic design of the mirrors is the same as the one used for ISO-LWS. The mirrors are made from Al-6061. They all have a standard interface with the structure, i.e. an M8 screw and a pin. Each mirror is machined in a single block of aluminium (diamond cutting). Before the final finishing of the machining process, the mirrors are annealed to remove any residual stresses that may cause distortions at cryogenic temperatures. The screw part of the attachment exerts pressure only on the shoulder part of the mirror, avoiding deformation of the optical surface. The mount of each mirror is located on the optical bench by

means of several hollow pins. These pins ensure that in case of dismounting of the mirror, it will be reassembled in the same position. During integration of the mirrors in the SPIRE structure, the mirrors are mounted on brackets. The mirror mounts are designed to have the first natural mode of vibration above 200 Hz. Figure 4-23 below shows a drawing of the CM5 mirror, which is the heaviest one.

For the mechanical interface between the mirror mounts and the SPIRE optical bench, the technique of using a hollow dowel pin as illustrated in Figure 4-40 is adopted. The mounting accuracy is nominally within 0.5 arc minute and 0.05 mm linearly. The mechanical interface between the mirror and the mirror mount is illustrated in Figure 4-24. This technique ensures that the rotational and translational degrees of freedom for the mirror are tightly constrained in a repeatable fashion.

The finish of the mirrors is to optical quality. This is to permit the alignment of the mirrors to be performed within the optical wave lengths (< 10 nm RMS, specular reflectivity > 80%). The emissivity of the surfaces within the sub-millimetre wavelength is to be less than 1% to minimise the spurious emissions transmitted to the detectors. The specular reflectivity in the same wavelength is in excess of 99%.

All the common mirrors, the photometer mirrors and the spectrometer mirrors are listed and briefly described in Table 4-3. The locations of the mirrors with respect to the other optical components are illustrated in Figure 4-25 and Figure 4-26. Information on the optical alignment of the instrument, and details of the corner cubes is found in the FIRST SPIRE: Optical alignment verification plan, (*Origne and Dohlen 2000*).

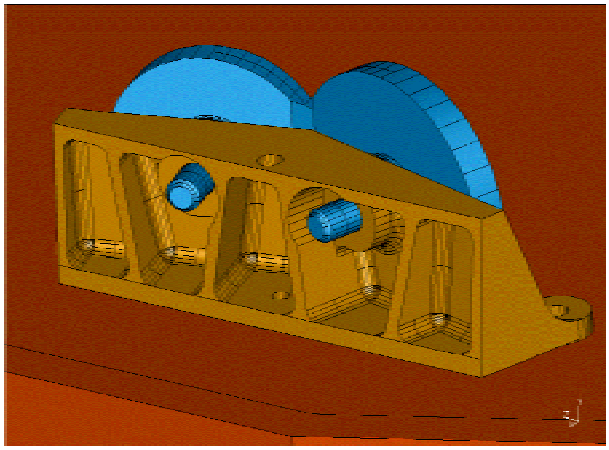

Figure 4-22 – Example of mirror mounts.

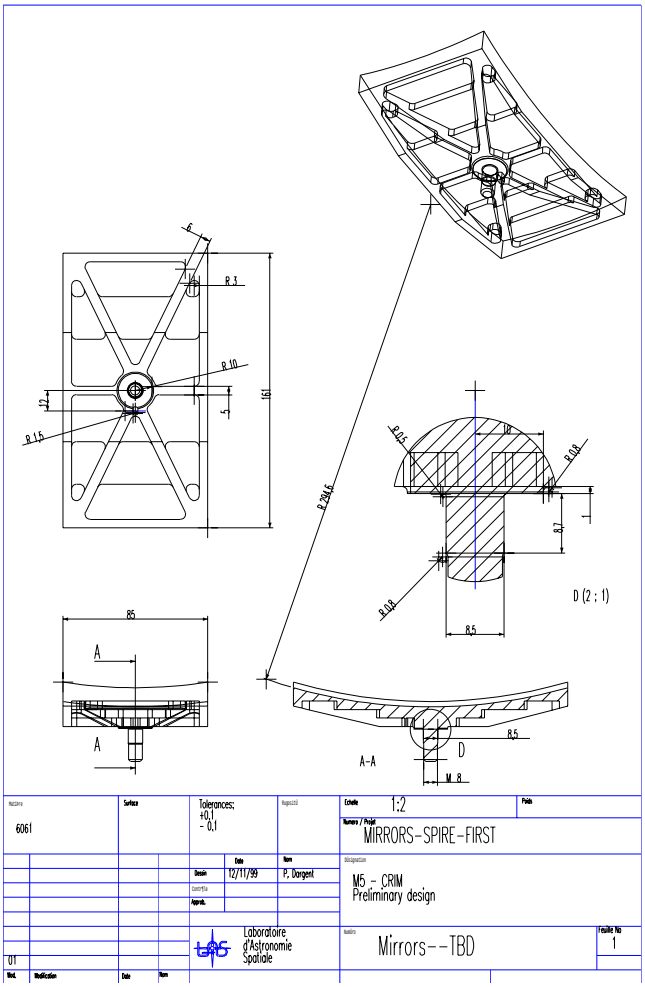

Figure 4-23 - Engineering drawing of CM5

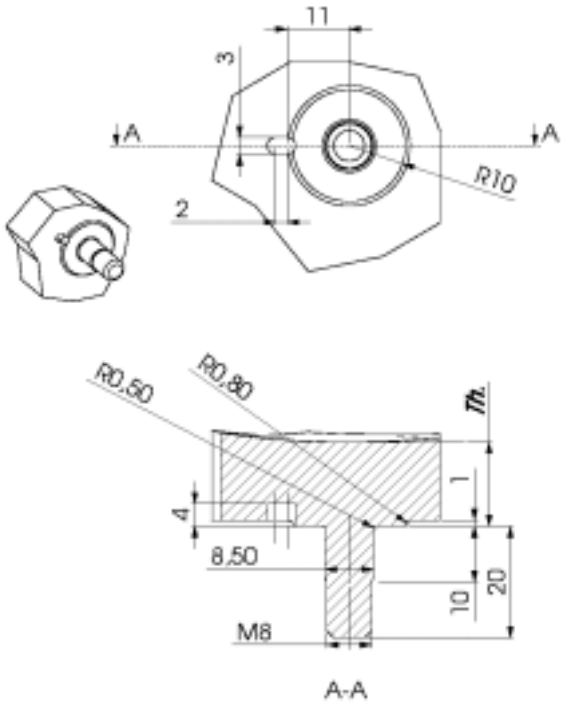

Figure 4-24 – Drawing of the Mirror/Mirror Mount mechanical interface.

Table 4-3 – General mirror specifications. The locations of these mirrors is illustrated in Figure 4-25 and Figure 4-26.

Subass'y	Mirror	Type	R or Ry (mm)	CC or Rx (mm)	Shape	Dimensions a x b or dia decenters [c , d] (mm)	Mass (kg)
Fore optics	CM3	Off-axis asphere	365.963	-0.5095	Rectangular	139x62 [-19.5, 145] See fig.	0.256
	CM4 (BSM)	Flat				15x16	0.021
	CM5	Toric	294.638	278.418	Rectangular	161x85 [19.5, -1.5]	0.360
Photometer	PM6 (Pick-off)	Toric	-307.49	-359.42	Rectangular	46x27	0.027
	PM7	Sphere	330.70		Rectangular	118x101 [0, -1.0]	0.300
	PM8	Sphere	-286.651		Circular	Ø 60	0.056
	PM9	Sphere	350.851		Circular	Ø 112	0.223
	PM10 (Fold mirror)	Flat			Rectangular	78x40 [2.5, 0]	0.065
	PM11 (Fold mirror)	Flat			Rectangular	56x53 [0, -2.75]	0.060
Spectrometer	SM6 (Pick-off)	Toric	523.79	269.92	Elliptical	9x12 [0, 1.0]	TBD
	SM7 (Fold mirror)	Flat			Rectangular	40x57 [0, 4.0]	0.044
	SM8A, B (Relay in)	Toric	230.34	202.00	Circular	Ø 60	0.112
	SM9A, B (Collimator)	Sphere	259.50		Special	Ø50	0.074
	CC face1	Flat			Special	40x60	0.044
	CC face2	Flat			Special	28x68	0.070
	CC face3	Flat			Special	28x68	0.070
	SM10A, B (Camera)	Sphere	260.00		Special	Ø60	0.112
	SM11A, B (Relay out)	Toric	196.99	169.84	Circular	Ø 74 [0, 1]	0.194
	SM12A, B (Fold mirrors)	Flat			Elliptical	21x16 [-1, 0]	0.050

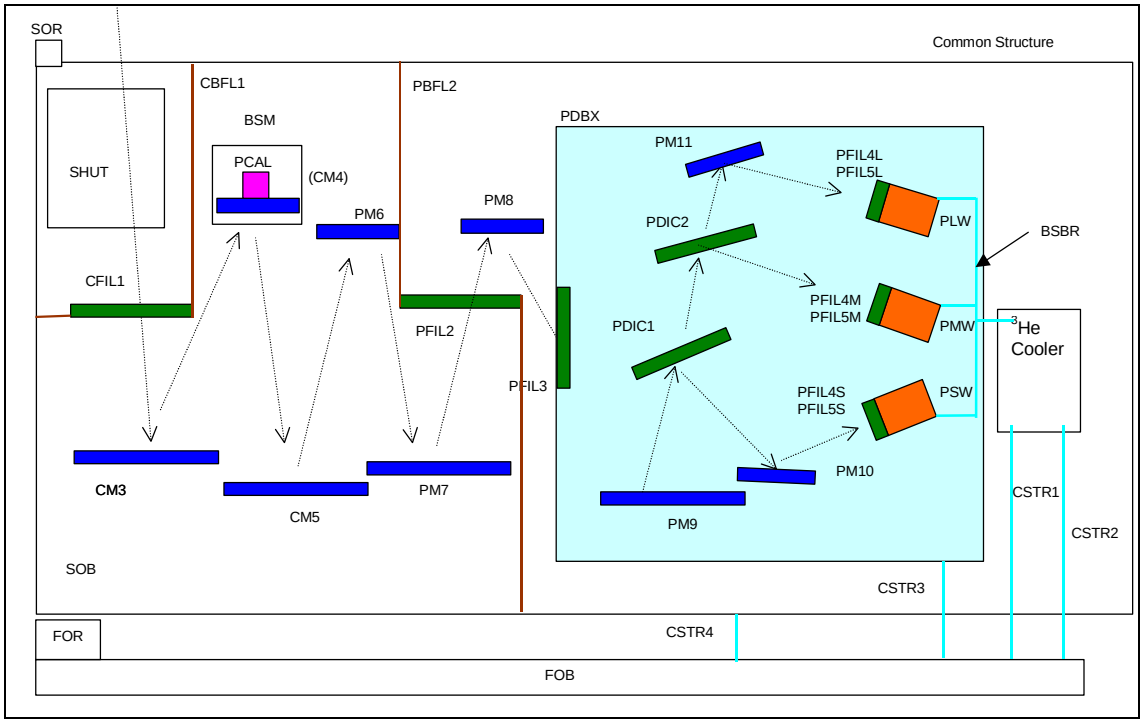

Figure 4-25 – Nomenclature for the SPIRE common and photometer mirrors, filters, beam splitters and dichroics.

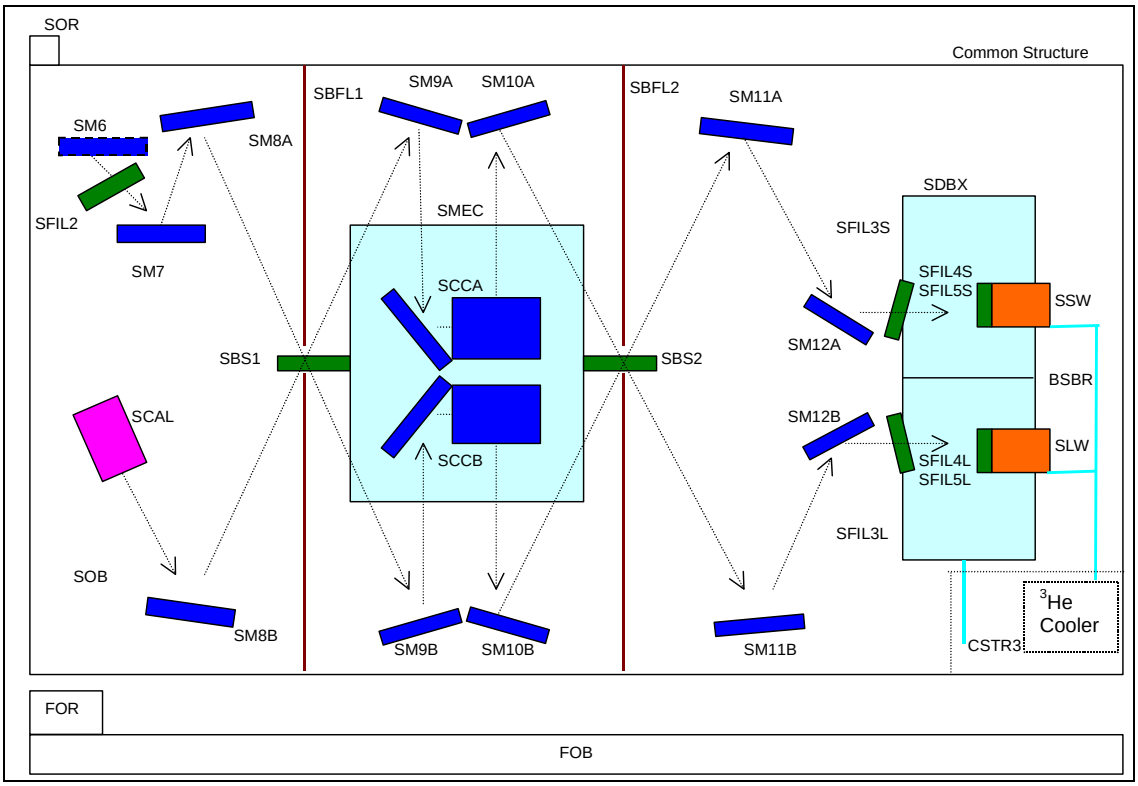

Figure 4-26 - Nomenclature for the SPIRE spectrometer mirrors, filters, beam splitters and dichroics.

4.6 Filters, beam splitters

Filters are placed at a number of positions within the SPIRE FPU, serving the following functions:

(i) definition of the spectral passbands;
(ii) minimisation of the thermal loading on the ^{3}He fridge, 2-K, and 4-K stages by rejecting short wavelength thermal energy;
(iii) minimisation of stray light getting to the detectors;
(iv) maximisation of the in-band spectral transmission.

The filters are implemented as combinations of capacitative and inductive grids formed by evaporation of copper on thin (~ 2 μm) mylar or polypropylene substrates (Lee *et al.*, 1996). Several grids are used in each filter. The grids must be maintained at accurate spacings. This is achieved either by the use of annular rings for vacuum-gap filters or solid dielectric spacers for "hot-pressed" filters. The latter are formed by pressing together a stack of grids and spacers while heating the combination. The result is a solid and robustly self-supporting filter.

The SPIRE filter chains are designed on the pessimistic assumption that the telescope surface is perfect even out to UV wavelengths. For complete blocking out to UV, 3 or 4 blocking filters are needed in the chain

The filters can withstand multiple cycling to low temperature, and are robust with respect to low temperature vibration. They are unaffected by UV and high energy particle irradiation and have a very low outgassing rate. They are based on technology developed and implemented in the ISO Long Wavelength Spectrometer and also used in numerous ground-based submillimeter instruments. The filters are interfaced to the structure by simple 3-point mounts to ensure that flatness of the grids is not affected by mechanical stress on the support rings.

4.6.1 Photometer filtering scheme

The photometer filtering and dichroic scheme is summarised in Table 4-4. The relative positioning of these items is illustrated in Figure 4-25 and Figure 4-26. The two dichoics allow the spectral bands to be directed to the three arrays with high efficiency

Table 4-4 Photometer filtering scheme.

Name	Location	Temp. (K)	Filter	Edges (cm-1)	Function (B=blocking T=optimum	Comment
CFIL1	input filter on 4K box	4K	90cm-1 low-pass edge	90% 85.5 50% 90 10% 94.5	T 17-48cm-1 B 90cm-1+	Thermal blocker. Common.
PFIL2	baffle between PM7 to	4K	75cm-1 low-pass edge	90% 71.3 50% 75 10% 78.8	T 17-48cm-1 B 75cm-1+	Thermal blocker. Common.
PFIL3	at 2K cold stop	2K	60cm-1 low-pass edge	90% 57 50% 60 10% 63	T 17-48cm-1 B 60cm-1+	Thermal blocker. Common.
PDIC1	after PM9	2K	34.3cm-1* low-pass edge	90% 32.6 50% 34.3 10% 36.0	T 17 - 34.2cm-1 R 34.4 - 47.9cm-1	Requires prototyping. Relects SW onto array. Transmits
PDIC2	after PDIC_1	2K	24.5cm-1* low-pass edge	90% 23.3 50% 24.5 10% 25.7	T 17.2 - 23.9cm-1 R 24.5 - 34.2cm-1	Requires prototyping. Relects MW onto array. Transmits
PFIL4S	LPE definer over SW array	300mK	47.9cm-1* low-pass edge	90% 45.5 50% 47.9 10% 50.3	T 34.4-47.9cm-1 B 50cm-1+	Band-defining edge. Requires protoyping. PDIC-1 defines
PFIL5S	blocker over SW array	300mK	55 cm-1 low-pass edge	90% 52.2 50% 55 10% 57.8	T 34.4-47.9cm-1 R 55cm-1+	Blocker for SW only.
PFIL4M	LPE definer over MW array	300mK	34.2cm-1* low-pass edge	90% 32.5 50% 34.2 10% 35.9	T 24.5-34.2cm-1	Unnecessary due to PDIC-1? Band-defining edge. Requires protoyping. PDIC_2 defines
PFIL5M	blocker over MW array	300mK	43cm-1 low-pass edge	90% 41 50% 43 10% 45	T 24.5-34.2cm-1 R 42cm-1+	Blocker for MW only.
PFIL4L	LPE definer over LW array	300mK	23.9cm-1* low-pass edge	90% 22.7 50% 23.9 10% 25.1	T 17.2-23.9cm-1	Unecessary due to PDIC_2? Band-defining edge. Requires
PFIL5L	LPE blocker over LW array	300mK	30cm-1 low-pass edge	90% 28.5 50% 30 10% 31.5	T 17.2-23.9cm-1 R 30cm-1+	Blocker for LW only.

Figure 4-27 shows a prototype photometer 350-µm band filter chain transmission profile on linear and logarithmic plots. The optical and UV transmissions of the individual elements have been measured separately and multiplied together to derive the overall transmission. The horizontal lines on the logaritmic plot indicate the out-of-band rejection requirements, which are comfortably met by the filter chain.

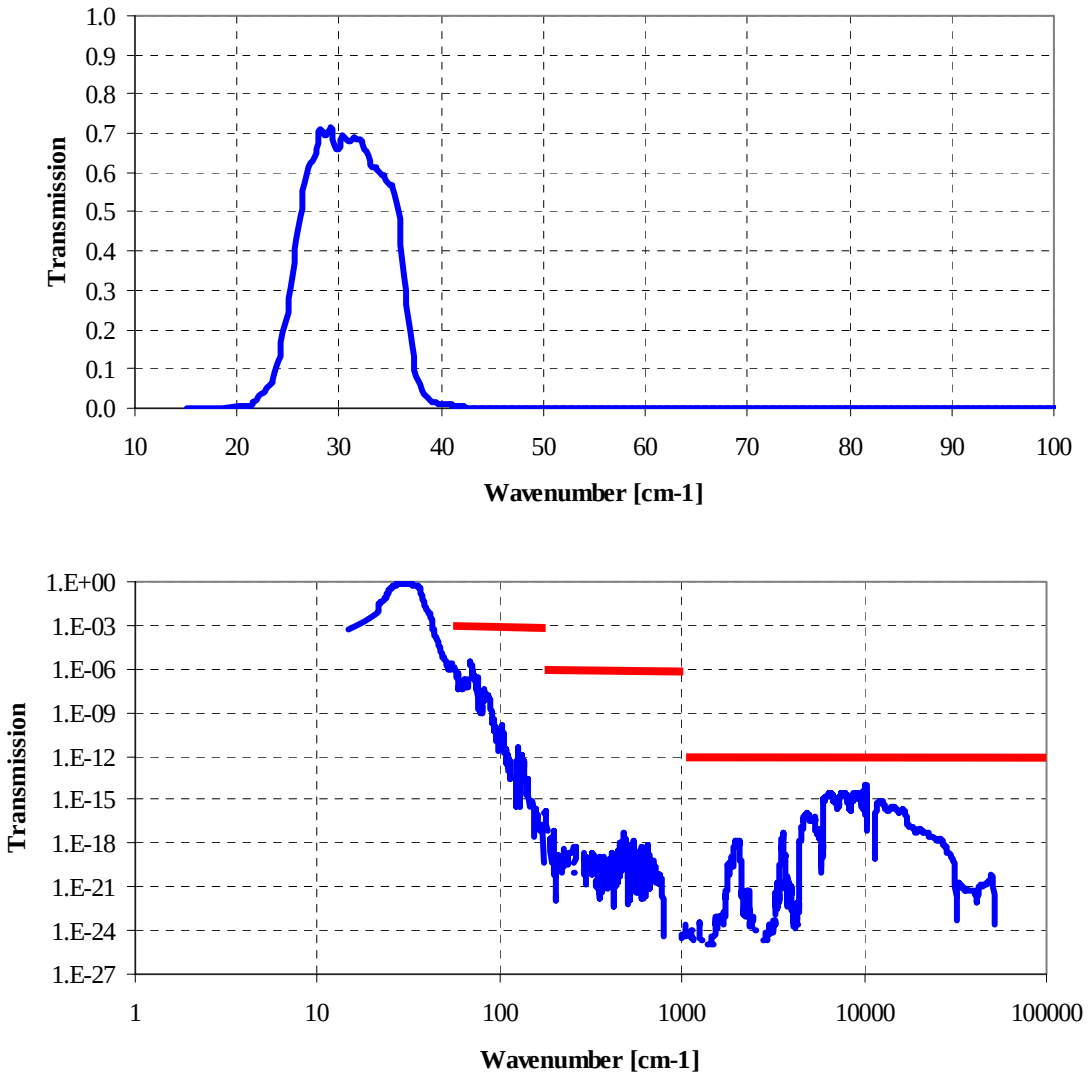

Figure 4-27 - Transmission characteristics of prototype 350-µm photometer filter chain

The SPIRE dichroics are implemented as capacitative low-pass edge filters placed at an angle to the beam. To maintain the sharpness of the edge, the angle of incidence is set at < 25°. Figure 4-28 shows typical transmission and reflection profiles for such a dichroic.

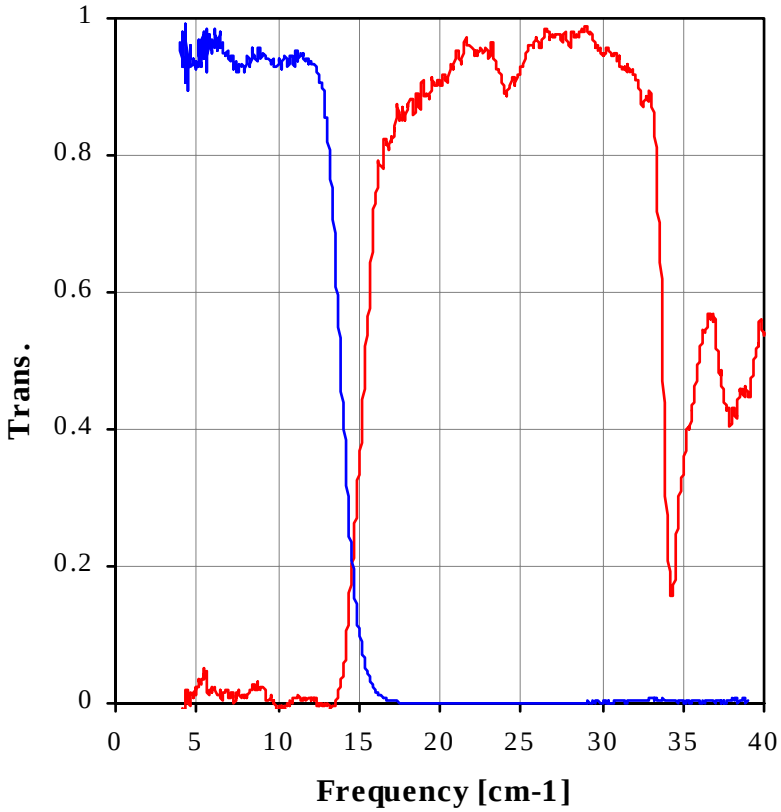

Figure 4-28 - Performance of a prototype 15-cm^{-1} dichroic (red: reflection; blue: transmission)

4.6.2 Spectrometer filtering scheme

The spectrometer filtering and beam-dividing scheme is summarised in Table 4-5. The first two filters are shared with the photometer, and the remaining ones are placed over the arrays. The beam splitters are designed to have near 50% transmitivity (T) and reflectivity (R) over the FTS spectral range. The beam splitter efficiencies as viewed by the two detector arrays are 4RT and $R^2 + T^2$, both of which should be close to 100%.

Table 4-5 Spectrometer filtering scheme.

Name	Location	Temp. (K)	Filter	Edges (cm-1)	Function (B=blocking T=optimum transmission)	Comment
CFIL1	input filter on 4K box	4K	90cm-1 low-pass edge	90% 85.5 50% 90 10% 94.5	T 17-48cm-1 B 90cm-1+	Thermal blocker. Common.
SFIL2	at pupil in SOB	4K	75cm-1low pass edge	90% 71.3 50% 75 10% 78.8	T 15-50cm-1 B 75cm-1+	Thermal blocker. Common.
SBS1	after SM8A	4K	15-50cm-1 beam splitter		T/R 15-50cm-1 (>90% 4RT)	
SBS2	after SM10A	4K	15-50cm-1 beam splitter (>90% 4RT)		T/R 15-50cm-1 (>90% 4RT)	
SFIL3S	2K cold stop (SW)	4K	60cm-1 low-pass edge	90% 57 50% 60 10% 63	T 33-50cm-1 B 60cm-1+	
SFIL4S_1	LPE definer over SW array	300mK	50cm-1* low-pass edge	90% 47.5 50% 50 10% 52.5	T 33-50cm-1 B 50cm-1+	
SFIL4S_2	HPE definer over SW array	300mK	33cm-1* HPE	90% 34.65 50% 33 10% 31.35	T 33-50cm-1 B 0-33cm-1	
SFIL5S	blocker over SW array	300mK	55cm-1 low-pass edge	90% 52.2 50% 55 10% 57.8	T 33-50cm-1 B 55cm-1+	
SFIL3L	2K cold stop (LW)	4K	55cm-1 low-pass edge	90% 52.2 50% 55 10% 57.8	T 15-33cm-1 B 55cm-1+	
SFIL4L_1	LPE definer over LW array	300mK	33cm-1* low-pass edge	90% 31.35 50% 33 10% 34.65	T 15-33cm-1 B 33cm-1+	
SFIL4L_1	HPE definer over LW array	300mK	15cm-1* HPE	90% 15.75 50% 15.0 10% 14.25	T 15-33cm-1 B 0-15cm-1+	
SFIL5L	blocker over LW array	300mK	40cm-1 low-pass edge	90% 38 50% 40 10% 42	T 15-33cm-1 B 40cm-1+	

Figure 4-29 shows the measured efficiency of a prototype beam splitter with the SPIRE wavelength range indicated by the shaded region.

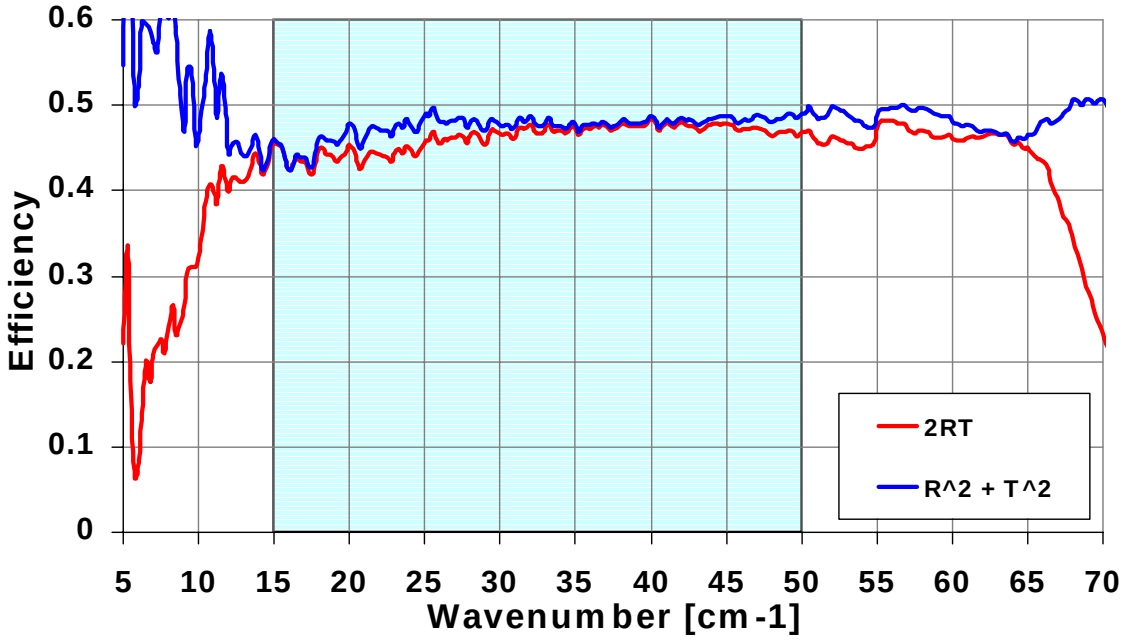

Figure 4-29 - Measured efficiency of FTS beam splitter prototype

4.7 Internal calibrators

4.7.1 Photometer calibrator (PCAL)

The purpose of the photometer calibrator is to provide a repeatable signal for monitoring of detector health and responsivity for ground testing and in-flight operation. It is not an absolute calibrator, but may be useful as part of the overall calibration scheme. The baseline design consists of a thermal source inside an integrating cavity, the body of which is at 4 K. The cavity has a light pipe output with a 1-mm diameter aperture. PCAL has a mass of < 30 gm and is located within the Beam Steering Mirror housing behind the beam steering mirror itself (M4), at an image of the system pupil (telescope secondary mirror). The fraction of M4 area obscured is 0.2%, and does not result in any loss of signal as the obscured central area is within the region of the pupil obscured by the hole in the primary mirror. PCAL shares the BSM wiring harness.

Because all of the detectors in the photometer arrays view the pupil with near equal efficiency, PCAL produces a very uniform illumination over the arrays (this is an advantage but not a requirement). It is envisaged that the calibrator will be operated in flight at regular but not frequent intervals (once per hour or more). Operation of PCAL requires the BSM to be switched off and the telescope pointing to be fixed, so that there are no sources of detector power modulation except the calibrator itself. A predetermined current excitation sequence will be applied over a period of ~ 10 seconds, and the corresponding detector signal measured.

The requirement for the brightness of PCAL is that it provide the equivalent of a unit emissivity black body temperature of 40 K or more over its 1-mm emitting area. PCAL occupies $(1/30)^2$ of the 30-mm diameter pupil area. The power level that it produces at the detectors can be compared to that due to the telescope (80-K 4% emissivity) by the following simple calculation. With a temperature of 40 K and unit emissivity, it

will produce a power at the detector of $(40/80)(1/0.04)(1/30)^2$ = 1.4% of the telescope background power. The latter is typically a few pW, so the signal level provided by PCAL is around 4 x 10^{-14} W. With a detector NEP of a few x 10^{-17} W $Hz^{-1/2}$, this provides a very large instantaneous S/N.

The 150 ms time constant requirement (30 ms goal) for PCAL is that it be comparable to or faster than the photometer detectors. A power dissipation requirement of < 2 mW has been adopted to ensure that PCAL operation makes a negligible contribution to the average load of the SPIRE FPU on the Herschel helium tank, and that local heating of the environment will not result when it is operated.

The baseline PCAL device is essentially an inverse bolometer, developed by J. Beeman of UC Berkeley for use in the SIRTF MIPS instrument. Figure 4-30 shows a photograph of a SPIRE PCAL prototype.

The device is similar in principle to the one used in the ISO Long Wavelength Spectrometer (but with lower power dissipation). A thin 1 x 1 mm dielectric substrate is coated with a metallic film and suspended from its 4-K copper housing by thin nylon threads. Electrical contacts allow a current to be passed through the metal film, heating it up to a temperature of 40 K or more. A photograph of a prototype device is shown in Figure 4-30. A typical resistance is 300 Ω, requiring ~ 2.5 mA drive current for 2 mW power. There is a 1% stability requirement on the constant-current drive, which translates to a comparable stability for the radiant power output. Prototype devices tested to date show that the radiant output requirement can be met comfortably, with some design iteration still needed to achieve the required time constant.

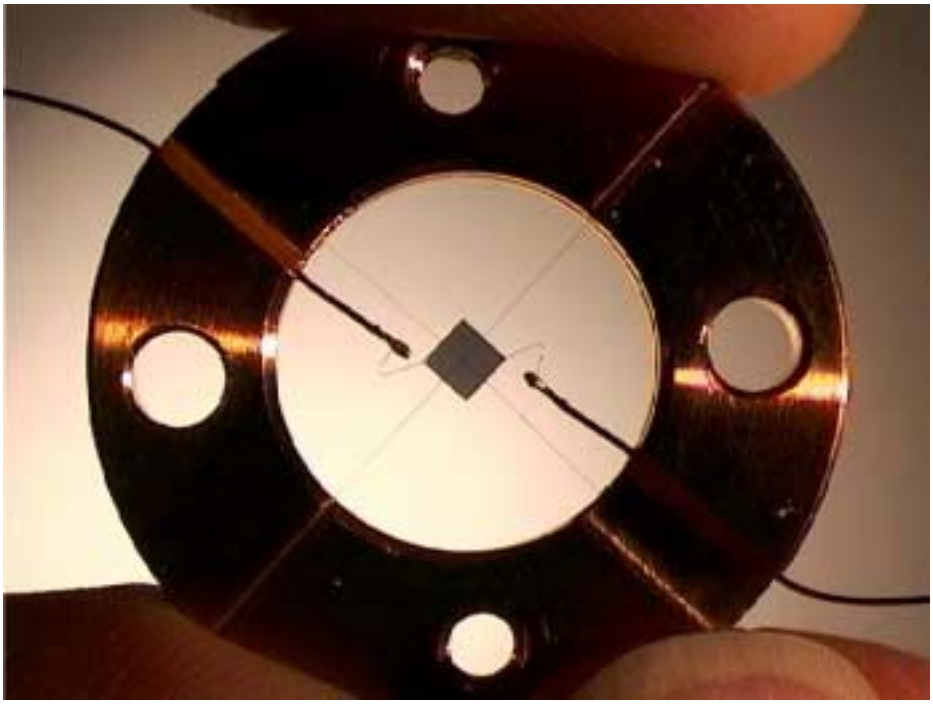

Figure 4-30 - Photograph of prototype PCAL device

4.7.2 Spectrometer calibrator (SCAL)

The signal output from one of the FTS detectors represents the difference between the spectra presented at the two input ports. When the FTS is at its zero path difference position, all frequencies are in phase and the signal is at its maximum. Astronomical signals will invariably be much smaller than the thermal background from the telescope. To minimise the required dynamic range for detector signal measurement, it is desirable to replicate the telescope spectrum in the second input port. This is the purpose of SCAL, which is designed to null the telescope emission to within 20% over the 200-400 μm range by minimising its spectrum and

brightness in the second input port of the FTS. It is located at the second input port to the FTS, at an image of the telescope pupil (diameter = 30 mm). The telescope is assumed to be at 80 K and to have an overall emissivity of 4%. It is assumed that the overall emissivity of the system is uncertain by a factor of two, and that the actual value will not be known before launch, and SCAL must therefore have sufficient adjustability to accommodate this uncertainty. The baseline SCAL design is shown in Figure 4-31. SCAL incorporates two active elements:

(i) a device similar to PCAL, designed to operate at a high temperature, filling a small fraction of the pupil area, which allows the responsivity of the spectrometer detectors to be monitored in the same way as for the photometer;
(ii) a large area heated plate to provide uniform illumination of the pupil and to replicate the dilute 80-K telescope spectrum.

The heated plate is supported on a thermally isolating tripod using Torlon struts, with the temperature measured by a Cernox thermometer. Full redundancy is implemented for both the heater and thermometer. The unit has a mass of < 200 gm and an allowed volume envelope of 50x50x70 mm. It interfaces directly to the 4-K structure.

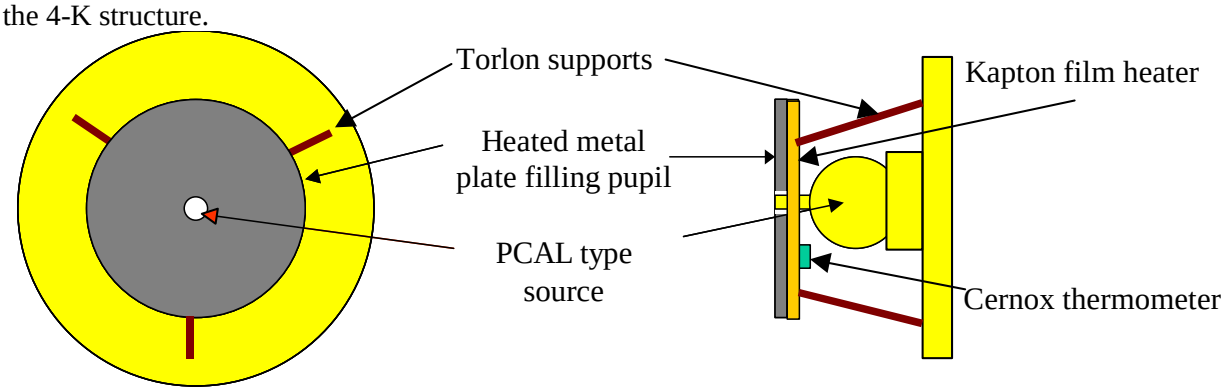

Figure 4-31 - Schematic diagram of SCAL. The diameter of the heated metal plate is approximately 30 mm.

In order to replicate the spectral shape of the telescope emission, SCAL must operate in the Rayleigh-Jeans part of the black body spectrum even at the longest wavelength covered by the FTS. This requires a temperature in excess of ~ 40 K. For a source of this temperature, filling the pupil, the emissivity must be considerably less than unity (approximately 8% if the telescope is at 80 K and has 4% emissivity). Two options are under consideration for achieving the desired SCAL heated plate emissivity:

(i) a neutral density filter may be placed in front of the device;
(ii) the plate may be coated with a suitable material to achieve the desired emissivity.

SCAL is required to have stable emission over the timescale of an FTS observation. The radiant output is required to be stable to within 1% over a period of > 1 hr. A long time constant is therefore desirable. A PID controller, implemented in software is baselined to control the SCAL temperature, and the device shall be designed to have a long intrinsic time constant. However, the cool-down time should not be excessive to prevent emission persisting after the FTS has been switched off (this could, for instance, create stray light problems for photometer observations). SCAL will be designed to have a cool-down time of ~ 15 minutes. The required SCAL power dissipation when switched on is < 5 mW with a goal of 2 mW.

Thermal testing of SCAL prototypes using a 2-mm thick aluminium plate indicate that an operating teperature of 80 K for the heated plate is achievable with power input of ~ 2 mW, comfortably within the requirement. A modelling and prototyping programme is continuing to optimise the device time constant and to control accurately the emissivity of the plate.

Note that failure of SCAL does not result in loss of the FTS, but the performance for low resolution spectrophotometery would be degraded.

Further details in of the PCAL and SCAL device may be found in the SPIRE Calibrators SSSD.

4.8 Beam Steering Mechanism (BSM)

The BSM is designed to allow the image of the sky to be positioned and moved across the detector arrays in a controlled manner. Its specifications are fully described in the BSM SSSD.

The BSM is mounted on the photometer side of the Spire Optical Bench, with the moveable mirror coincident with an image of the system pupil stop, the Herschel secondary mirror. The BSM must be able to steer the FOV in two independently controlled orthogonal axes. Rotations of the mirror around the Y-axis of the satellite represent “chopping” motions of the FOV while rotations about the Z-axis represent jiggling motions. Various observation modes of the telescope call for simultaneous rotations in both axes.

The key specifications of the BSM are summarised in Table 4-6.

Table 4-6 - Key specifications of the BSM.

	Chop stage	**Jiggle Stage**
On-sky rotation	± 2 arcminutes	± 30 arcseconds
Mirror rotation	± 2° 24’	± 0° 36’
Frequency	2 Hz (design), 5 Hz (goal)	0.5 Hz (design), 1 Hz (goal)
Maximum power dissipation	4 mW	
Settling time to within 5% of demand position	10 msec	50 msec
Angular measurement resolution	0.002°	
True angular position accuracy	0.04°	
Angular position repeatability	0.004°	

The BSM is composed of the following components:
(i) Mechanism (BSMm)
(ii) Mirror and Photometer calibration source (P-Cal)
(iii) Flex-pivots
(iv) Gimbal frame
(v) Magnetic actuators
(vi) Position sensor
(vii) Stray light baffle
(viii) Thermometer
(ix) Structural interface to the SPIRE Optical Bench (BSMs)
(x) Warm electronics (BSMe)
(xi) Launch-lock device

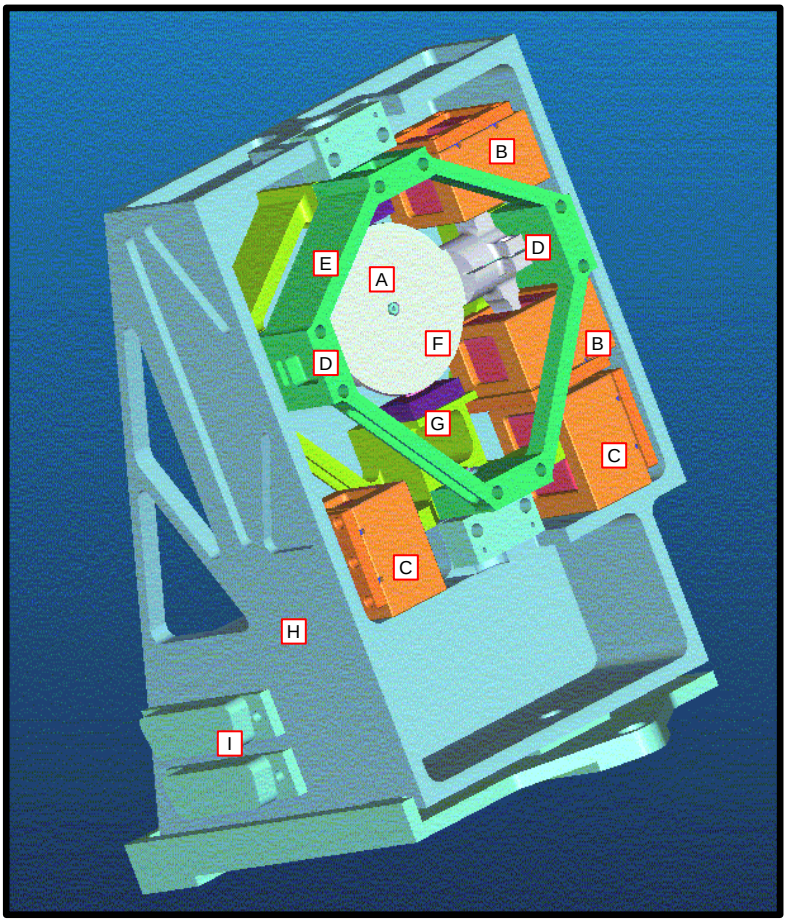

Figure 4-32 Beam Steering Mechanism: A. P-Cal, B. Chop stage motors, C. Jiggle Stage Motors, D. Chop Stage Flexure Pivots, E. Gimbal frame, F. Mirror surface, G. Chop Stage Magneto-resistive position sensor, H. BSM Structure, I. Electrical connectors. Not shown; stray light baffle.

Mirror/Chop Stage: The mirror has a diameter of 32 mm and is machined from a monolithic block of Al-6160. The mirror has an integrally machined shaft about which it rotates. And thus forms the chop stage of the BSM. The front reflecting surface is machined flat to within 1 μm rms and polished to within 10 nm RMS. The mirror has a specular reflectivity in excess of 99% and an emissivity of less than 1% in the wavelength range 200-670 μm. Perpendicular stiffening ribs machined into the rear surface of the mirror minimise the mass while retaining sufficient in plane stiffness. There is a 2.0-mm diameter (TBC) hole at the centre of the mirror, through which PCAL, the photometer calibration source (see §4.7.1), radiates when operated. This hole is conjugate with the central obscuration of the Herschel telescope. The PCAL source is mounted behind the BSM mirror with a short length of light-pipe coupling the radiation to the aperture at the centre of the mirror. The underside of the mirror is light-weighted and has pockets for the iron plates for the magneto-resistive position sensors. The moment of inertia of the chop stage is 2.1 kg.mm^2 and has been minimised to reduce power consumption during chop transitions.

Flexure Pivots: The Flexural Pivots allow rotation of the mirror while constraining translational degrees of freedom. Lucas 5010-800 Flexure Pivots are used for the chop axis while Lucas 5010-600 Flexure Pivots are used for the jiggle axis. These pivots have high radial stiffness, which virtually eliminates unwanted rotation of the mirror due to bearing flexibility. They have minimal static friction to overcome which would greatly complicate the design of the control system and possibly increase the power demand on the actuator. The torsional spring rate of these pivots is 5.02 Nm/° for the 5010-600 and 0.631 Nm/° for the 5010-800. This restoring force ensures that the mirror returns to the neutral position in the event of power failure to the BSM. The mounts for the pivots are designed in such as way so that if the pivots fracture, they are held in place and effectively become journal bearings. This aspect of the design renders this contingency a soft failure mechanism.

Jiggle Stage: The jiggle stage is in the form of a split frame split and clamps together around the flex pivots. To balance the jiggle stage the framework in the opposite corner to the coils of the actuator has been made solid. This also increases the stiffness of the structure. This structure carries the chop stage, and is inevitably heavier. Since the amplitude and frequency requirements in this axis a stiffer flexures pivot is used for increased strength and reliability.. The static load on the jiggle axis flex-pivots at 50g is 27N, well below the 245N load capacity.

Position sensors for the chop axis are mounted on the jiggle stage, which means flexible cable connections are required, unlike the jiggle stage position sensors, which mount directly on the non-moving housing. An alternative to this may be to place the chop axis sensor also to the housing and compensate for the movement in the jiggle axis in the look up table using this in conjunction with the jiggle axis position. The gimbal frame is fabricated from Al-6061.

Magnetic Actuators: The magnetic actuators are located at the edge of each stage of the BSM. There is a primary and a redundant motor for each axis. The estimated power consumption is 0.4 mW when chopping at 2Hz with maximum amplitude and an average power consumption of 1.6 mW when jiggling at 1 Hz with maximum amplitude. Depending on implementation, the motor for a single axis will either have:

(i) the prime coil on one side of the rocker beam and the redundant on the other, leading to an unbalanced load but a more rugged coil, or

(ii) a balanced set of coils with the prime and redundant motor coils wound onto the same bobbin.

The coils may be potted (encapsulated) if required, and will certainly require extensive magnetic shielding and strong thermal linking to the thermal straps. All the motor coils mount directly to the BSMs, i.e. the chop stage air gaps must be slightly over-size to accommodate chopping whilst in various jiggle modes.

Position sensors: These sensors are Infineon (ex-Siemens) FP 212 L100-22 differential field plates that sense the position of soft iron pieces in the moving parts. The sensors are dual InSb/NiSb magneto-resistive elements, biased with a permanent magnet and forming part of a bridge circuit**.** As the position of the gimbal frame moves relative to the position of the sensor, the resistance of the element changes in proportion to the displacement. The sensor is connected in a Wheatstone bridge configuration driven by a constant current source. Hence, the voltage measured across the bridge is proportional to the displacement of the mirror.

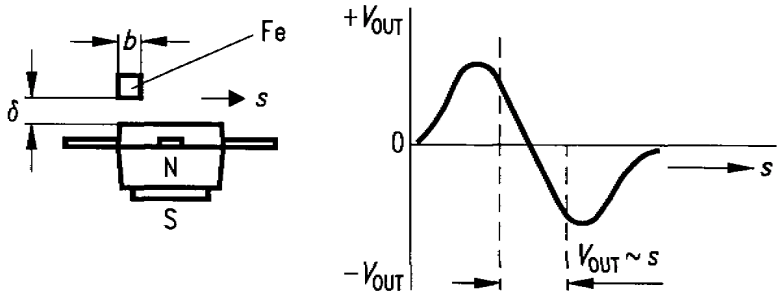

Figure 4-33 – Schematic drawing of the Infineon magneto-resistive position sensor.

Position sensors for the chop axis are mounted on the jiggle stage, which means flexible cable connections are required. The jiggle stage position sensors mount directly on the non-moving housing and do not require these flexible wires.

Stray light baffle: Parasitic losses in the actuators, electronics and wiring may cause the temperature of some of the items mounted on the BSM to rise above the 4 K temperature of the Level-1 enclosure. Any radiation emitted from these items must be shielded from the detector arrays. This is achieved through a baffle made from 0.25-mm thick (TBC) Al-6160 (TBC) placed over the components and around the mirror. The baffle fits tightly around the mirror allowing full movement without interfering with the primary beam.

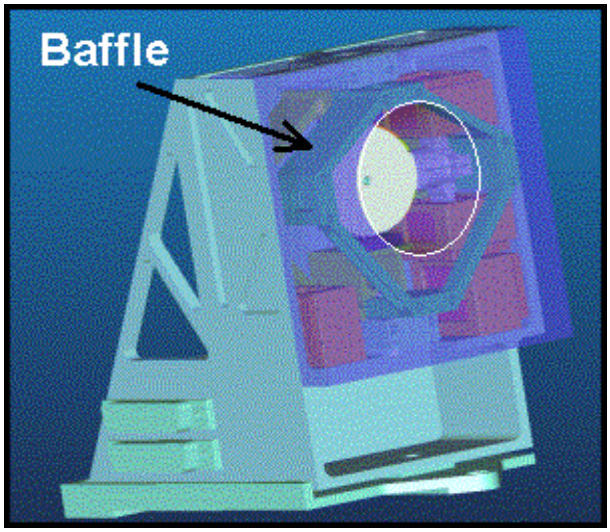

Figure 4-34 - View of the BSM with the stray light baffle covering the electrical components.

Structural interface to SPIRE Optical Bench: The mirror needs to be accurately mounted on the SPIRE optical bench. The mounting interface is shown

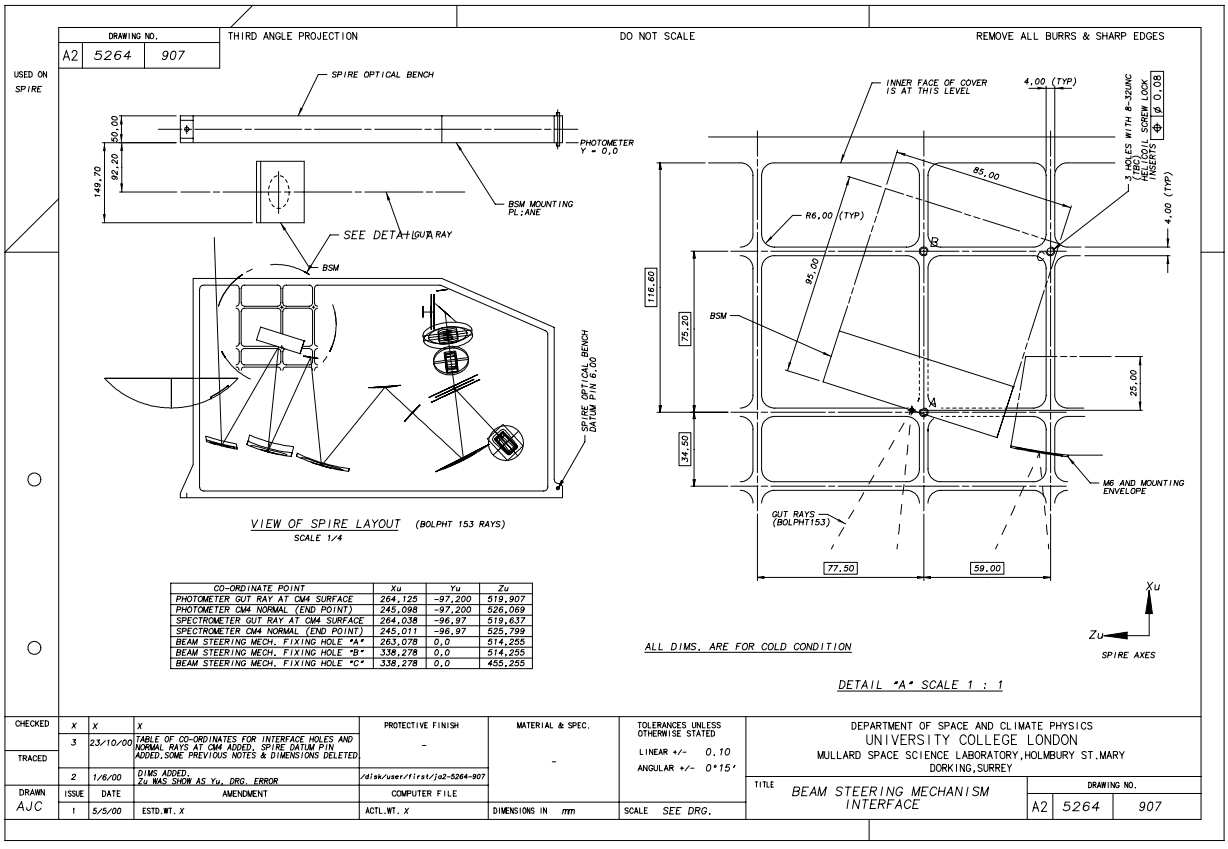

Figure 4-35 - Mechanical interface drawing between the BSM and the SPIRE optical bench.

Electrical connector: Two 37 way connectors (one prime and one redundant) accommodates all electrical connections to the BSM and the PCAL device. These connectors are located on the mounting frame.

Launch-lock device: During the launch (and operation) of Herschel, failure the BSM Flexure Pivots could result in the mirror being fixed in an undesirable off-axis position. The spectrometer functionality is particularly susceptible to this failure mode - if the BSM gets stuck at one extreme of its angular range, then the field of view of the FTS detectors could be projected outside the SPIRE field of view resulting in loss of the spectrometer. To prevent this from happening, a launch lock device is incorporated into the BSM. This device is a solenoid-driven locking device that reduces the maximum travel range of the Chop and Jiggle axes. During launch or in the event of failure of one or more of the Flexure Pivots, the launch lock solenoids can be energised, constraining the mirror to point ± 1"(TBC) in each axis of the telescope boresight resulting in a soft failure mode. The state of the launch lock solenoid is monitored by a prime and redundant micro-switch.

Control system: The BSM has a prime and redundant electrical interface with the FCU to provide the necessary feedback control of the mirror pointing angle. The position of the mirror is controlled via a PID algorithm which is part of the OBS of the MCU. The control scheme treats each rotational axis of the mirror independently of the other. More detail on the hardware implementation of the actuator control and power system is described in §4.1.2.2.

4.9 Spectrometer Mechanism

The Spectrometer mirror MEChanism subsystem (SMEC) controls the movement of the rooftop mirrors inside the SPIRE spectrometer. The movement of the mirrors causes there to be an optical path difference between the two beams that enter the spectrometer 2-K detector box. The critical performances of SMEC are the mirror velocity and its stability, the mirror movement around its travel axis and the required accuracy of the mirror position measurements.

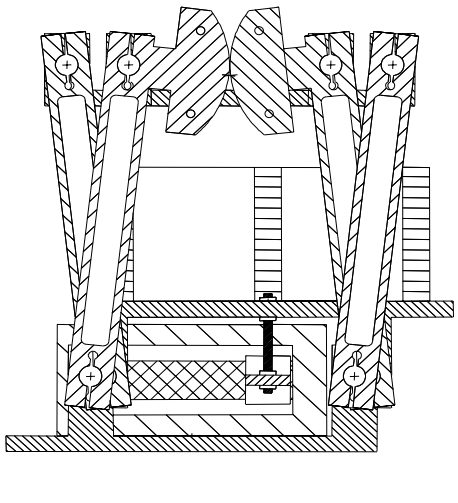

Figure 4-36 - CAD drawing of the link mechanism used for the SMEC.

4.9.1 Requirements on the mirror mechanism

The design of the FTS spectrometer (see §3.4.2) means that there is an effective folding of the optical path difference of a factor of four between the actual movement of the mirror mechanism and the change in the optical path difference (OPD). The required resolution of the spectrometer is for a maximum $\Delta\sigma$ = 0.4 cm^{-1} at all points in the field of view with a goal of reaching 0.04 cm^{-1} for at least point sources viewed on axis. There is a further requirement that the systematic noise induced by the movement of the mirrors will not prevent low resolution spectroscopy down to at least $\Delta\sigma$ = 2 cm^{-1}. The goal resolution imposes a maximum

change in the OPD of ~ 12 cm or 3 cm in actual mirror movement. In order to Nyquist sample the interferogram at the highest frequency present in the optical band (50 cm^{-1}) , the optical path difference must be sampled every 20 microns, or every 5 microns of actual mirror movement.

The most efficient method of operating an FTS is the so-called rapid scanning method. Here, the mirror is kept in constant motion while the signal and mirror position are sampled. This method of operation effectively transforms the optical frequency to audio frequencies by the relationship $f = v_{opd}\sigma$. Where f is the detection frequency, v_{opd} the rate of change of the optical path difference and σ the optical frequency. The maximum OPD velocity required will be determined by the frequency response of the detectors. For an assumed detector response of 20 Hz the maximum v_{opd} will be 0.4 cm/s or 0.1 cm/s in actual mirror speed. In fact some "head room" may required in case of problems with microphonic interference so the maximum velocity requirement on the mirror mechanism has been set at 0.2 cm/s.

I

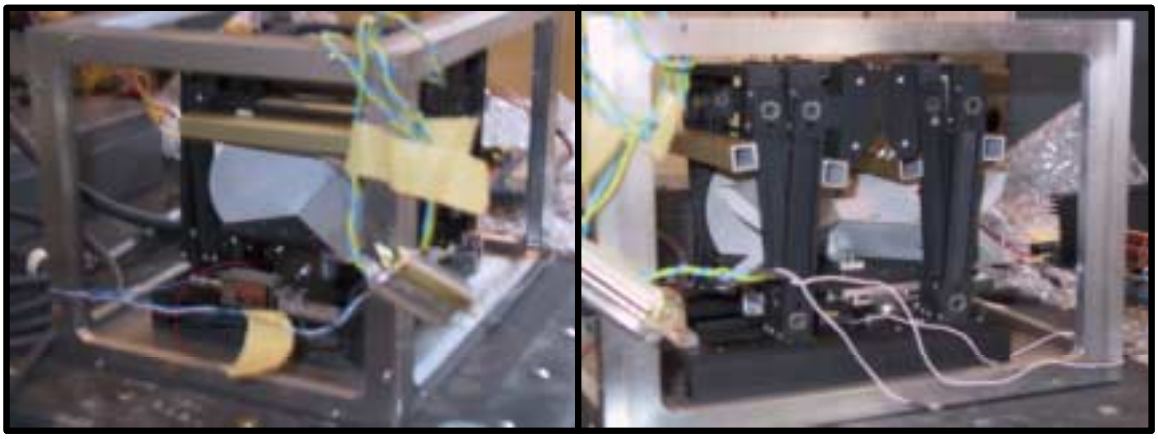

Figure 4-37 - Views of the engineering model of the SMEC.

In order to further improve efficiency, the interferograms can be taken "single sided". That is only a short movement is needed on one side of the zero path difference (ZPD) to enable the position of the ZPD to be established and as long a distance as necessary is scanned beyond that to achieve the required resolution.

As in the photometer, the signal in the recorded interferograms will be dominated by the telescope emission. The shape of the optical pass band means that the rate of change of the signal is greatest over the scan region close to the ZPD (Figure 4-39); that is at low resolution. In order to fulfil the requirement on the low resolution performance of the spectrometer it is necessary to have good control of the variation in the velocity and knowledge of the mirror position over the scan range close to the ZPD. Further away from the ZPD the requirement is less strict as the rate of change of the signal is much reduced.

These scientific and operational requirements impose the following baseline performance on the FTS mirror mechanism or SMEC:

(i) maximum mirror travel required (w.r.t. the ZPD position): – 0.32 to +3.2 cm;
(ii) minimum measurement interval of 5 μm is required;
(iii) required mirror position measurement accuracy 0.1 μm over +- 0.32 scan range and 0.3 μm thereafter;
(iv) the mirror velocity shall be within 0.001 cm/s r.m.s. within a band width of 0.03 to 25 Hz over the entire scan range;
(v) additionally movement of the mirrors must not impose any translation or rotation on the optical beam such as to affect the fringe visibility in the recorded interferogram.

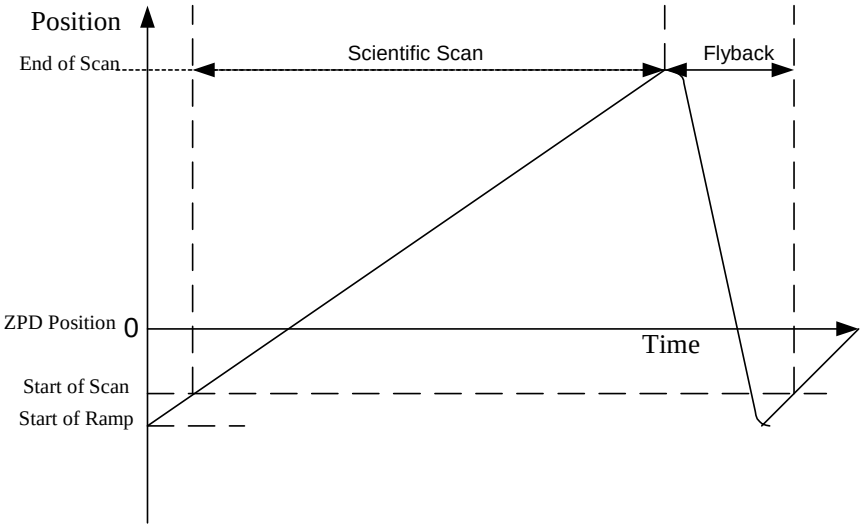

Figure 4-38 - Definition of a typical scan trajectory for the SMEC.

4.9.2 Control System and Readout

The baseline design of the spectrometer is that it should be operated in “rapid scan” mode with a constant mirror velocity and the time at which each position is passed recorded. The mirror movement will be controlled by a digital feed back loop that uses the time between successive pulses from the optical encoder to control the speed of the mirrors. In order that the mirror velocity jitter in the signal detection band (essentially 0.03-25 Hz) does not affect the signal to noise ratio achieved, the feedback loop will be operated at about 2 kHz. The digital feedback loop is implemented using the TEMIC TSC21020 digital signal processor which is also used as the CPU in the DPU. The detectors could be read out in one of two methods given the encoder type we plan to implement:

Position sampling with synchronised detector readout. In this technique, the mirror position pulse is used to trigger the readout of the detectors. The time taken to readout the detector array will need to include any possible uncertainty in the time interval between positions due to the uncertainty in the mirror velocity. This method has the advantage that each frame will be recorded at a known mirror position within the uncertainty of the mirror velocity from one position sample to the next. This means the interferograms can be safely co-added with no need to interpolate the data onto a common position grid. The disadvantage of this method is that it requires both a synchronisation pulse from the mirror drive electronics to the detector read-out electronics (and therefore makes the electronics more complicated) and a higher readout rate for the detectors.

Time sampling. Here the time of each pulse from the position sensor is recorded and the detectors are independently sampled; with perhaps a start pulse at the start of the scan to synchronise the readout. The advantage of this technique is that it is simpler to implement in the electronics and will be less prone to operational difficulties associated with timing between the position readout and detector readout. The disadvantage is that, because of the uncertainty in the mirror velocity and any hysteresis or scan-to-scan variability in the positioning of the mirror, the detector readouts will have to be interpolated onto a common position grid before co-addition of the interferograms. In practical terms, this will probably prevent on board co-addition of the interferograms and the mirror scan speed will therefore have to be adjusted to allow the data sampling rate to fit within the 100 kbs telemetry bandwidth available for the Herschel instruments.

After an assessment of the implementation of the two methods in the electronics system for the SPIRE instrument, it was decided to adopt the time sampling method as the default operating mode.

4.9.3 The cryogenic mechanism (SMECm)

The SMECm is the mechanism which moves the mirrors. The mirrors are considered a part of SMECm. Basically, the movement of the mirrors is a translation only, obtained through the action of a linear actuator. The mechanical design is based on a prototype Goddard Space Flight Center design for a balloon project (Figure 4-36 and Figure 4-37). A base plate supports the mechanism and is mounted on the SPIRE Optical Bench. On the base plate are mounted the fixed part of the actuator and the optical encoder. A moving plate supports the rooftop mirrors and the rule for the optical encoder. The base plate and the moving plate are linked by four "legs", each of which has two arms; one linking the base plate and the intermediate moving plate, the other linking the intermediate moving plate and the moving plate. The articulations at both extremities of the legs use flex pivots. The stiffness of the articulation is very low to keep the actuator power consumption within the specified limits. Consequently, for SPIRE, a launch latch item is added to allow the mechanism to sustain the launch vibrations without damage. The latch is placed between the baseplate and the mirror moving plate.

4.9.4 Position measurement

For the position measurement system, a Heidenhain LIP interferential linear encoder is used over the complete travel range of the mirror with a linear variable differential transformer (LVDT) transducer implemented over the movement range around ZPD as a redundant device. The LVDT also provides absolute position measurement close to the ZPD, unlike the optical linear encoder, which only provides relative position information. LVDT devices have already flown on many previous space experiments and were used cryogenically on the ISO LWS grating mechanism. Cryogenic tests indicate that the Heidenhain encoder may be used at liquid helium temperatures with only minor modifications to the optical head. The optical encoder will have a resolution of 0.1 mm or better and gives a “pulse” as each position is passed rather than an absolute distance measurement. The encoder will be fitted to the outside of the mirror carriage.

Measuring the position at a distance from the signal beam imposes stringent requirements on the “nodding” movement of the mirror mechanism, possibly stricter than those imposed by the optical requirements of the spectrometer. The actual value of the requirement will depend on the final configuration of the flight optical encoder and the final carriage design.

4.9.5 The preamplifier (SMECp)

Due to the loss of current on the output signals of the optical encoders when they are cooled down to 4 K, a preamplifier is necessary. The electronic components (JFETs, etc..) are implemented on a card integrated in a separate box on the SPIRE structure. The temperature of the components is set around 100 K.

The driving and control of the SMEC is carried out by the SMEC and MAC boards in the MCU. This

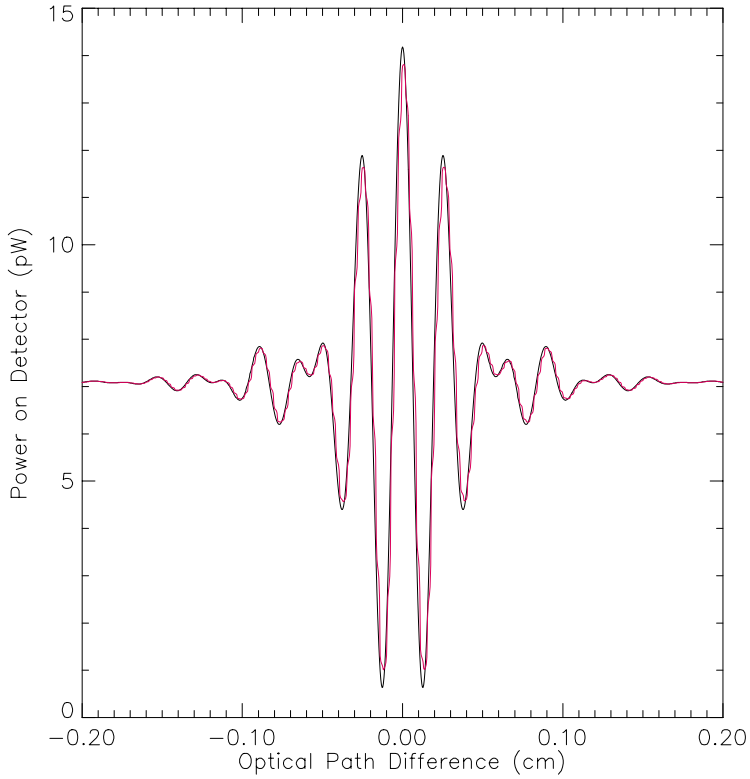

Figure 4-39 - Simulated spectrum of the 80 K telescope seen through the SPIRE FTS with representation optical filtering. The black line is before applying the frequency response of the detectors the red line after. Note the much larger rate of change of the sign

4.10 FPU structure

Parameter	Specification
L1 Heat leak to FPU from FIRST Optical Bench	6mW (for ΔT = 11-4.2 = 6.8K)
L0 Conductive heat leaks down 2K box supports	1mW (for ΔT = 4.2 - 1.7 = 2.5K)
300mK Parasitic heat leak on 300mK detector stage	<1.6μW per array <8μW total
300mK Heat leak down the Photometer 300mK strap supports	<0.6μW
300mK Heat leak down the Spectrometer 300mK strap supports	<0.4μW

The structure has three main requirements:

1. To mechanically support and positively locate the components (optical or otherwise) of the photometer and the spectrometer;
2. To provide the correct thermal isolation between the various temperature stages of the instrument; and

3. To provide adequate EM shielding and stray light shielding to the photometer and spectrometer such that the detectors see no spurious sources of EM power.

The structure is comprised of three main components; the Spire Optical Bench (SOB), the photometer cover and the spectrometer cover. The Spire Optical Bench is machined from a single block of Al-6061 approximately 675 mm long (aligned with the Spacecraft Z axis, See Figure 2-2) by 410mm high (aligned in the X axis) and 50 mm thick. All the optical components of the spectrometer are located on the +Y side of the SOB while all the components of the photometer are located on the –Y side. The mass of the SOB is minimised by machining ribbed pockets (nominally 70 x 70 mm) on both sides. The nominal thickness of the ribs is 2 mm and the centreline plane of the bench is 2 mm (TBC) as shown in Figure 4-40-A.

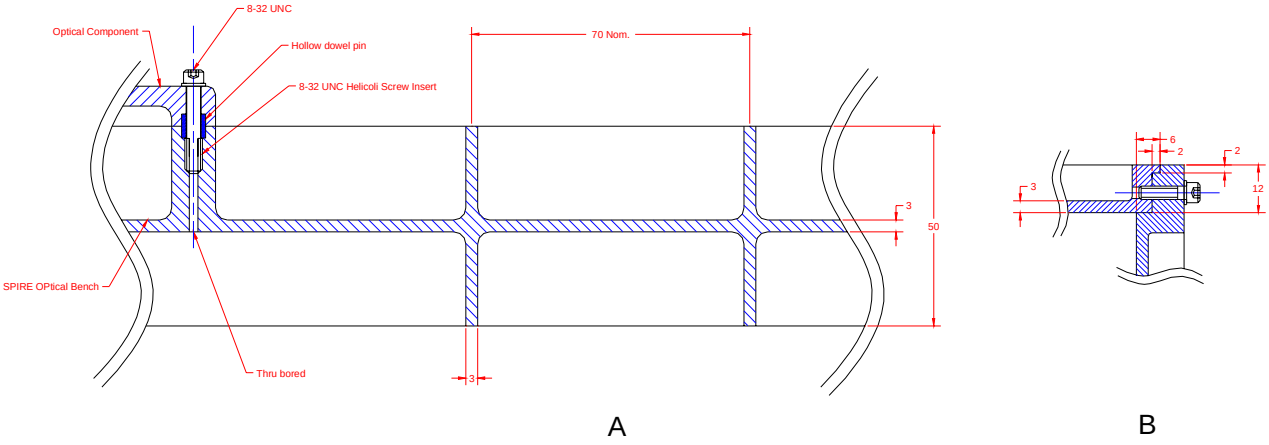

Figure 4-40 Details of (A) SOB lightweighting and optical component interfaces and (B) cover joint design.

The optical components are located on the bench by hollow dowel pins and 8-32 UNC screws provide positive the mechanical attachment. The SOB is manufactured and toleranced in such a way so that the position of the components located on the bench are in the correct position when the bench has undergone the contraction during cooling from room temperature to the nominal operating temperature of 4K.

Figure 4-41 - FPU/HOB interface strut.

The ribbed design of the SOB gives it excellent bending stiffness but it will have a relatively low torsional stiffness. The required torsional stiffness is achieved through the photometer and spectrometer covers. The

covers are created by screwing a series of lightweighted, 12mm thick plates together in the manner shown in Figure 4-40-B. The integration plan for the FPU structure sees the covers being loosely assembled with the screws not being fully tightened. The covers are then screwed tightly onto the SOB and the cover screws fully tightened thus forming a monocoque cover structure that will not be subsequently disassembled. Access to the SOB with integrated optical components will be done by removing either the photometer or the spectrometer covers. The remaining cover and optical bench give the required stiffness to the structure. The two covers and the SOB are machined from Al-6082. After final machining, it is passivated with Aluchrome treatment.

The FPU structure is connected to the Herschel Optical Bench via three feet structures. These feet have to:

(i) provide a rigid connection between SPIRE and Herschel so that the first natural frequency of the integrated instrument is higher than 100 Hz and prescribed in the IRD.

(ii) provide adequate thermal isolation between the 10K HOB and the FPU structure so that the heat load requirements are met and that the temperature of the structure does not rise above the nominal operating temperature;

(iii) allow for contraction and expansion between the FPU and the Herschel optical bench without inducing high stresses.

This is achieved through the use of two struts illustrated in Figure 4-41 attached to the covers and a single conical pin joint attached to the central SPIRE optical bench. Each of these three supports have a high thermal impedance and help to isolate the FPU structure from the HOB. The conical pin joint restrains the three translation degrees of freedom of the structure. The two struts in combination with the pin restrain the three rotational degrees of freedom. Vespel washers electrically isolate the

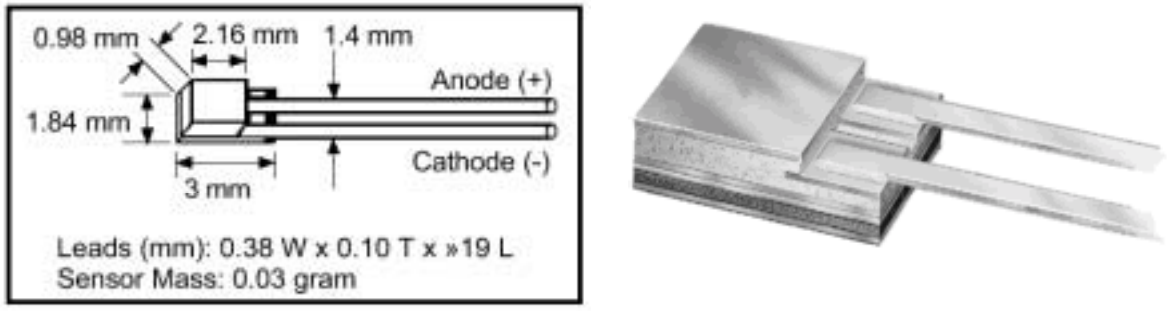

Figure 4-42 - View of the Lakeshore, Cernox SD hermetically sealed RTD thermometers.

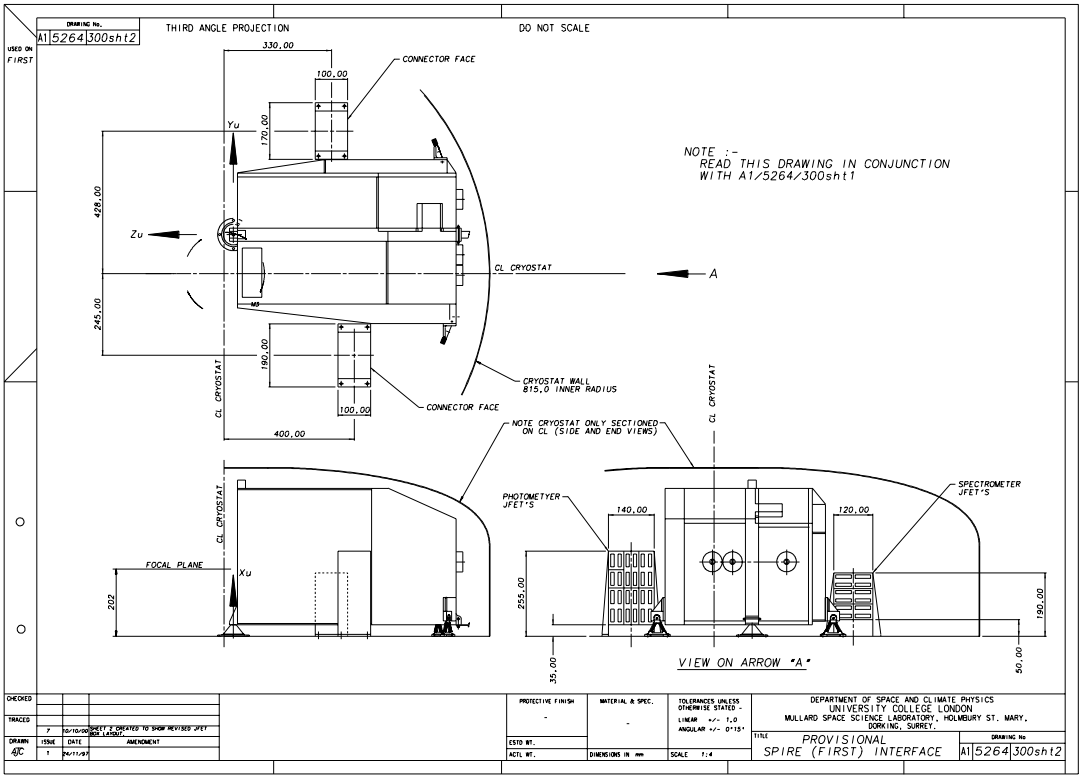

Figure 4-43 Interface drawing for the FPU structure within the CVV showing the positions of the photometer and spectrometer JFB**,** and the 2K strap feed throughs.

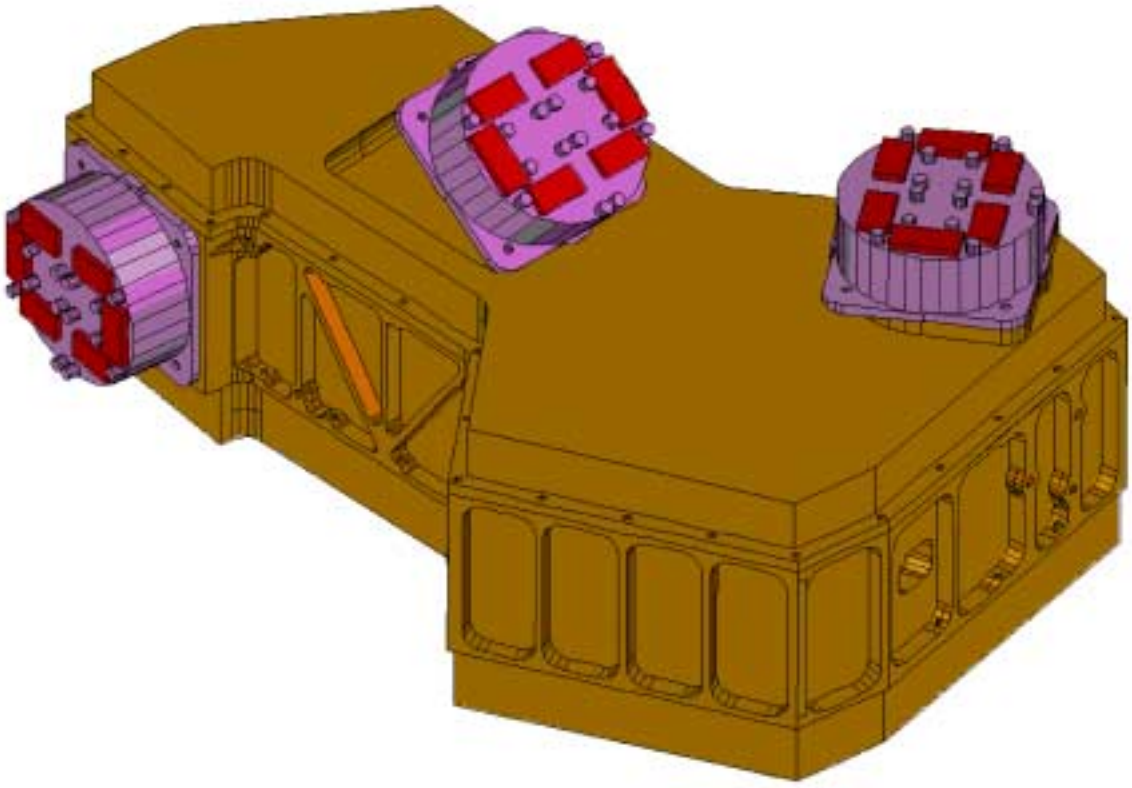

Figure 4-44 – View of the spectrometer 2-K Detector Box. The BDAs are shown in magenta. The PSW is on the right, the PMW is in the centre and the PLW is on the left.

4.11 Helium-3 Cooler

The cooling of the SPIRE detectors down to 300 mK is performed by a ^{3}He sorption cooler. This sub-Kelvin sorption cooler relies on the capability of porous materials to adsorb or release a gas when cyclically cooled or heated. Using this physical process one can design a compressor/pump which by managing the gas pressure in a closed system, condenses liquid at some appropriate location and then perform an evaporative pumping on the liquid bath to reduce its temperature. The cooler has no moving parts, is vibrationless and is designed to be self contained and compact with a high duty cycle efficiency.

As shown is **Figure 4-46**,

The cooler is basically made of 6 components designated as a sorption pump (SP) and an evaporator (EV) connected via a pumping line to a thermal shunt (TS) comprising a heat exchanger, two gas gap heat switches (HSP) and (HSE) respectively connected to the sorption pump (SP) and evaporator (EV), and finally a support structure (SST). SP, EV, TS and the pumping line are assembled to form a single component which is the actual “heart” of the cooler. This component is held within SST, which provides firm mechanical support (launch environment) while minimising any parasitic conductive load on the cooler (low temperature environment).

Two heat switches are required for operation of the cooler. The two switches are used to control the temperature gradient; during the condensation phase they are set such that the sorption pump can be heated to release the helium gas and such that liquid condensation occurs into the evaporator maintained as the coldest point. The liquid is held in the EV by capillary action inside the porous material: both the surface tension and the vapour pressure provide forces that drive and hold the liquid at the coldest point. Then the

switches are set such that the sorption pump is thermally grounded to the heat sink and such that the evaporator is thermally isolated. The sorption pump provides an evaporative pumping on the liquid helium bath which temperature quickly drops to sub-Kelvin temperature. Gas gap heat switches have been selected as the preferred design for the present project (see Figure 4-45). Gas gap heat switch utilises concentric copper cylinders separated by a small gap which is filled with or emptied of He gas to achieve the switching action. The thermal separation between the two ends is achieved by a thin-walled tube which also provides the mechanical support. The presence or absence of gas is controlled by a miniature cryogenic adsorption pump that can be temperature regulated. Thus one of their main feature is the absence of any moving part, and consequently operation of the cooler is almost then fully controlled by three heaters.

For operation in a zero-G environment two aspects are addressed: the liquid confinement and the structural strength required for the launch. The confinement within the evaporator is provided by a porous material which hold the liquid by capillary attraction, and a suspension system using Kevlar cords is designed to firmly support the refrigerator during launch while minimising the parasitic heat load on the system.

The sorption cooler is mounted off a 4 K plate and 1.7 K thermal paths will be provided for the heat switches and thermal shunt for the operation of the cooler. The radiative environment will be 4 K. The recycling time shall be as short as possible, compatible with the warm heat sink heat evacuation capability. This recycling time has no real impact on the design of a cooler operated from a helium bath. It only has an impact on the recycling procedure (timing, control of heat switches, peak dissipation). The sorption cooler is able to be operated in any orientation under 1g. However it is understood that during ground test some specific orientations shall be avoided because of potential convective effect. This constraint only applies during the recycling phase while the pump is heated to above 20 K.

(i) the temperature of the evaporator cold tip should not drift by more than 0.1 mK/h under active temperature control;
(ii) the temperature fluctuations at the evaporator cold tip shall be no more than 10 $\mu K/Hz^{-1/2}$ in a frequency band from 0.1-10 Hz;
(iii) the energy dissipated per cycle due to cooler operation shall be no more than 860 J - the 4 K/1.7 K

The ^{3}He cooler is required to maintain the temperature of the BDA below the nominal Two chambers, the evaporator and the charcoal sorption pump, are joined by thin-walled stainless steel tubes via the condenser, which is in good thermal contact with the cold heat sink (we will assume a temperature of 2K for the purpose of this description). The refrigerator is charged with 3He gas, and permanently sealed by a crimped tube.

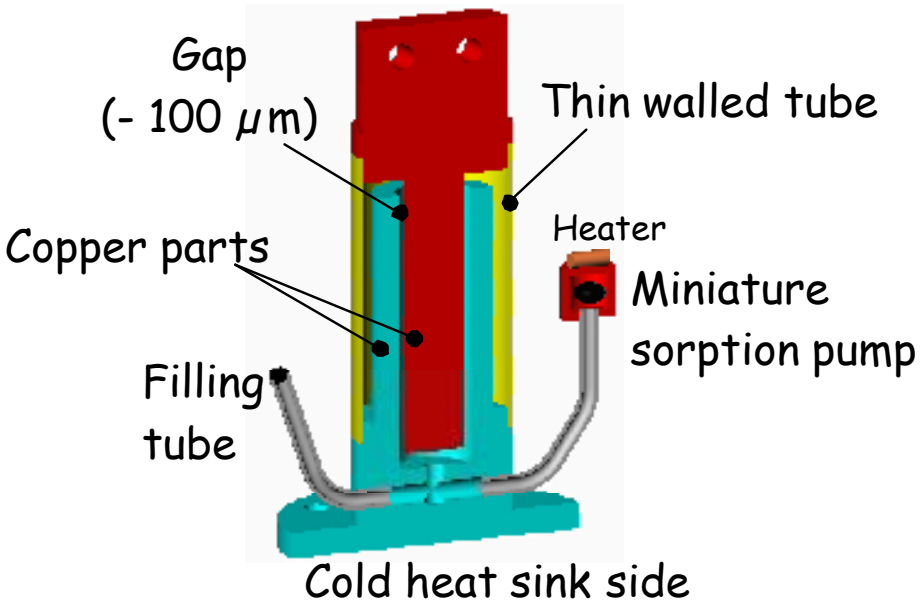

Figure 4-45 - Schematic representation of the gas gap heat switch.

48 hours recycle
hard mounted to 4K FPU Optical Bench
Separate straps from Pump and Evaporator to L0 Helium Tank, both via heat switches.
Separate straps necessary to prevent warming of evaporator during cooler recycling.
Evaporator strap has high conductance requirement (>100mW/K @ 2K) in order to limit temperature at end of recycling.
Leak before burst
titanium alloy (Ta6V Eli
3He cooler : 264 mK ultimate T, 20 μW @ 300 mK

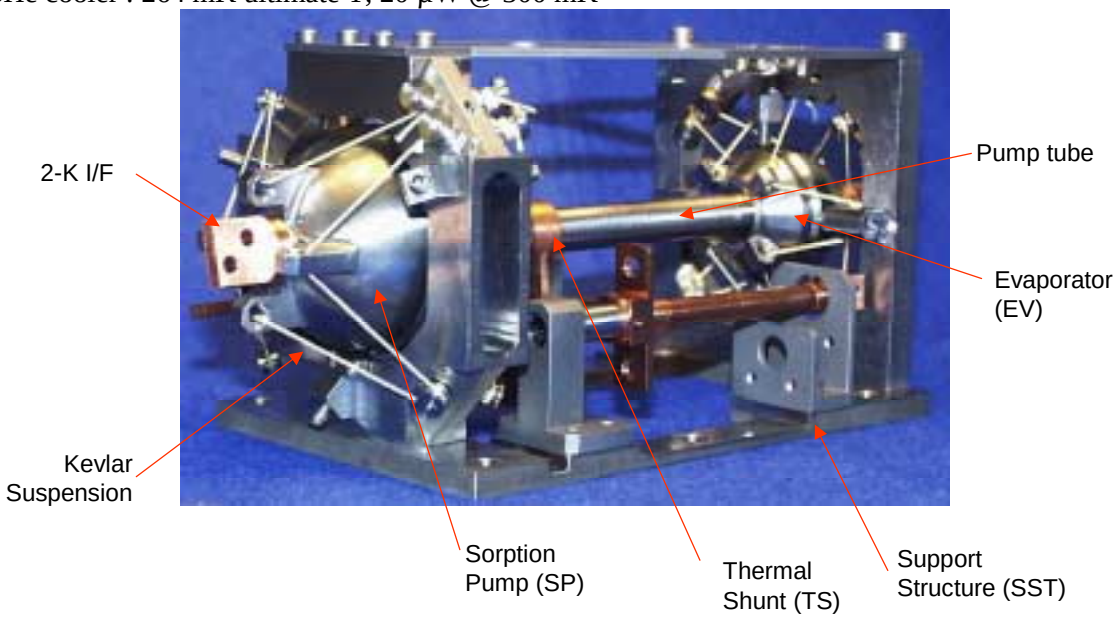

Figure 4-46 - Illustration of the 2-K cooler.

Figure 4-47 illustrates the operation of the cooler during recycle. At the end of the cooling cycle, there is no liquid ^{3}He remaining in the evaporator and therefore no more cooling power can be delivered to the cold tip. At this point in time, all the ^{3}He will be contained in the sorption pump. Current is fed to ES1 (see Figure 4-48) and the Helium absorbed in the miniature sorption pump is driven off and fills the gap between the copper cylinders in the gas gap heat switch. The thermal conductivity of the switch rises greatly and the evaporator becomes thermally shorted to the 2-K stage of the cryostat. At the same time, no current is passed

to the evaporator heat switch and all the Helium remains in the gas gap miniature sorption pump. A vacuum exists between the copper cylinders in the gas gap switch and the evaporator remains thermally insulated from the 2-K stage. The evaporator heater (PH1, Figure 4-48) is switched on and the temperature rises to approximately 40 K. This state can be seen in Figure 4-47A. A shunt halfway along the pump tube prevents heat leaking from the pump to the evaporator. At 40 K, the ^{3}He that has been held in the pump is driven off and recondenses in the evaporator. Once all the ^{3}He has condensed in the evaporator, the pump heat switch is closed to cool the pump back down to approximately 2-K while the evaporator heat switch is opened to thermally isolate it and allow it to cool below the 2-K stage. This state is represented by Figure 4-47B. Once the pump nears 2 K, it starts to pump on the evaporator and liquid ^{3}He starts to boil off. The latent heat of evaporation of the ^{3}He causes the temperature of the liquid to drop below 300 mK and simultaneously provide cooling power to the BDAs. (see Figure 4-47C).

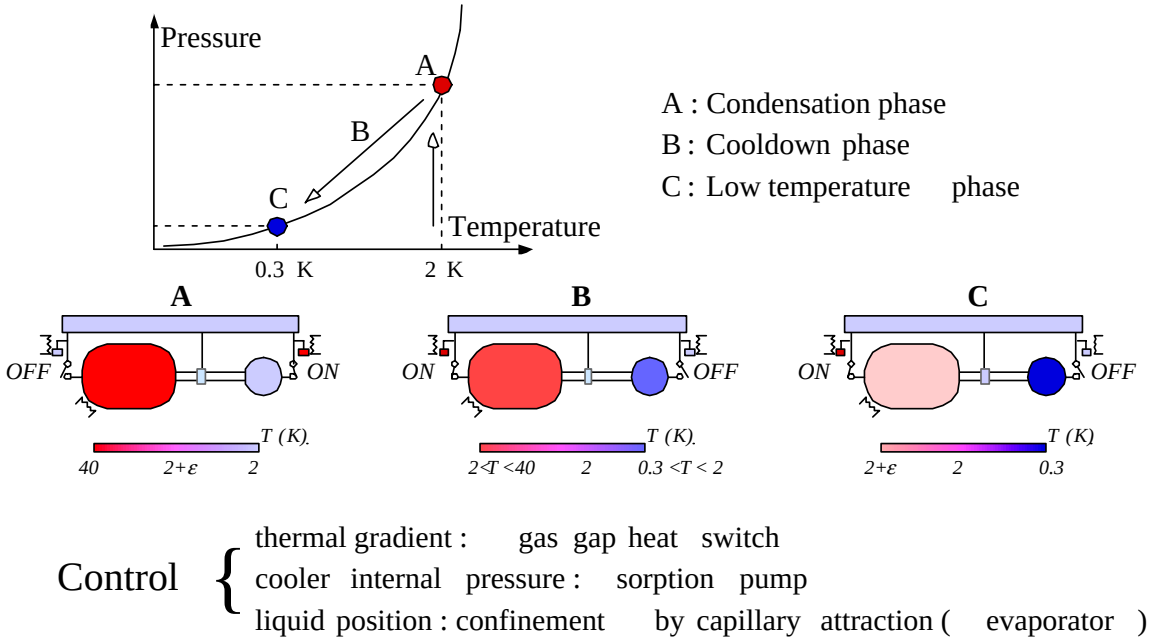

Figure 4-47 - Operation of the ^{3}He cooler during recycle, (A and B) and normal operation (C).

Figure 4-48 illustrates the redundancy scheme adopted for the cooler. There is full redundancy on the drive electronics. The possibility of implementing parallel heat switches for the evaporator and the condenser was investigated. This was discarded as (i) the heat switches provide a parasitic heat load to the evaporator even when the switch is open, and (ii) the switch can fail in either the open or the closed state. The addition of an extra switch does not correct a failed closed switch.

During operation, the pump is capable of providing a net heat lift of 10 μW at a cold tip temperature of 290 mK. The pump has a capacity of 6 litres of ^{3}He at STP which provides for up to 72 hours of operation of the pump. The recycling of the pump takes approximately two hours.

As can be seen Figure 4-46, the evaporator, condenser and the pump tube are all suspended in the support structure be a series of Kevlar cords. These cords are intended to provide a stiff mechanical interface between the two parts of the subsystem while providing a high degree of thermal isolation between them. The parasitic heat load passed down through the Kevlar is less than 12 μW. The whole cooler is housed in a structure (shown in Figure 4-50

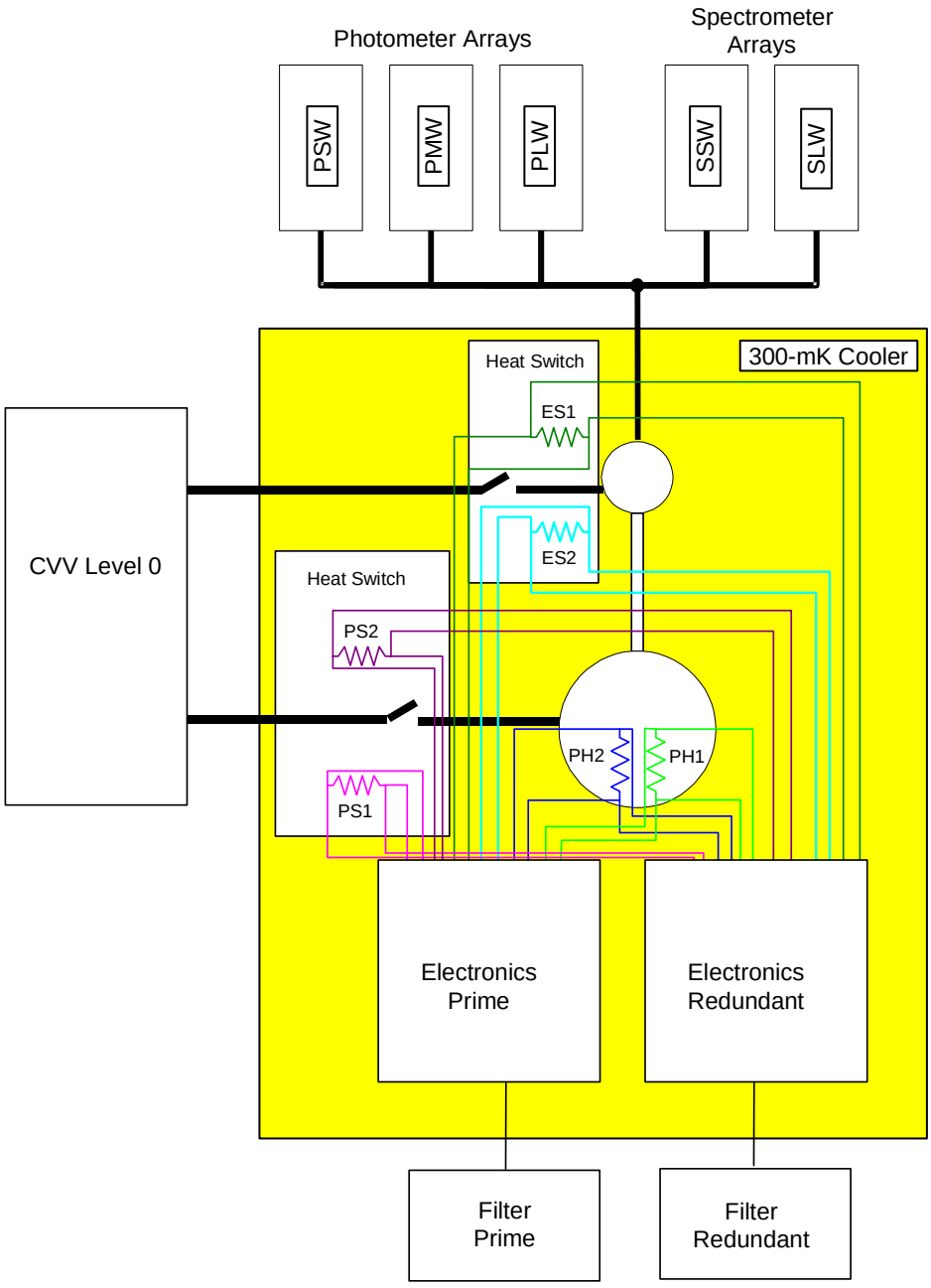

Figure 4-48 - ^{3}He Cooler cryogenic redundancy scheme.

4.12 Thermal straps

4.12.1 4-K to 10-K

The ^{3}He cooler and the detector boxes require thermal straps from the Herschel Level-0 stage of the cryostat to maintain the correct temperature. These straps are fabricated from Copper and are supplied to SPIRE by the satellite platform.

As shown in Figure 4-48, the cooler requires two straps; one connected to the evaporator and one connected to the condenser. These two straps must pass through the cover of the photometer which is a part of the FPU from the CVV. A further strap passes through the cover of the spectrometer to the detector boxes. The

temperature immediately outside the FPU is at a temperature of between 10 and 15 K and is therefore radiating strongly in the frequency band of the detectors. A stray light baffle is therefore required to greatly attenuate this stray light from entering the FPU close to the detectors. Two possible

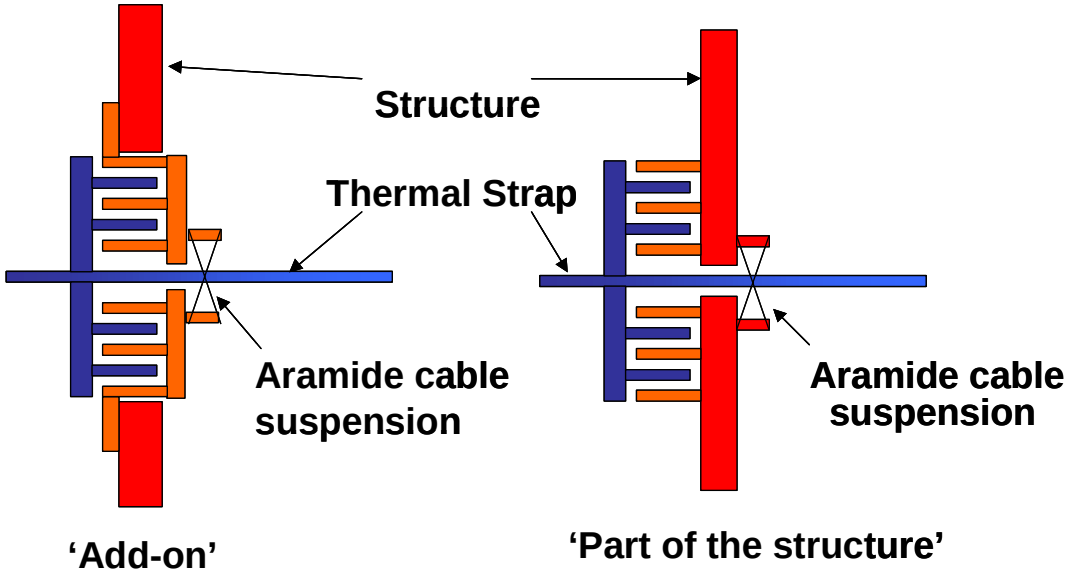

Figure 4-49 – Conceptual design of the stray light baffle on the 2-K straps entering the FPU.

light baffle on 2-K straps
power limits on 2-K strap during recycle (IID-B Ch 5)

FIRST Interface	SPIRE Interface	IID-A (Sect. 5-26)	Instrument Temperature Requirement	Instrument Conductance Requirement
L2	Photometer JFET Enclosure	T < 15K	-	TBD
L2	Spectrometer JFET Enclosure	T < 15K	-	TBD
L1	FPU 4K Optical Bench	T < 6K	T < 3.5K (at FPU Flange)	TBD
L0	FPU 1.8K Boxes	T < 2K	T < 1.75K (at FPU Flange)	TBD
L0	Cooler Evaporator	T < 2K	T < 1.75K (at FPU Flange)	G>100mW/K @ 2K
L0	Cooler Pump	T < 2K	T < 1.75K (at FPU Flange)	G>50mW/K @ 2K

4.12.2 300 mK

For the photometer and spectrometer detectors to operate correctly, they have to be maintained below a temperature of 300 mK during operation. Power is constantly being dissipated within the bolometers due to ohmic heating caused by the bias current and power is being absorbed due to photon thermailization, and conduction from warmer parts of the instrument. This heat needs to be carried away from the bolometers to prevent them from heating up. Two 300-mK straps between the photometer and spectrometer BDAs to the ^{3}He cooler conduct this heat away. The routing of the photometer 300mK strap is shown in Figure 4-50 and Figure 4-51 shows the routing of the spectrometer strap.

The design of these straps is challenging. They have the following requirements:
(i) the straps need to be supported rigidly so that the first mode of vibration is above 120 Hz (TBC);

(ii) the entrance of the strap into the 2-K detector box must not allow excessive stray light to enter. The stray light requirements for this are far less stringent than those emplaced on the entrance of the 2-K straps into the FPU;

(iii) the mechanical supports must positively and reliably locate the straps so the there can be no possibility of the strap touching the surrounding structure and causing a thermal short. This contingency is highly undesirable as it could compromise the functionality of the detectors by either greatly reducing the hold time of the cooler at the operating temperature or preventing the cooler from maintaining the detectors at the required 300 mK;

(iv) the suspension system must not place an excessive heat load directly to the strap. This is limited to 1 μW per strap (TBC).

The strap will be fabricated from ∅3 mm copper rod with a flexible lighter gauge copper wire running the last tract to the BDAs. These joints are formed by electron beam welding. A Kevlar suspension system will provide the mechanical support for the strap while maintaining a sufficient thermal impedance so as to meet the thermal requirements.

There is a stray light baffle around the entrance of the strap into the detector box. This is to prevent unfiltered 4-K stray from entering the detector box. It's design will be similar to the concept illustrated in Figure 4-49 but will be less complicated due to the less stringent shielding requirements. Several concepts of the support structure are currently being developed.

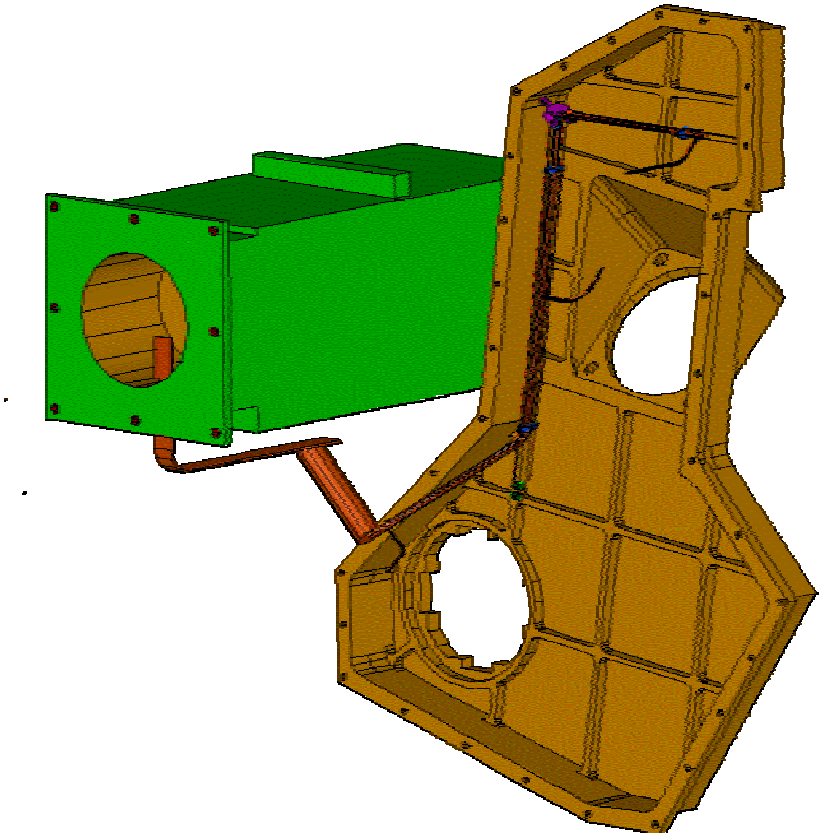

Figure 4-50 - Routing of the 300-mK strap from the cooler tip (inside the green box) to the 2-K photometer detector box.

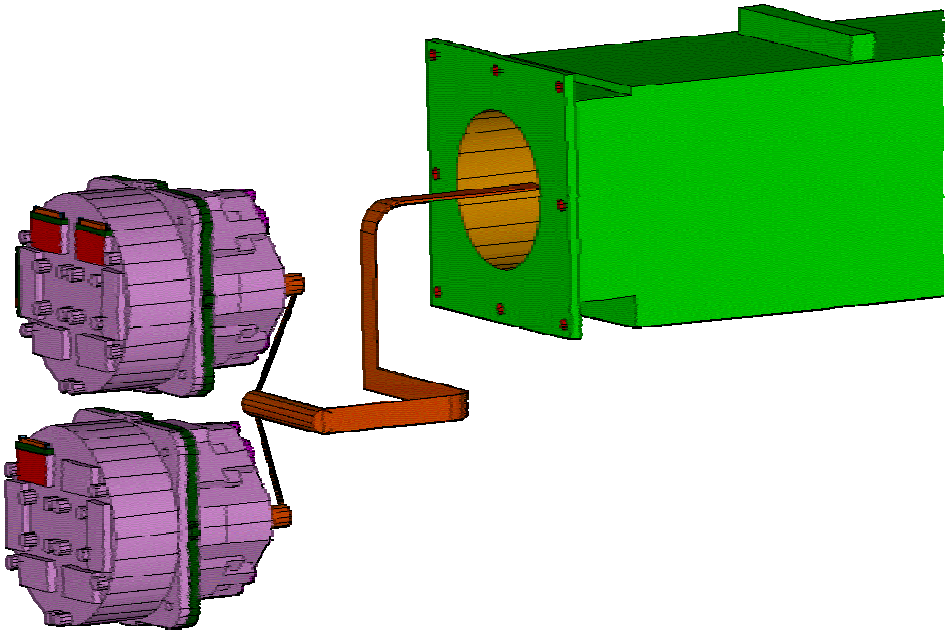

Figure 4-51 - Routing of the 300-mK strap from the cooler tip to the spectrometer BDAs inside the 2-K detector box. The strap crosses the SPIRE optical bench.

4.13 Harness

There are five sets of harnesses for the SPIRE instrument. They are briefly described below in Table 4-7.

Table 4-7 – SPIRE harnesses.

Name	Prefix	Connection One	Connection Two	Description
FPU Harnesses	F	JFP, JFS, RF Filters	FPU subsystems	Internal connection within FPU RF shield
Cryo-harnesses	C	CVV Wall bulkhead connectors	JFP, JFS, FPU	Relays FPU signals within CVV
Interconnect Harness	I	DCU, FCU	CVV Wall bulkhead connectors	Relays analogue signals from CVV wall
Warm Interconnect Harness	W	DPU	DCU, FCU	Digital and power interfaces
Test	T	EGSE	HSDPU, HSFCU	Test harnesses only used during testing of integrated electrical systems

The cryo-harnesses represents a critical part of the design. Previous experience in cryogenic harnesses for space application has shown that they are a common failure point. For this reason, great care is to be taken in the thermal/mechanical deign, connector selection, fabrication and routing design.

The harnesses from the detectors to the JFET boxes also represent a critical part of the design of the instrument. As previously stated in §3.7.3, the detectors are very susceptible to signal disturbances caused by microphonic vibrations of the harnesses To minimise this, these harnesses have the following provisions:

(i) they are mechanically clamped at intervals of approximately 10 mm to raise the first mode of vibration of the harnesses as high as possible;

(ii) they have mechanical supports for the free runs from the detectors down to the SPIRE optical bench and for the free run from the FPU to the JFET boxes;
(iii) the length is minimised as far as it practical;
(iv) the supporting structure is as rigid as is practical.

The harnesses that are contained within the FPU are shown in Figure 4-52 while the harnesses that run from the FPU to the warm electronics is shown in Figure 4-53.

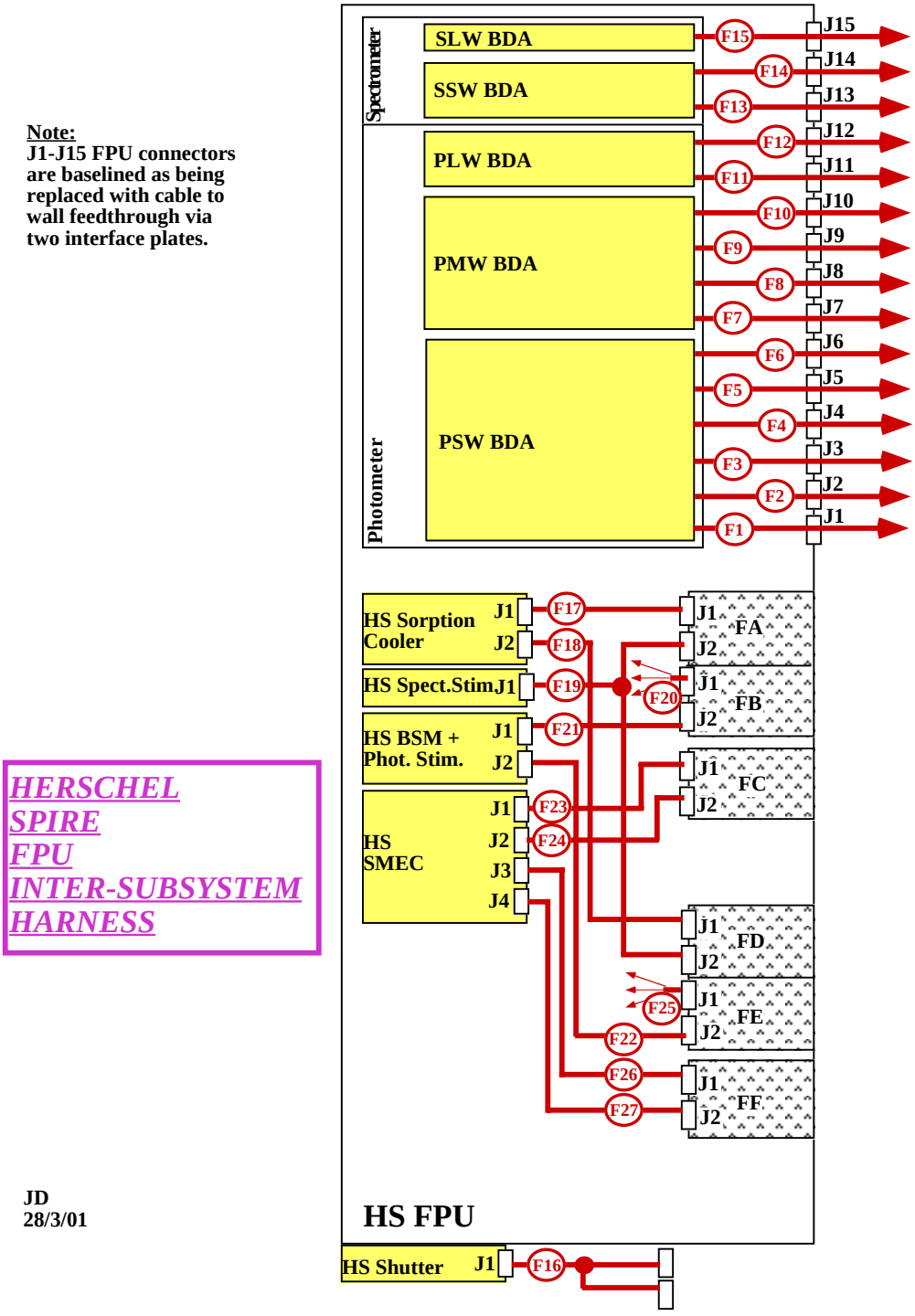

Figure 4-52 – SPIRE harnessing inside FPU.

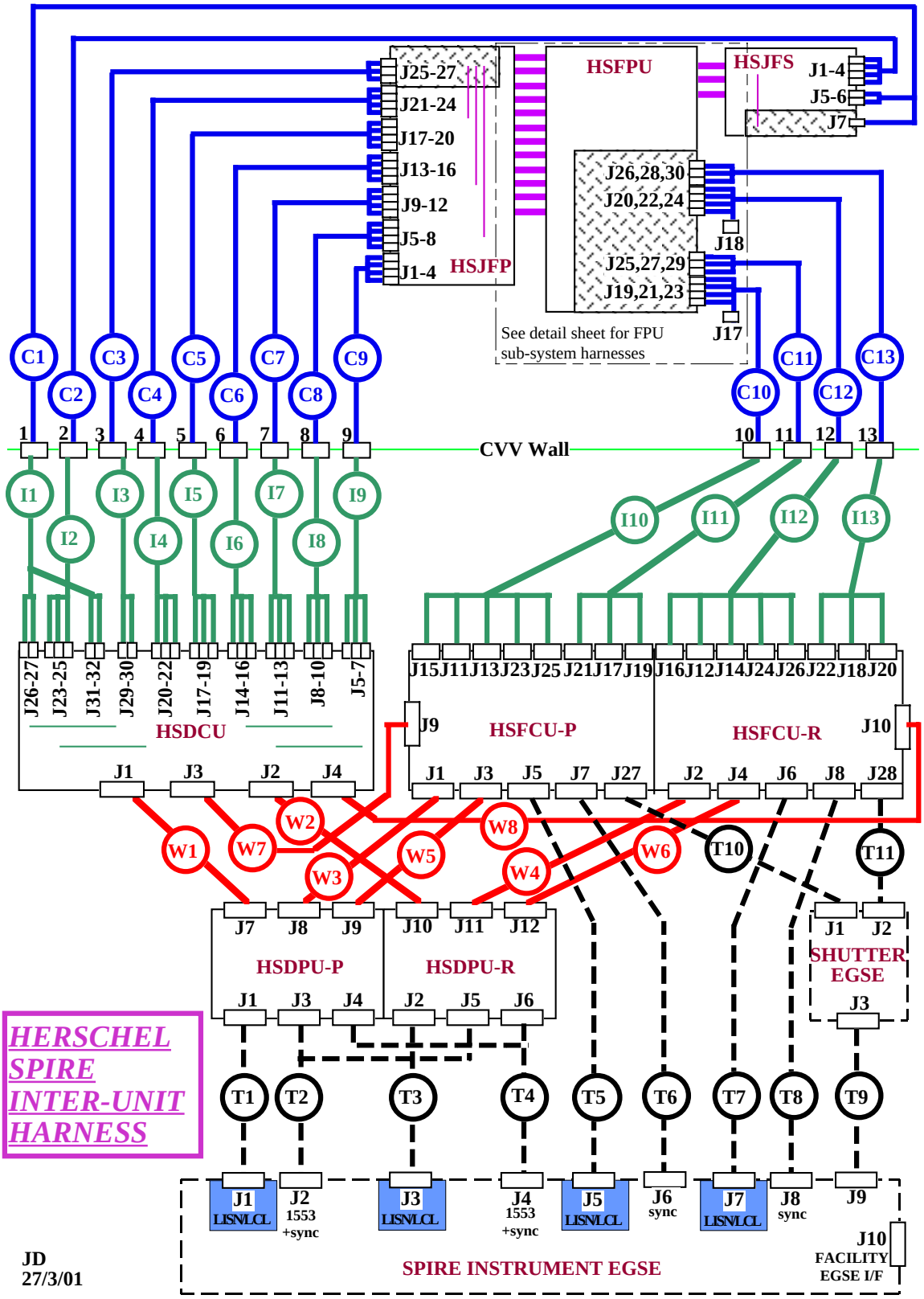

Figure 4-53 - SPIRE harnesses outside the FPU.

4.14 Shutter

During the period between final integration of the SPIRE instrument into the Herschel spacecraft and launch (a period of approximately two years), it is desirable to be able to verify that the photometer and spectrometer detectors and the cold and warm read out electronics are operating correctly. To test the optical readout system inside the spacecraft cryostat prior to launch, the background flux of light falling onto the detectors must be similar to the flux seen by the detector when the instrument is imaging astronomical objects during operation. In orbit, this background arises primarily from the self emission of the primary and secondary telescope mirrors which are assumed here to be at 80 K with an overall emissivity of 4%.

Prior to launch, the cryostat must cool the all the Herschel instruments in the focal plane to the nominal cryogenic flight temperature. To do this, a lid must seal the opening at the top of the cryostat vessel. This lid will however be at around 200 K (TBC) due to the relatively inefficient thermal insulation and will provide a very large background flux of photons onto the detectors (see Figure 4-54). To prevent this energy from flooding the detectors, a shutter mechanism is employed to prevent the thermal background from the cryostat lid from entering the SPIRE instrument.

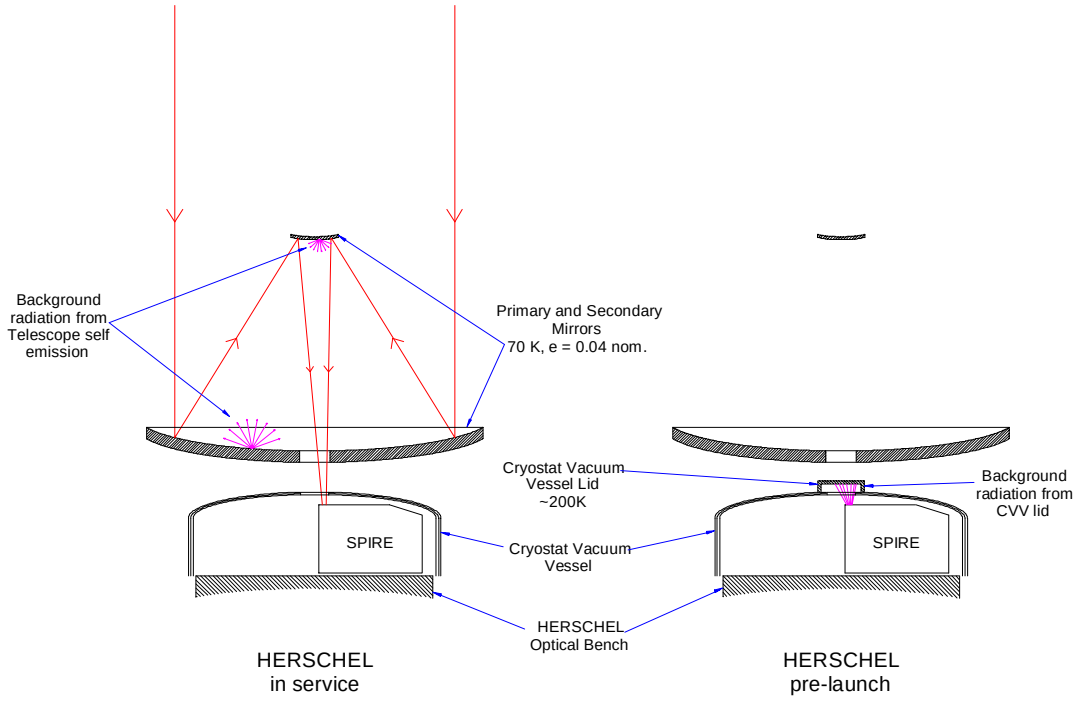

Figure 4-54 - Background radiation on the SPIRE detectors in space and on-ground.

When the shutter is closed, the detectors must see the same background flux in the spectrally sensitive band of the instrument as that used to test the detectors in the ground calibration facility (and expected from the telescope in flight). To achieve this, the inside surface of the shutter has a high emissivity coating, and can be heated electrically. Figure 4-55 shows the power absorbed by the photometer detectors as a function of shutter temperature (based on the same assumptions used in §6 for the SPRIE sensitivity estimation).

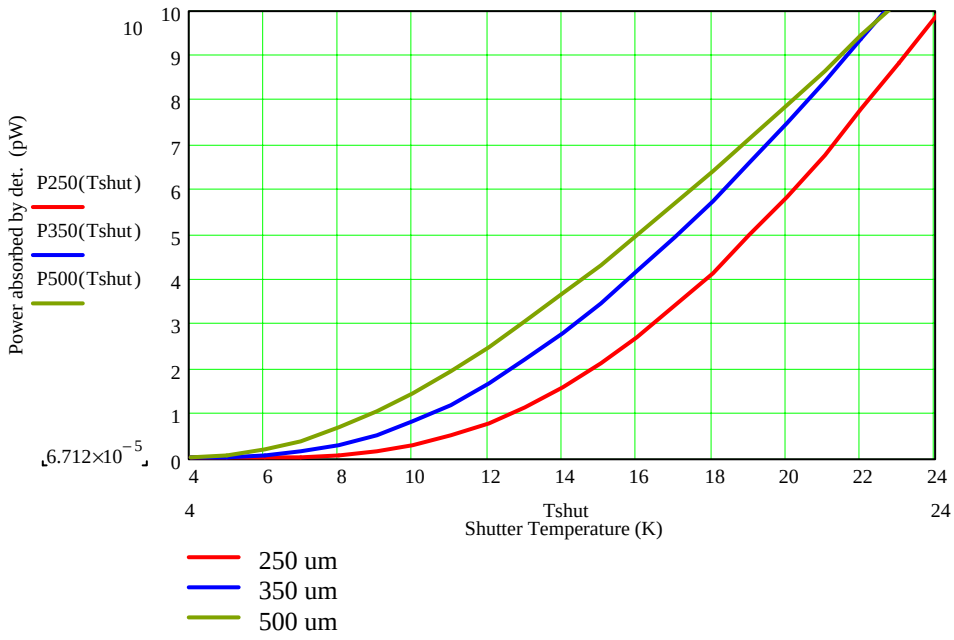

Figure 4-55 - Detector power vs. shutter temperature for the three photometer bands.

The telescope power levels that must be reproduced are nominally 3.9, 3.2 and 2.4 pW at 250, 350 and 500 μm, respectively (see §6). These correspond to shutter temperatures of approximately 17, 14.5, and 12 K. The effective emissivity of the telescope in-orbit is highly uncertain, and the instrument will be tested in the AIV facility over a range of backgrounds. Allowing for a factor of at least two in the power levels to be reproduced, the shutter is therefore designed to operate at up to 25 K. Note that the shutter is not required to reproduce the correct background levels on all arrays at the same time.

With the shutter thus providing a representative background radiation flux, the photometer and spectrometer calibration sources can be used to stimulate the detectors and the resulting signal read out from the read out electronics. These tests can be carried out in the AIV facility and again in the Herschel cryostat, to ensure that the system is operating nominally.

The baseline location of the shutter is shown in Figure 4-56. As this shutter is only used in the pre-launch testing of the detectors there is a launch lock device that will prevent the shutter from closing during flight. This launch lock mechanism is a passive device, in that it requires no power to keep the shutter in the locked open position.

The other components of the shutter are described below.

Vane: A metal vane blackened on one side is used to block off the input radiation.

Heater: An electrical heater mounted on the vane of the shutter provides power to heat the vane up to the design temperature.

Temperature sensor: A single Lakeshore Cernox thermistor is mounted on the shutter vane to monitor its temperature.

Actuator: A single rotary stepper motor is used to actuate the shutter vane. It can be driven by a primary set of two windings or alternatively by a separate set of two windings.

Launch latch position indicator: This is a micro switch that indicates the state of the launch lock. The contact on the switch can only be closed when the Shutter has returned to the open position and the launch lock successfully deployed.

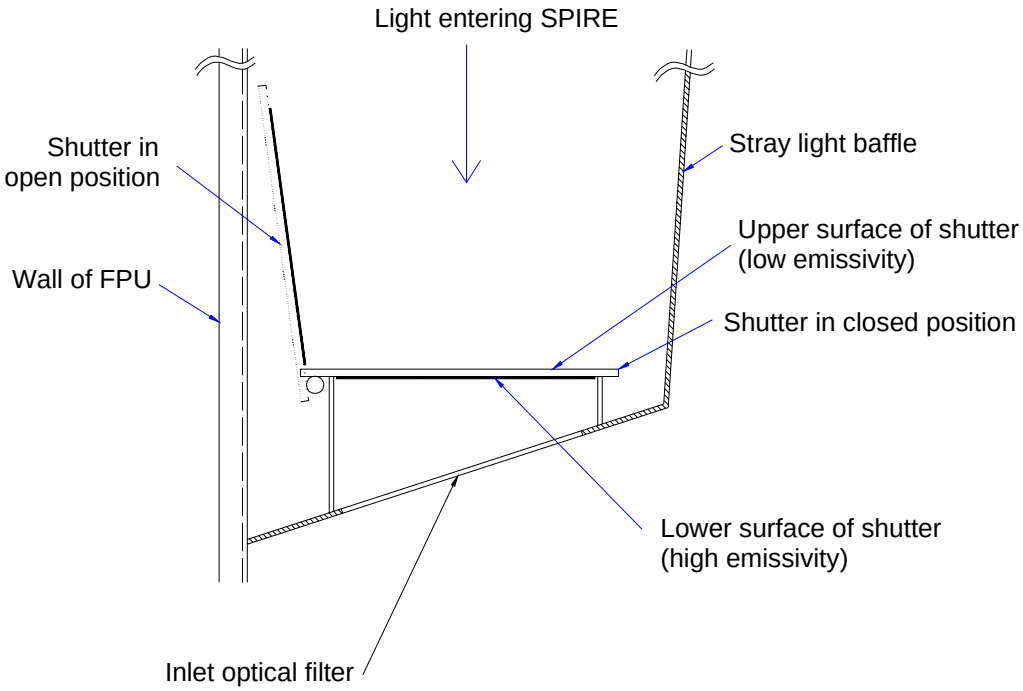

Figure 4-56 - Physical layout of shutter within the inlet of the FPU enclosure.

The powering, thermal control and the monitoring of the shutter sub-system are all carried out with the EGSE. When the EGSE is disconnected, the shutter is unable to be operated or controlled. The state of the launch lock indicator must be read out by the spacecraft housekeeping electronics.

5. INSTRUMENT OPERATING MODES

The operational modes of the SPIRE instrument are documented in detail in the OMD. These operating modes can be summarised as being the sequence adopted to turn the instrument on, preparing it for scientific observations, making the observations, the recycling of the cryogenic cooler and the abnormal and normal shut down. The implementation of the astronomical observing modes will be briefly described here.

5.1 Spacecraft pointing

It is assumed that SPIRE pointing will be defined with respect to the telescope boresight by two offset positions, one for the centre of the photometer arrays and one for the centre of the spectrometer arrays, as shown below. When the telescope is pointed at a source at the request of SPIRE, it shall be aligned on one of the two positions defined in Figure 5-1 below. Any offsetting by the SPIRE BSM or the AOCS shall then be defined with respect to this position.

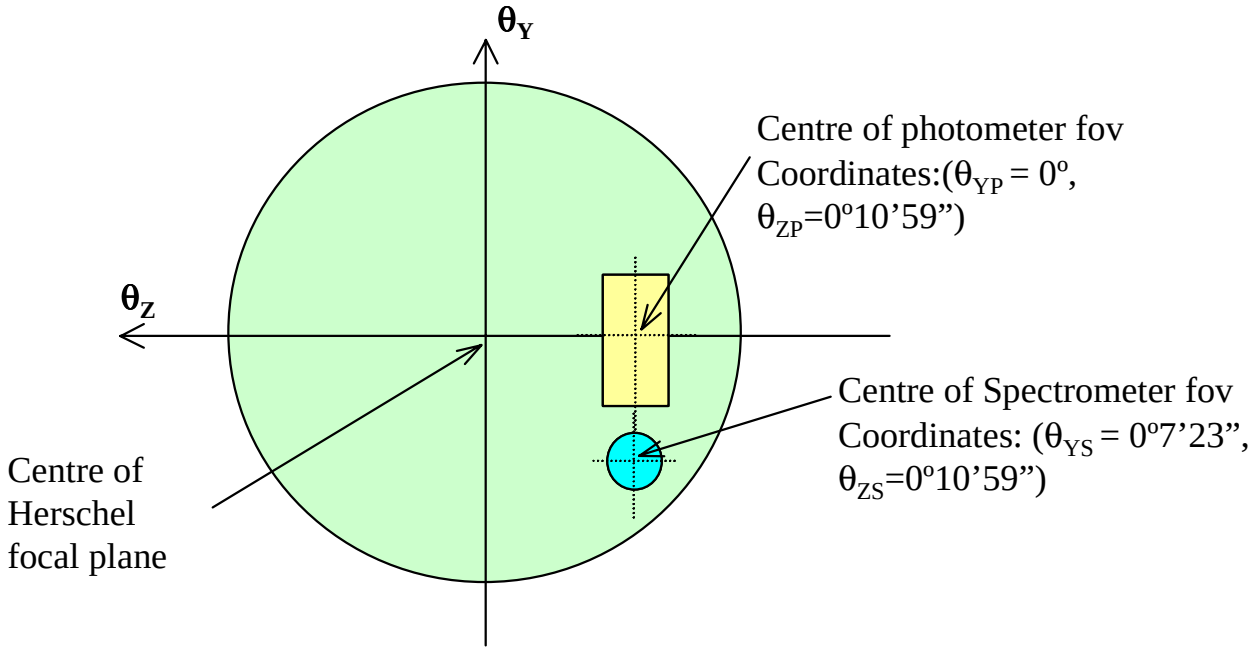

Figure 5-1 - Definition of SPIRE pointing offsets with respect to the telescope boresight.

5.2 Spacecraft movements during SPIRE observing

The Herschel spacecraft is capable of executing various controlled movements to allow observations of various kinds by the three instruments. These are described in detail in the IID-A. SPIRE will mainly use the following spacecraft movements.

5.2.1 Nod

The NOD function of the telescope is an operation in which the target source is periodically moved from one instrument chop position to the other chop position by re-pointing the satellite. The pointing direction will change in the direction of the chopper throw - see Figure 5-2.

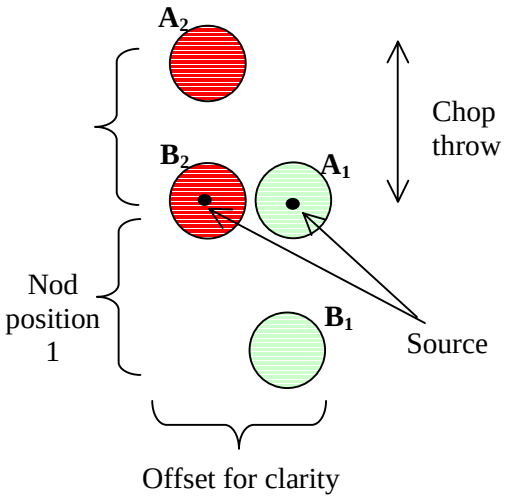

Figure 5-2 - Pointing positions for a telescope NOD function. The circles represent the size of the telescope Airy pattern projected onto the sky. The two nod positions have been offset left and right for clarity.(A_1 and B_2 are co-aligned).

The purpose of nodding is to subtract out the signal offset that will be present at some level due to the fact that the detector will receive different amounts of ambient background power in the two chop positions. This offset is likely to be larger than low-level signals to be detected, and may also vary significantly with time over the course of an observation if the primary mirror has a time-varying temperature gradient in the chopping direction (Griffin, 1998). Nodding takes out the offset in the following way:

Let S = Source signal O_A = Offset signal for beam A O_B = Offset signal for beam B

Then if we subtract the total signals measured in the two nod positions, we get

(A1 - B1) - (A2 - B2) = [(S + OA) - OB] - [OA - (S + OB)] = 2S.

5.2.2 Raster

The RASTER Spacecraft Function is a series of fine pointing operations of separated by slews such that the pointing of the telescope axis moves in a raster pattern. Figure 5-3 shows how the raster pattern will be constructed.

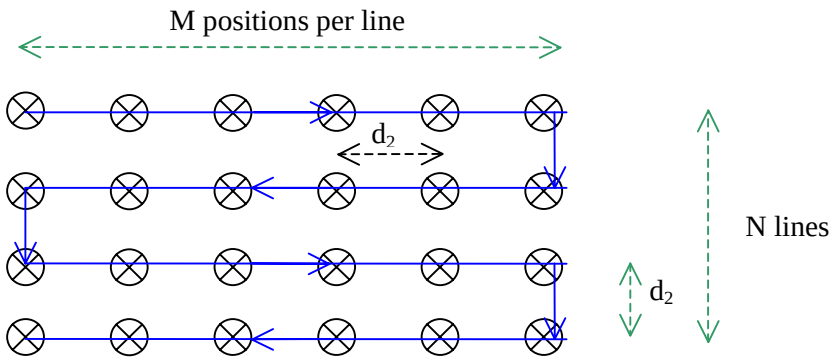

Figure 5-3 - Pointing positions for a telescope RASTER function. The observation is specified in terms of M pointings per line separated by d_1 by N lines separated by d_2 arcsec.

5.2.3 Line Scan

In the LINE SCAN Spacecraft Function the satellite is slewed at a constant angular velocity along short parallel lines on the sky. Figure 5-4 shows how the operation is carried out.

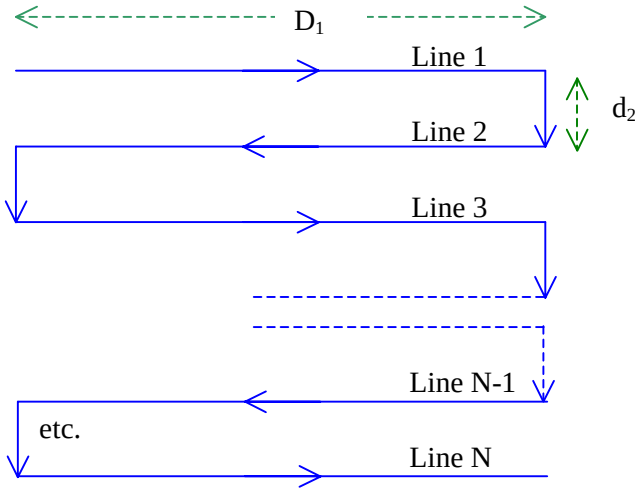

Figure 5-4 - The LINE SCAN function of the telescope consists of a number of short slews of length D_1 separated by a distance d_2. The slews will be carried out in the order shown here

SPIRE observations are implemented by combinations of the following:

Spacecraft Functions: These are the operations that can be carried by the spacecraft to point the telescope, such as line scan; raster; staring etc. They are fully described in the IID-A. Spacecraft Functions also include operations by the CDMS to switch power to the instrument; send commands; collect data etc.

Instrument Functions: These are the operations to be carried out with the instrument such as chopping , jiggling, scanning the FTS mirror, operation of the internal calibrators, etc. Combined with the Spacecraft Functions they fully define how an observation is to be carried out.

Instrument Data Configurations: In addition to specifying how the instrument is to be operated for a given operation, the on-board data processing needs to be specified along with the data to be sampled and the manner in which the detector data is sampled. This will be done be choosing from a number of Data Configurations such as **Photometer Full Field Chop**, **Spectrometer Single Pixel**, etc.

Observatory Functions: Combinations of Spacecraft and Instrument Functions and Instrument Data Configurations which, with the appropriate input parameters, allow any **Observation** to be carried out. There are two categories of Observatory Functions: **Photometer Observatory Functions (POFs)** and **Spectrometer Observatory Functions (SOFs).**

5.3 Photometer Observatory Functions

Table 5-1 - Photometer Observatory Functions

Observation	Observatory Function	Name	Comments
Point source Photometry	POF1	Chop without jiggling	Accurate pointing and source position
	POF2	Seven-point jiggle map	Inaccurate pointing or source position
Jiggle Mapping	POF3	n-point jiggle map	Field mapping
	POF4	n-point jiggle map with raster	Extended field mapping
Scan Mapping	POF5	Scan map (no chopping)	Large-area mapping
	POF6	Scan map with chopping	Large area mapping (with 1/f noise)
Peak-up	POF7	Photometer peak-up	Determination of pointing offsets
Calibrate	POF8	Photometer calibrate	Responsivity tracking
Engineering Modes	POF9	Special engineering/ commissioning modes	

5.3.1 Point Source Photometry (POF1 and POF2)

For point source photometry, pixel-pixel chopping is used as described in Section 2.2.1.3. The required chop throw is 4Fλ at 500 μm, corresponding to a 10-mm motion of the beam on the array and to a chop angle on the sky of θ_{chop} = 126 arcsec.

Simple pixel-pixel chopping (POF1) requires pointing accuracy sufficiently good that the loss of signal due to the pointing error is acceptable. The signal loss factors for the photometer beams are shown in Figure 5-5a.

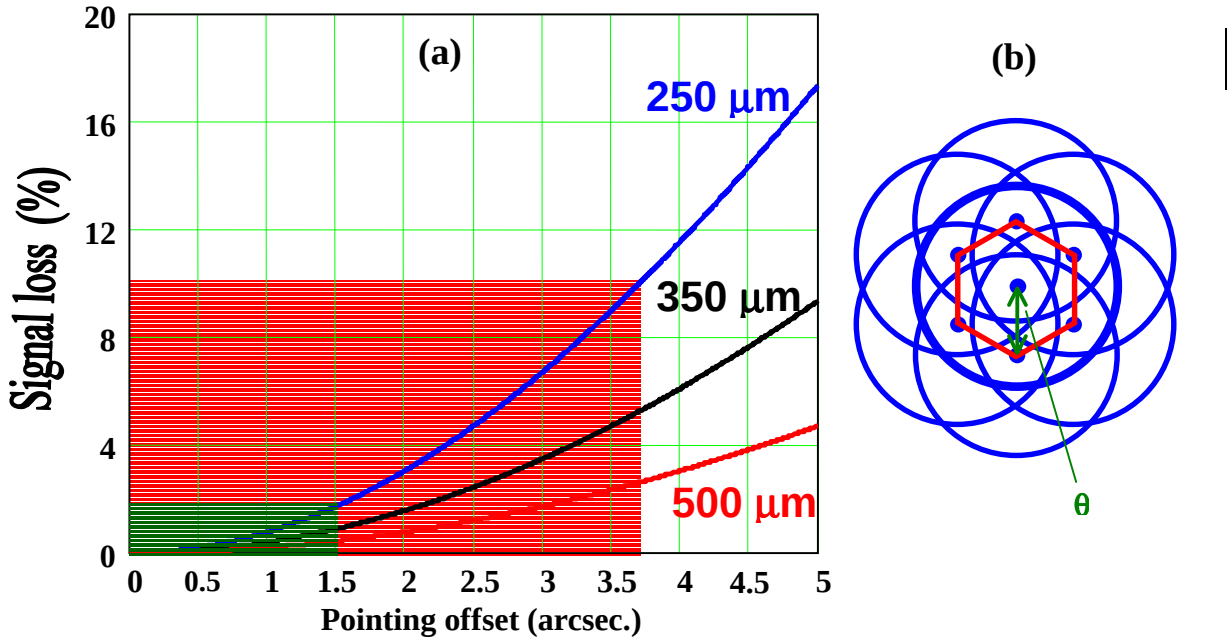

Figure 5-5 - (a) Signal loss vs. pointing error for the three SPIRE photometer bands; (b) beam positions for 7-point map with angular offset θ.

The required Absolute Position Error (APE) for Herschel (3.7 arc seconds) corresponds to 11%, 6%, and 3% signal loss at 250, 350, and 500 μm respectively. The corresponding figures for the goal APE value (1.5") are 2%, 1%, and 0.5%. For most observations, 11% is not acceptable, but 2% is. Therefore, the required APE is not good enough to allow accurate photometry at 250 μm without peaking up, but the goal is sufficient to allow this.

In order to avoid calibration errors due to satellite pointing errors or inaccurate knowledge of the source co-ordinates, it is envisaged that many point source observations will be carried out by making a 7-point map (POF2). The BSM is used to do to do small map 7-point hexagonal jiggle map with spacing θ arcsec., as shown in Figure 5-5b. A suitable value for θ is ~ 6 arc seconds: this spacing is 1/3 of the beam at 250 μm (so consistent with full sampling), and is almost twice the APE. From such a 7-point map, the total flux of the source can be computed, and the source position can be recovered with an accuracy that depends on the S/N. The central position is made to coincide with one of sets of three overlapping detectors to allow simultaneous optimised observations in the three bands. The chop throw can be set at any desired value within the available range. A value of 126" improves the overall efficiency by allowing the source to be observed all the time in all bands.

5.3.2 Jiggle Mapping (POF3 and POF4)

Jiggle-map mode is for mapping objects or regions that are extended with respect to the SPIRE beam but smaller than a few arcminutes in size.

The BSM is used to make an n-point jiggle map while chopping with a throw greater than the size of the object to be mapped. The maximum throw is 4 arcminutes (± 2 arcminutes) as illustrated below.

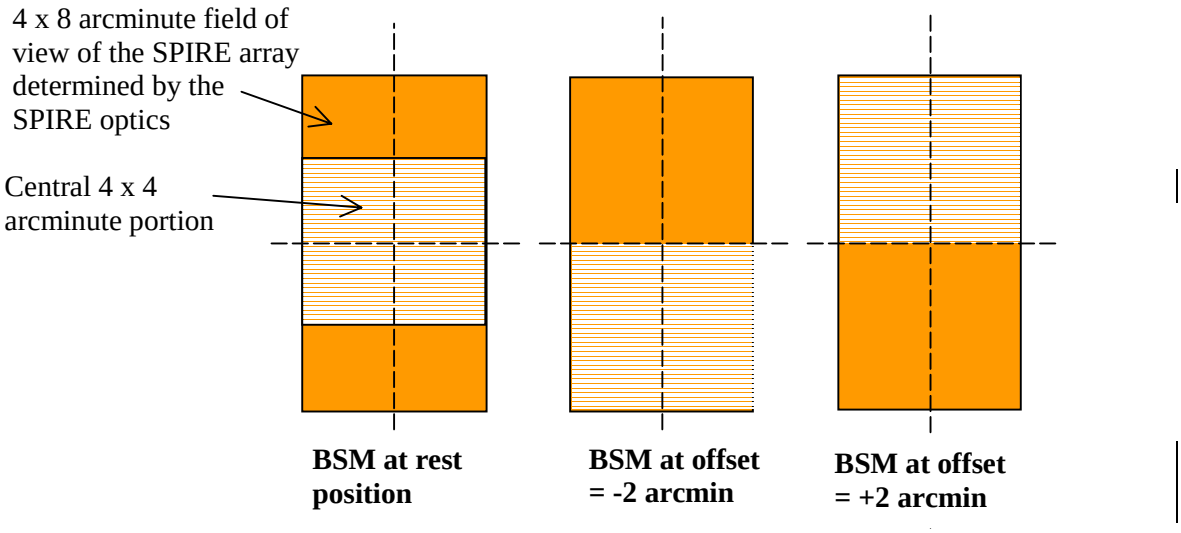

Figure 5-6 Field mapping with maximum chop throw of 4 arcminutes. The detectors in the central square 2 x 2 arcminute portion of a photometer array are deflected by ± 2 arcminutes by the BSM, so that they are alternately chopped from one side of the available field of view to the other.

For full sampling at all wavelengths, n = 64. Considering the simplified case of square-packed horns, the step size must be 0.5λ/D = 9 arcseconds at 250 μm and the number of steps must accommodate the need to cover the distance between two beams at 500 μm: 2λ/D = 72 arc seconds. Eight steps in each orthogonal direction are thus required. The geometry of the juggle pattern is hexagonal for the hexagonally packed feedhorns, but the number of steps required is still 64. To allow flexibility in the use of this mode, permitted values of n shall be 16, 32 and 64. The jiggle positions shall be defined by angles $\Delta\theta_Y$ and $\Delta\theta_Z$ in the Y and Z directions (with respect to the BSM rest position). The sequence in which the jiggle positions are visited is

yet to be determined. It is envisaged that a typical time per 64-point jiggle cycle will be 64 seconds, allowing two chop cycles per jiggle position at the maximum chop frequency of 2 Hz.

POF4 involves a sequence of repetitions of POF3 with the telescope performing the steps of a raster scan between the individual jiggle cycles in order to build up a map of a larger area.

5.3.3 Scan mapping (POF 4 and POF5)

This mode is for mapping a large region of sky by scanning the telescope to provide modulation of the signal. It does not require the beam steering mechanism and is the preferred observing mode for deep extragalactic surveys because it is more efficient and requires simpler data analysis. It also avoids increasing confusion noise as happens with chopped observations if the individual signals in the two chop half-cycles are not both transmitted to the ground. This will be done in the case of SPIRE, so chopping can be performed if necessary without degrading the S/N in principle.

All SPIRE mechanisms are inactive. The spacecraft operates in line scan mode with the scan direction across the sky at an angle of 14.5^{o} to one of the array axes so that the individual strips of the map are fully sampled (1/2 beam spacing) in the cross-scan direction. The length of each line-scan should be such that the turn-around time of the telescope (here assumed to be 10 seconds) does not constitute a large overhead. Each line should therefore take at least 60 seconds. The scan rate will depend on the 1/f stability of the whole system, but with a maximum limit of 60 arcseconds/second, determined by the spacecraft AOCS. The fastest beam-crossing time (for a 250-μm detector) at this scan rate is 18/60 = 0.3 seconds. This is comfortably longer than the time constant of the detectors (< 30 ms). It will be desirable to scan as slowly as possible to minimise telescope turn-around overheads.

In the event of some 1/f noise component resulting in noise fluctuations on the timescale of a scan, the BSM can perform chopping.

5.3.4 Photometer peak-up (POF7)

This mode is designed to allow SPIRE to peak up the pointing on a sufficiently strong point-like source. As far as the observations are concerned, it is the same as a 7-Point Jiggle Map). It may not be necessary to use this mode in flight. It is not needed for very bright objects (carrying out a small map is quick compared to overheads from slewing etc.). Nor is it practical for very faint objects (poor S/N of the 7-point data would lead to inaccurate offset calculation). It is therefore only likely to be useful for a particular band of source strengths. POF7 may therefore be deleted for simplicity. For the moment, it is included to account for the possibility that peaking up involving autonomous computation of the required pointing corrections by the SPIRE DPU may be needed in some cases.

SPIRE does a standard seven-point jiggle observation. The offset of the source with respect to the commanded pointing is computed by the DPU using the recorded data. The calculated pointing offsets are (a) implemented by the BSM (baseline) or (b) transmitted to the spacecraft AOCS. If (b), the AOCS checks that the required telescope movement is within the acceptable limits and executes it. SPIRE waits for a standard period of time to elapse before flagging the data as valid.

5.3.5 Operation of photometer internal calibrator (POF8)

It is envisaged that the photometer calibrator will be operated at intervals of an hour or more. Its function is to present a repeatable signal to the detectors. This will allow characterisation of (i) any responsivity or system gain drifts; (ii) any variation of the detectors' responsivity with radiant loading (e.g., non-linear response when viewing very bright sources).

In operation, it will be powered by a pre-selected waveform, and the corresponding signals will be recorded. A typical duration of the whole sequence will be ~ 10 sec. The BSM must be fixed at its rest position, and the telescope pointing must also be fixed so that the only signal modulation is from the calibrator. To allow

calibration to be performed flexibly, it may be advantageous to incorporate this function within some of the other POFS (e.g., to enable calibrator flashes to be interspersed between the rows of line scanning observations).

5.4 Spectrometer Observatory Functions

There are two different Spectrometer Observatory Functions:

SOF1: Point Source Spectrum
SOF2: Fully sampled spectral map

5.4.1 Point source spectrum (SOF1)

This mode is for measuring the spectrum of a point source that is well centred on the central detectors of the FTS arrays. The telescope is pointed at a known position, with the source lying on the chosen detector pair - nominally the central detectors of the two arrays - pointing offset (θ_{YS}, θ_{ZS}).

The FTS mirror mechanism is scanned over the required range with the velocity controlled by the drive electronics. Each scan will take between 7 and TBD seconds to complete. The detectors and the position sensor are read out asynchronously whilst the mechanism is moving – i.e. time-sampling of the FTS mechanism position. Each interferogram for each detector is stored in the DPU memory. The scan is repeated until the desired integration time has been reached.

5.4.2 Fully-sampled spectral map (SOF2)

This mode allows imaging spectroscopy of a region of sky or an extended source that is within the FOV of the spectrometer – i.e. less than 2.6 arcminutes circular. This is achieved by using the beam steering mirror to perform a low-frequency jiggle and taking one or more interferograms at each point of the jiggle pattern. The sequence of operations for an individual pointing is as for SOF1, and the BSM is used to make an n-point jiggle map as in POF3. The mirror is held at each position while the desired number of FTS scans is carried out. For full sampling at all wavelengths, n = 25. Considering the simplified case of square-packed horns, the step size must be $0.5\lambda/D$ = 9” at 250 μm and the number of steps must accommodate the need to cover the distance between two beams at 350 μm: $2\lambda/D$ = 45”. Five steps in each orthogonal direction are thus required. The geometry of the juggle pattern is hexagonal for the hexagonally packed feedhorns, but the number of steps required is still 25.

The number of interferograms required per position is selectable (a minimum of three would seem sensible, and could be built up either by repeating the jiggle three times or doing three scans at each position of a single jiggle). With three scans per position, it will take at least 525 seconds to take a fully sampled R = 0.4 cm^{-1} 2.6 arcminutes circular map - with overheads this will be around ten minutes.

6. SPIRE SENSITIVITY ESTIMATION

The sensitivity of SPIRE has been estimated under the assumptions listed below. Pessimistic overall optical efficiencies of 30% for the photometer and 15% for the FTS are assumed, taking into account all losses including filter transmission, mirror reflectivity, diffraction within the instrument and pupil alignment errors.

Table 6-1 - Assumptions for SPIRE sensitivity estimation

Telescope temperature (K)		80		
Telescope emissivity		0.04		
Telescope used diameter (m)	(1)	3.29		
No. of observable hours per 24-hr period		21		
Photometer				
Bands (μm)		250	350	500
Numbers of detectors		139	88	43
Beam FWHM (arcseconds)		17	24	35
Bolometer DQE	(2)	0.6	0.7	0.7
Throughput		λ^2		
Bolometer yield		0.8		
Feed-horn/cavity efficiency	(3)	0.7		
Field of view (arcminutes) Scan mapping Field mapping		4 x 8 4 x 4		
Overall instrument transmission		0.3		
Filter widths ($\lambda/\Delta\lambda$)		3.3		
Observing efficiency (slewing, setting up, etc.)		0.9		
Chopping efficiency factor		0.45		
Reduction in telescope background by cold stop	(4)	0.8		
FTS spectrometer				
Bands (μm)		200-300	300-670	
Numbers of detectors		37	19	
Bolometer DQE		0.6	0.7	
Feed-horn/cavity efficiency		0.70		
Field of view diameter (arcminutes)		2.6		
Max. spectral resolution (cm^{-1})		0.04		
Overall instrument transmission		0.15		
Signal modulation efficiency		0.5		
Observing efficiency		0.8		
Electrical filter efficiency		0.8		

Notes:

(i) The telescope secondary mirror is the pupil stop for the system, so that the outer edges of the primary mirror are not seen by the detectors. This is important to make sure that radiation from highly emissive elements beyond the primary reflector does not contribute stray light.

(ii) The bolometer DQE (Detective Quantum Efficiency) is defined as the $\left[\frac{NEP_{ph}}{NEP_{Total}}\right]^2$ where NEP_{ph} is the photon noise NEP due to the absorbed radiant power and NEP_{Total} is the overall NEP including the contribution from the bolometer noise.

(iii) This is the overall absorption efficiency of the combination of feed-horn, cavity and bolometer element.

(iv) A fraction of the feedhorn throughput falls outside the solid angle defined by the photometer 2-K cold stop and is thus terminated on a cold (non-emitting) surface rather than on the 4% emissive 80-K telescope. This reduces the background power on the detector.

The detailed calculations for the photometer and spectrometer are presented in *Sensitivity Models for SPIRE* (Griffin). The main results are summarised below.

Background power and photon noise levels: The background power levels (which are dominated by the telescope emission), and the corresponding photon noise limited NEP values are given in Table 6-2.

Table 6-2 - Background power and photon noise-limited NEPs for SPIRE.

		Photometer band (μm)			FTS band (μm)	
		250	350	500	200-300	300-670
Background power/detector	PW	3.9	3.2	2.0	6.0	11
Background-limited NEP	W $Hz^{-1/2}$ x 10^{-17}	8.1	6.1	4.5	10	11
Overall NEP (inc. detector)	W $Hz^{-1/2}$ x 10^{-17}	10	7.3	5.4	12	14

Instrument sensitivity: The estimated sensitivity levels for SPIRE are summarised in Table 6-3. The figures quoted are the nominal values, with an overall uncertainty of around 50% to take into account uncertainties in instrument parameters, particularly feedhorn efficiency, detector DQE, and overall transmission efficiency. The pixel size will be increasingly mis-matched to the diffraction spot size. The trade-off between wavelength coverage and sensitivity of the long-wavelength FTS band must be studied in detail. At the moment, we estimate an effective loss of efficiency of a factor of two at 670 μm, and scale linearly for wavelengths between 400 and 670 μm. Performance beyond 400 μm may have to be compromised to maintain the desired sensitivity below 400 μm.

Table 6-3 - Estimated sensitivity of SPIRE for broad-band photometry, line spectroscopy and low-resolution spectrophotometry.

Photometry					
λ	μm		250	350	500
ΔS(5-σ; 1-hr)	mJy	Point source (7-point mode)	2.5	2.6	2.9
		4' x 4' jiggle map	8.8	8.7	9.1
		4' x 8' scan map	7.3	7.2	7.5
Time (days) to map 1 $deg.^2$ to 3 mJy 1-σ		1^o x 1^o scan map	1.8	1.7	1.9

Line spectroscopy Δσ = 0.04 cm^{-1}					
λ	μm		200	400	670
ΔS (5-σ; 1-hr)	W m^{-2} x 10^{-17}	Point source	3.4	3.9	7.8
		2.6' map	9.0	10	21

Low-resolution spectrophotometry Δσ = 1 cm^{-1}					
λ	μm		200	400	670
ΔS (1-σ; 1-hr)	mJy	Point source	110	130	260
		2.6' map	300	350	700

For the FTS, limiting flux density is inversely proportional to spectral resolution (Δσ). Limiting line flux is independent of spectral resolution (for an unresolved line).

7. REFERENCES

Ade, P A R., P A Hamilton, & D A Naylor, "An absolute dual beam emission spectrometer", *In Fourier transform spectroscopy: new methods and applications*, OSA, 90, 1999.

Bock, J J, H G LeDuc, A E Lange, & J Zmuidzinas, "A monolothic bolometer array suitable for FIRST", *Proceedings of ESA Symposium on The Far Infrared and Submillimetre Universe*, Grenoble, 15-17 April 1977, ESA SP-401, 349, 1997.

Bock J., "Temperature Stability Requirements for SPIRE", SPIRE-JPL-NOT-000623.

Caldwell, M E, B M Swinyard, & A Richards, "Beam pattern (diffraction) aspects in design of the SPIRE instrument", *Proc. SPIE* 4013, 210, 2000.

Dohlen, K, A Orignea, D Pouliquen, & B Swinyard, "Optical design of the SPIRE instrument for FIRST", *Proc. SPIE* 4013, 119, 2000.

Duband, L, "Spaceborne helium adsorption coolers", *Proceedings of ESA Symposium on The Far Infrared and Submillimetre Universe*, Grenoble, 15-17 April 1977, ESA SP-401, 357, 1997.

Duband, L, "A thermal switch for use at liquid helium temperature in spaceborne cryogenic systems", *Proceedings of the 8th International Cryocooler Conference*, Vail, Colorado, p731, 1995.

Goldsmith, P F, "Quasi-optical techniques at millimeter and submillimeter wavelengths", *Infrared and mm Waves*, Vol. 6, Chap. 5, K J Button, Ed., Academic Press, 1982.

Griffin, M J, & W S Holland, "The influence of background power on the performance of an ideal bolometer." *Int. J. Infrared mm Waves* 9, 861, 1988.

Griffin, M J. "The design of a bolometer instrument for FIRST", *Proceedings of ESA Symposium on The Far Infrared and Submillimetre Universe*, Grenoble, 15-17 April 1997, ESA SP-401, 31, 1997.

Griffin *et al.* "SPIRE: A bolometer instrument for FIRST", proposal submitted in response to ESA's Announcement of Opportunity for FIRST payload instruments, 1998a.

Griffin, M, L Vigroux, B Swinyard, and C Cunningham, "SPIRE - a bolometer instrument for FIRST", *Proc. SPIE* 3357, 404, 1998b.

Griffin, M, "Observing speed for SPIRE feedhorn and filled array options", SPIRE-QMW-NOT-000334, Jan. 24, 2000.

Griffin, M., "Sensitivity Models for SPIRE", SPIRE-QMW-NOT-000XXX.

Holland, W S, E I Robson, W K Gear, C R Cunningham, J F Lightfoot, T Jenness, R J Ivison , J A Stevens, Ade, P A R, M J Griffin, W D Duncan, J A Murphy, & D A Naylor, *Mon. Not. R. Astron. Soc.* 303, 659, 1999.

Lee, C, P A R Ade, and C V Haynes, "Self-supporting filters for compact focal plane designs", in *Proc. Submillimeter and far-Infrared Space Instrumentation*, 30th ESLAB Symposium, Noordwijk, ESA S-P 388, 1996.

Martin, D H, "Polarising interferometric spectrometers for near- and sub-millimetre spectra", Int. J. *Infrared mm Waves*, 6, 65, 1982.

Mather, J, "Bolometer noise: non-equeilibrium theory" Appl. Opt. 21, 1125, 1982.

Mauskopf, P D, J J Bock, , H del Castillo, W L Holzapfl, & A E Lange, “Composite infrared bolometers with Si_3N_4 micromesh absorbers”, *Appl. Opt.* Vol. 36, No. 4, 765, 1997.

Origne, A. and Dohlen, K. “FIRST SPIRE: Optical alignment verification plan,” LOOM. KD. SPIRE. 2000.001-2, 16 May 2000.

Richards, P L, "Bolometers for infrared and millimeter waves", *J. Appl. Phys*. 76, 1, 1994.

Swinyard, B M, P A R Ade, M J Griffin, P A Hamilton, K Dohlen, J-P Baluteau, D Pouliquen, D Ferand, P Dargent, G Michel, J Martignac, L Rodriguez, D E Jennings, M E Caldwell, & A G Richards, "FIRST-SPIRE spectrometer: a novel imaging FTS for the submillimeter" *Proc. SPIE* 4013, 196, 2000.

Swinyard, B., “Assessment of System Level Failure Effects for SPIRE”, SPIRE-RAL-NOT-000319.